

A Multi-omics Perspective
on Osmoadaptation and
Osmoprotection
in *Bacillus subtilis*

Dissertation

zur Erlangung des Grades
des Doktors der Ingenieurwissenschaften
der Naturwissenschaftlich-Technischen Fakultät III
Chemie, Pharmazie, Bio- und Werkstoffwissenschaften
der Universität des Saarlandes

vorgelegt von

Michael Kohlstedt

Saarbrücken

2014

Tag des Kolloquiums: 25. Juli 2014

Dekan: Prof. Dr. Volkhard Helms

Berichterstatter: Prof. Dr. Christoph Wittmann
Prof. Dr. Elmar Heinzle
Prof. Dr. Jörg Stülke

Vorsitz: Prof. Dr. Manfred J. Schmitt

Akademischer Mitarbeiter: Dr. Björn Becker

Für meine Mama

Publications

Partial results of this work have been published in advance authorized by the Institute of Biochemical Engineering (Technische Universität Braunschweig) and the Institute of Systems Biotechnology (Universität des Saarlandes) represented by Prof. Dr. Christoph Wittmann.

Peer-reviewed articles

Kohlstedt, M., Becker, J., and Wittmann, C. (2010). Metabolic fluxes and beyond – systems biology understanding and engineering of microbial metabolism. *Appl Microbiol Biotechnol* **88**: 1065-1075. DOI: 10.1007/s00253-010-2854-2.

Becker, J., Schäfer, R., Kohlstedt, M., Harder, B.J., Borchert, N.S., Stöveken, N., Bremer, E., and Wittmann, C. (2013). Systems metabolic engineering of *Corynebacterium glutamicum* for production of the chemical chaperone ectoine (2013). *Microb Cell Fact* **12**: 110. DOI: 10.1186/1475-2859-12-110.

Kohlstedt, M., Sappa, P.K., Meyer, H., Maaß, S., Zaprasis, A., Hoffmann, T., Becker, J., Steil, L., Hecker, M., van Dijl, J.M., Lalk, M., Mäder, U., Stülke, J., Bremer, E., Völker, U., and Wittmann, C. (2014). Adaptation of *Bacillus subtilis* carbon core metabolism to simultaneous nutrient limitation and osmotic challenge: A multi-omics perspective. *Environ Microbiol*, in press. DOI: 10.1111/1462-2920.12438.

Conference contributions

Kohlstedt, M., Becker, J., Korneli, C., Sappa, P.K., Meyer, H., Maaß, S., Lalk, M., Mäder, U., Bremer, E., Hecker, M., Völker, U., and Wittmann, C. (2011). Osmotic stress response in *Bacillus subtilis* – integration of the fluxome with the regulatory networks. VAAM Jahrestagung, Karlsruhe, Germany.

Kohlstedt, M., Korneli, C., Becker, J., Meyer, H., Sappa, P.K., Mäder, U., Maaß, S., Hoffmann, T., Lalk, M., Völker, U., Hecker, M., Bremer, E., and Wittmann, C. (2011). Towards systems understanding of *Bacillus subtilis* – integrating metabolic fluxes and cellular components under osmotic stress. Biotransformations, Bad Herrenalb, Germany

Meyer, H., Kohlstedt, M., Maaß, S., Sappa, P.K., Hoffmann, T., Völker, U., Wittmann, C., Bremer, E., and Lalk, M. (2011). Osmotic stress response in *Bacillus subtilis* – a combined 'omics' study, Metabomeeting, Helsinki, Finland.

Sappa, P.K., Kohlstedt, M., Meyer, H., Burian, M., Mäder, U., Steil, L., Lalk, M., Hoffman, T., Bremer, E., Wittmann, C., and Völker, U. (2012). Absolute quantification of central carbon metabolism in growing and stressed *Bacillus subtilis*. EuPA congress, Glasgow, United Kingdom.

Sappa, P.K., Kohlstedt, M., Meyer, H., Steil, L., Mäder, U., Becker, J., Burian, M., Hoffmann, T., Lalk, M., Bremer, E., Wittmann, C., and Völker, U. (2013). Multi-omics based investigation of central carbon metabolism of glucose starved *Bacillus subtilis* under osmotic stress and osmoprotection. Proteomic Forum, Berlin, Germany.

Kohlstedt, M. (2014) Systems understanding of salt-stressed and osmoprotected *Bacillus subtilis* – an integrated multi-omics perspective on carbon core metabolism. 2nd UniGR Workshop "Systems Biology", Esch-sur-Alzette, Luxembourg.

Kohlstedt, M., Sappa, P.K., Meyer, H., Maaß, S., Hoffmann, T., Becker, J., Steil, L., Hecker, M., van Dijl, J.M., Lalk, M., Mäder, U., Stülke, J., Bremer, E., Völker, U., Wittmann, C. (2014) Adaptation of *Bacillus subtilis* carbon core metabolism to simultaneous nutrient limitation and salt stress: a multi-omics perspective. Trends in Metabolomics, Frankfurt, Germany.

Vorwort

Bei der Entstehung der vorliegenden Arbeit hat mich eine Vielzahl von Menschen begleitet und unterstützt, denen mein großer Dank gilt.

Besonders danken möchte ich meinem Doktorvater Prof. Dr. Christoph Wittmann für die stets gute Betreuung der Arbeit, die vielen wissenschaftlichen Diskussionen und die wertvollen Ratschläge fürs Leben. Seine stets offene Tür und die lockere Atmosphäre haben in meinen Augen die Arbeit in vielerlei Hinsicht vereinfacht, sodass am Ende *alles gut wurde*.

Mein Dank gilt den Professoren Elmar Heinzle und Manfred Schmitt für den herzlichen Empfang an der Universität des Saarlandes und die kurzfristige Übernahme des Zweitgutachtens bzw. des Prüfungsvorsitzes.

Den Professoren Jörg Stülke, Erhard Bremer und Uwe Völker sei für das stete Voranbringen des Projektes und die Zurverfügungstellung ihres umfassenden *Bacillus*-Know-hows gedankt.

Bedanken möchte ich mich bei allen Mitarbeitern des Instituts für Bioverfahrenstechnik der Technischen Universität Braunschweig für die angenehme Arbeitsatmosphäre und die bereitwillige Unterstützung bei experimentellen und technischen Fragen. Ganz besonders seien die zahlreichen *Samplinghelfer* erwähnt, ohne die ein Erfolg des BaCell-SysMo-Projektes nicht möglich gewesen wäre. Tausend Dank gehen insbesondere an Claudia Korneli, Judith Becker und Christoph Bolten für die *süßen Momente* im Labor während der anfänglichen Nachtschichten. Zusätzlicher Dank geht an Judith für das Einweihen in die Kunst der metabolischen Flussanalyse und der Enzymassays, sowie für das Korrekturlesen der Arbeit. Ein großes Dankeschön geht an Yvonne Göcke für alle *Ratschläge* in HPLC-Fragen und ihren *radspportlichen* Ehrgeiz. Vielen lieben Dank auch an meine ehemaligen Bürokollegen Jasper und Steffi für ihre offene Art, ihren Humor, ihre grenzenlose Hilfsbereitschaft und ihre Freundschaft. *Office Combo for Life*.

Ein besonderer Dank gilt *meinen* Studenten Daria Kaptan, Eugenie Sibakina, Dave Hartig und Benjamin Gola, die die bearbeitete Thematik mit den Ergebnissen ihrer experimentellen Arbeiten im Rahmen ihrer Abschlussarbeiten maßgeblich bereichert haben.

Danke an das Greifswalder Analytiktrio Hanna Meyer, Sandra Maaß und Praveen Kumar Sappa für den offenen Austausch der gewonnenen Daten, das engagierte Krisenmanagement bei aufgetretenen Schwierigkeiten und die schönen Tage in Greifswald.

Ganz herzlich möchte ich meiner Frau Anne danken, die mir während dieser intensiven Zeit den Rücken frei hielt, mich wieder aufbaute, wenn einmal der Frust drohte Überhand zu nehmen und mit ihrer unbeschwerten Art meine Gedanken auf die wichtigen Dinge des Lebens lenken konnte. *Wer, wenn nicht wir. Wo, wenn nicht hier. Wann, wenn nicht jetzt. Ans Ende denken wir zuletzt.* Meiner lieben Tochter Emma danke ich für ihr papafreundliches Schlafpensum und für ihr Verständnis, dass ihr Kampf um meine Aufmerksamkeit nicht selten zugunsten der Arbeit ausging.

Ein großer Dank geht schließlich an meine Eltern, Kerstin und Elger, und meinen Bruder Martin für ihren Antrieb und ihre Unterstützung, für ihr Interesse an meiner Arbeit und ihr Vertrauen, das richtige zu tun, für ihre verführerischen Ausflüge in die Welt der Musik und für ihre, mir mitgegebene Kraft.

Table of Content

Abstract	X
Zusammenfassung	XI
1 Introduction	1
1.1 <i>Bacillus subtilis</i> – paradigm of gram-positive bacteria and versatile cell factory	1
1.2 Central metabolism of <i>Bacillus subtilis</i>	2
1.3 Osmoregulation in <i>Bacillus subtilis</i>	8
1.4 Metabolic flux analysis and its use in combination with other omics methodologies.....	11
2 Materials and Methods.....	20
2.1 Strain	20
2.2 Chemicals	20
2.3 Media	20
2.4 Cultivation	21
2.5 Analytical techniques.....	23
2.6 Determination of rates and yields.....	40
2.7 Multi-omics data integration and visualization.....	39
2.8 Experimental workflow.....	40
3 Results and Discussion.....	42
3.1 First insights into cellular metabolism of <i>B. subtilis</i> BSB1	42
3.2 Systems biology setup for multi-omics analysis	54

3.3	Adaptation of <i>Bacillus subtilis</i> carbon core metabolism to simultaneous nutrient limitation and osmotic challenge	61
3.4	Adaptation of <i>Bacillus subtilis</i> carbon core metabolism under nitrogen limitation, ionic and non-ionic osmotic stress	81
3.5	Biotechnological production of the high-value compatible solute ectoine	93
4	Conclusion and Outlook	96
5	References	97
6	Appendix	109
6.1	Abbreviations and Symbols.....	109
6.2	Supplementary information	111

Abstract

In its natural environment, the soil bacterium *Bacillus subtilis* permanently encounters nutrient limitations and increases in osmotic stress. The present study investigated the systems-wide response of *B. subtilis* to different simultaneously imposed stresses by combining chemostat experiments under conditions of carbon and nitrogen limitation, ionic and non-ionic osmotic stress and osmoprotection with multi-omics analyses of the transcriptome, proteome, metabolome and fluxome. Surprisingly, the flux through central carbon and energy metabolism is very robust under all conditions studied. The key to achieve this robustness is the increased production of several enzymes of central carbon metabolism to compensate for their reduced activity in the presence of high salt. A major response of the cell during osmotic stress is the production of the compatible solute proline through the concerted adjustment of multiple reactions around the 2-oxoglutarate node, which drives metabolism towards the precursor glutamate. Co-regulations between the individual cellular components under the investigated stress conditions indicate that the fine-tuning of the transcriptional and metabolic networks involves functional modules that outreach single pathways. Additionally, the work shortly describes the salinity-decoupled fed-batch production of the compatible solute ectoine in *Corynebacterium glutamicum* and the contribution of precursor amino acids of the aspartate family.

Zusammenfassung

Das Bodenbakterium *Bacillus subtilis* ist in seiner natürlichen Umgebung permanenten Schwankungen des Nährstoffangebots und osmotischem Stress ausgesetzt. Die vorliegende Arbeit untersucht die systemweite Anpassung von *B. subtilis* an verschiedene, gleichzeitig auftretende Umweltstresse. Dazu wurden Chemostatexperimente, die sowohl Kohlen- und Stickstofflimitierung, als auch osmotischen Stress und Osmoprotektion nachbilden, mit Analysen des Transkriptoms, Proteoms, Metaboloms und Fluxoms kombiniert. Überraschenderweise ist die metabolische Flussverteilung im zentralen Kohlenstoffwechsel unter allen untersuchten Bedingungen sehr rigide. Eine erhöhte Produktion wichtiger Enzyme des zentralen Kohlenstoffwechsels kompensiert deren reduzierte Aktivität in Gegenwart von hohen Salzkonzentrationen im Cytosol. Eine weitere Reaktion der Zelle auf erhöhten osmotischen Stress ist die verstärkte Synthese des kompatiblen Soluts Prolin. Dies wird ermöglicht durch eine abgestimmte Anpassung der Reaktionen bis zum 2-Oxoglutarat-Knoten, die den Kohlenstofffluss in Richtung des Vorläufers Glutamat treibt. Regulatorische Interaktionen innerhalb funktionaler Module ermöglichen dabei eine systemweite Feinabstimmung des metabolischen Netzwerks über einzelne Stoffwechselwege hinaus. Die Arbeit beschreibt weiterhin die erfolgreiche, Hochsalz-unabhängige Produktion des kompatiblen Soluts Ectoin mit *Corynebacterium glutamicum* und geht kurz auf die Rolle beteiligter Aminosäuren der Aspartatfamilie ein.

1 Introduction

1.1 *Bacillus subtilis* – paradigm of gram-positive bacteria and versatile cell factory

At present, *Bacillus subtilis* is Nature's best-characterized gram-positive bacterium. The rod-shaped, prokaryote is a member of the Firmicutes and inhabits all kinds of ecosystems including the upper layers of the soil, aqueous milieus, the rhizosphere of plants and even the human gastrointestinal tract (Earl *et al.*, 2008). The bacterium serves as paradigm to study cell physiology and cellular differentiation processes, e.g. metabolism, gene regulation, sporulation, competence, biofilm formation or responses to environmental stresses. Therefore, its genome was sequenced as one of the first in 1997 and has been re-sequenced in 2009, providing valuable insights into the genetic repertoire of the *Bacillus* clade (Kunst *et al.*, 1997; Barbe *et al.*, 2009). The *Bacillus* genome consists of 4,215 kb pairs coding for over 4,100 proteins, of which the half has yet to have a function assigned. Moreover, *B. subtilis* is a model system for the study of pathogens, such as *Bacillus anthracis*, *Clostridium perfringens*, *Staphylococcus aureus*, *Streptococcus pneumoniae* and *Listeria monocytogenes* (Michna *et al.*, 2014). Apart from the scientific interest, a multitude of *Bacillus* species is used for the commercial production of fine chemicals, antibiotics and vitamins, as well as food, feed and technical enzymes (Harwood, 1992; Schallmeyer *et al.*, 2004; Papagianni, 2012). Among the most important biotechnological products are α -amylases, lipases, proteases (e.g. subtilisin), riboflavin (vitamin B₂), the polypeptide antibiotic bacitracin, insecticidal toxins and flavor-enhancing nucleosides (e.g. inosine, guanosine). Today, modern recombination techniques furthermore allow biosynthesis of medically relevant antibody fragments (Wu *et al.*, 1993; Wu *et al.*, 2002), hyaluronic acid (Widner *et al.*, 2005; Chien and Lee, 2007) or even biocommodities (Romero *et al.*, 2007; Romero-Garcia *et al.*, 2009; Zhang *et al.*, 2011; Zhang and Zhang, 2011) using *B. subtilis*. In agriculture *B. subtilis* strains serve as biological control agents (BCAs), protecting plants against pathogens, thus promoting plant growth (Cazorla *et al.*, 2007; Galindo *et al.*, 2013). *B. subtilis* is free of exo- and endotoxins in such a way as the respective products can be generally regarded as safe (GRAS).

1.2 Central metabolism of *Bacillus subtilis*

Carbon substrate uptake

B. subtilis uses glucose as its preferred carbon and energy source (Stülke and Hillen, 2000). The sugar is metabolized via three main pathways of carbon metabolism: glycolysis (or Embden-Meyerhof-Parnas (EMP) pathway), the tricarboxylic acid (TCA) cycle and the pentose phosphate (PP) pathway (Figure 1.1). Uptake and simultaneous phosphorylation of glucose and various other carbon sources is realized via a phosphoenolpyruvate (PEP):carbohydrate phosphotransferase system (PTS). Phosphotransferase systems can be found in numerous gram-positive and gram-negative bacteria and are composed of two general components: i) phosphotransferases enzyme I (EI) and histidine protein (HPr), and ii) several sugar-specific enzymes II (EII). In *B. subtilis* EII, HPr and EI are encoded by the operon *ptsGHI*, in which *ptsH* and *ptsI* are constitutively expressed. In the presence of glucose, a phosphoryl group is transferred from PEP, which serves as energy source and phosphate donor, to the sugar, eventually yielding glucose 6-phosphate. Other substrate uptake mechanisms active in *Bacilli*, are ATP-binding cassette (ABC) transporters, facilitated diffusion and secondary active transport (Stülke and Hillen, 2000; Deutscher *et al.*, 2003).

Central carbon metabolism

Glucose 6-phosphate is simultaneously metabolized via the EMP and the PP pathway (Figure 1.1). Under unperturbed growth conditions and in a large number of mutants the split ratio between the two catabolic pathways is about 2:1 (Fischer and Sauer, 2005). Both pathways fulfill different cellular functions. Whereas the EMP pathway yields 2 moles of pyruvate with concomitant formation of ATP and NADH, the PP pathway, on the other hand, is a major source of NADPH and pentose phosphates for anabolic purposes (Zamboni *et al.*, 2004; Commichau *et al.*, 2009). Through the EMP pathway, phosphorylated glucose is initially split into triose phosphates, which are further metabolized to pyruvate through the total action of eight enzymes (Figure 1.1) (Ludwig *et al.*, 2001; Commichau *et al.*, 2009).

In the oxidative part of the PP pathway, 2 moles of NADPH are generated by action of glucose 6-phosphate dehydrogenase and phosphogluconate dehydrogenase.

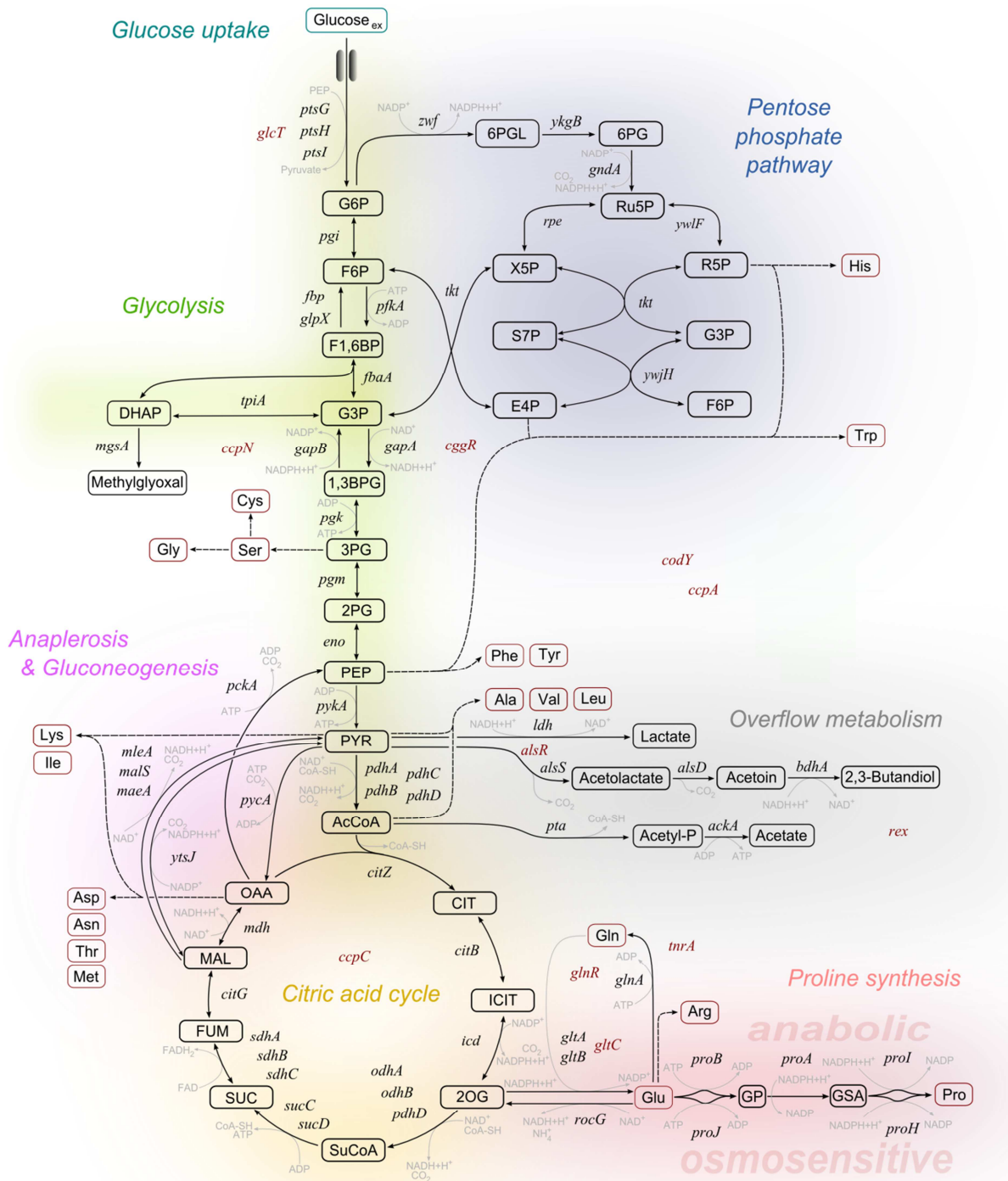


Figure 1.1: Central carbon metabolism and proline biosynthesis in *B. subtilis*. Metabolites are displayed in CAPITALS and encoding genes are displayed in *italics*. Dark red gene names indicate regulators of particular pathways. Metabolite abbreviations: G6P, Glucose 6-phosphate; F6P, Fructose 6-phosphate; F1,6BP, Fructose 1,6-bisphosphate; DHAP, Dihydroxyacetone phosphate; G3P, Glyceraldehyde 3-phosphate; 1,3BPG, 1,3-bisphosphoglycerate; 3PG, 3-phosphoglycerate; 2PG, 2-phosphoglycerate; PEP, Phosphoenolpyruvate; PYR, Pyruvate; AcCoA, Acetyl-CoA; CIT, Citrate; ICIT, Isocitrate; 2OG, 2-oxoglutarate; SuCoA, Succinyl-CoA; SUC, Succinate; FUM, Fumarate; MAL, Malate; OAA, Oxaloacetate; 6PGL, 6-phosphogluconolactone; 6PG, 6-phosphogluconate; Ru5P, Ribulose 5-phosphate; X5P, Xylulose 5-phosphate; R5P, Ribose 5-phosphate; S7P, Sedoheptulose 7-phosphate; E4P, Erythrose 4-phosphate; GP, Glutamate 5-phosphate; GSA, Glutamate 5-semialdehyde.

In the non-oxidative part, different pentoses are interconverted and the enzymes transketolase (Tkt) and transaldolase (YwjH) transfer 2-carbon and 3-carbon groups to form fructose 6-phosphate and glyceraldehyde 3-phosphate, thereby linking PP and EMP pathway (Figure 1.1) (de Wulf, 1998; Zamboni *et al.*, 2004). NADH mainly serves for cell respiration to build ATP via the electron transport chain, whereas NADPH from PP pathway is needed for biosynthetic purposes in anabolism. Both routes, EMP and PP pathway, additionally provide intermediates which serve as precursors for the synthesis of numerous biomass building blocks, especially amino acids, cell wall components and nucleotides (Table 1.1). The alternative Entner-Doudoroff pathway is not present in *B. subtilis* (Stülke and Hillen, 2000).

In case of glucose excess, *B. subtilis* converts a significant portion of glucose into pyruvate and acetyl-CoA, respectively, and drains the respective carbon flux towards overflow metabolism; i.e. the synthesis and secretion of lactate, acetate, acetoin and 2,3-butanediol (Sonenshein, 2007). The synthesis of overflow metabolites quickly regenerates NAD⁺ for continued glycolysis and additional ATP is gained via substrate-level phosphorylation when for instance acetate is formed. The pyruvate dehydrogenase complex (PdhABCD), whose action leads to formation of acetyl-CoA, links EMP pathway, overflow metabolism and the TCA cycle (Stülke and Hillen, 2000). Acetyl-CoA can be converted to acetate through phosphotransacetylase and acetate kinase, or serves as precursor for the biosynthesis of fatty acids.

In the TCA cycle, pyruvate is completely oxidized into carbon dioxide. Enzymes of the TCA cycle generate ATP, reducing power in the form of NADH, FADH₂ and NADPH for oxidative phosphorylation and anabolic biosyntheses, respectively, as well as different biomass precursors (Table 1.1). At the same time, the membrane-bound TCA cycle enzyme succinate dehydrogenase (SdhABC) is involved in electron transport in the respiratory chain (Sonenshein, 2003; von Wachenfeldt and Hederstedt, 2003). *B. subtilis* has no glyoxylate shunt and is thus unable to grow on acetate or fatty acids as sole carbon source (Sonenshein, 2003).

In the absence of glucose, *B. subtilis* is able to perform gluconeogenesis to generate glucose from TCA cycle intermediates by the action of phosphoenolpyruvate carboxykinase (PckA) and glyceraldehyde 3-phosphate dehydrogenase (GapB). All remaining steps are reversible reactions of glycolysis.

Table 1.1: Major biomass building blocks of a *B. subtilis* cell, their corresponding precursor metabolites and the involved metabolic pathways.

Precursor metabolite	Building blocks	Biomass component	Pathway
Glucose 6-phosphate	UDP-glucose, glucosyldiacylglycerols, lipoteichoic acids, teichoic acids	cell wall, lipids	EMP
Fructose 6-phosphate	<i>N</i> -acetylglucosamine, lipoteichoic acids, minor teichoic acids	cell wall, lipids	EMP
Glyceraldehyde 3-phosphate	fatty acids, lipoteichoic acids, teichoic acids	cell wall, lipids	EMP
3-phosphoglycerate	serine, cysteine, glycine, nucleotides	protein, DNA, RNA	EMP
Phosphoenolpyruvate	phenylalanine, tryptophan, tyrosine	protein	EMP
Pyruvate	alanine, lysine, isoleucine, valine, leucine, branched-chain fatty acids	protein, lipids	EMP
Ribose 5-phosphate	histidine, tryptophan, nucleotides, ATP, GTP	protein, DNA, RNA	PP
Erythrose 4-phosphate	phenylalanine, tryptophan, tyrosine	protein	PP
Acetyl-CoA	fatty acids, lipoteichoic acids, minor teichoic acids	cell wall, lipids	TCA
2-oxoglutarate	arginine, glutamate, glutamine, proline	protein, hemes	TCA
Oxaloacetate	aspartate, asparagine, isoleucine, lysine, methionine, threonine, nucleotides	protein, DNA, RNA	TCA

The 2-oxoglutarate-glutamate-glutamine hub

The 2-oxoglutarate pool is from outmost importance for the cell. It represents the hub between carbon and nitrogen metabolism as it is the direct precursor of glutamate, the most abundant metabolite in the cytosol with about $800 \mu\text{mol g}_{\text{DCW}}^{-1}$ (Bolten *et al.*, 2007; Commichau *et al.*, 2008). Glutamate and glutamine serve as the major amino group donors for most nitrogen-containing metabolites (e.g. amino acids, RNA, DNA) and they are direct precursor metabolites for *de novo* synthesis of the amino acid proline, an important compatible solute involved in protection against osmotic stress (Brill *et al.*, 2011; Gunka and Commichau, 2012). It is thus evident, that the intracellular glutamate pool has to be kept sufficiently high and that flux through this metabolic hub has to be tightly controlled. In *B. subtilis*, this is realized by the concerted cyclic action of the glutamate synthase complex (GltAB, also GOGAT) and glutamine synthetase (GlnA, also GS) (Figure 1.1).

The PEP-pyruvate-oxaloacetate node

Continued operation of the TCA cycle depends solely on the action of pyruvate carboxylase. This anaplerotic reaction replenishes the TCA cycle with oxaloacetate. Together with pyruvate kinase (PykA) and the corresponding gluconeogenic enzyme PEP carboxykinase (PckA), the metabolite triangle PEP-pyruvate-oxaloacetate forms a flexible node that links anabolism, catabolism and energetic cellular needs (Figure 1.2) (Sauer and Eikmanns, 2005).

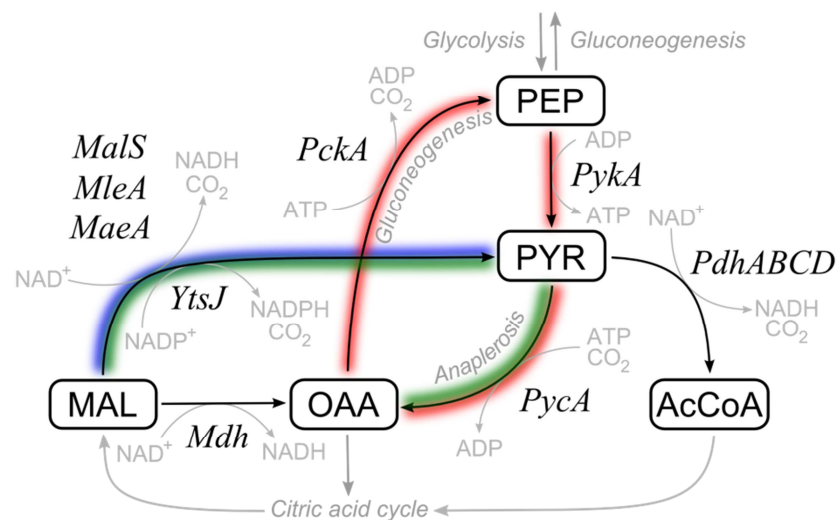


Figure 1.2: The PEP-pyruvate-oxaloacetate node in *B. subtilis* as switch point between anabolism and catabolism; including a transhydrogenation cycle to interconvert NADPH and NADH via 4 different malic enzymes (blue) (Lerondel *et al.*, 2006; Rühl *et al.*, 2012), an ATP-dissipating futile cycle (red) (Dauner *et al.*, 2001a; Dauner *et al.*, 2002) and the pyruvate shunt as bypass to malate dehydrogenase (Mdh) which provides additional OAA at the cost of one mole of ATP (green) (Diesterhaft and Freese, 1973; Sauer and Eikmanns, 2005).

Additionally, *B. subtilis* possesses four different malic enzyme isoforms which decarboxylate malate to pyruvate. Thereby MalS, MleA and MaeA use NAD⁺ as cofactor, whereas the YtsJ isoform uses NADP⁺ and plays a major physiological role under most growth conditions (Lerondel *et al.*, 2006). Fuhrer *et al.* detected *in vitro* activity of a not yet identified transhydrogenase working in *B. subtilis* (Fuhrer and Sauer, 2009), which can directly transfer electrons from NADH to NADP⁺ and the other way around. Together with transhydrogenation cycles, i.e. enzyme pairs that operate in reverse directions and in this way interconvert the two redox equivalents NADH and NADPH, the cell is able to balance its intracellular demand for redox equivalents (Lerondel *et al.*, 2006; Rühl *et al.*, 2012). Especially at lower growth rates, a significant portion of carbon is withdrawn from the TCA cycle via

gluconeogenic PEP carboxykinase or malic enzyme, even in the presence of glucose. However, carbon is reintroduced into the TCA cycle via pyruvate kinase (PykA) and pyruvate carboxylase (PycA) resulting in net loss of one mole of ATP (Dauner *et al.*, 2001a; Dauner *et al.*, 2001b). The latter pathway via malic enzyme and pyruvate carboxylase is also known as pyruvate shunt and serves as bypass to malate dehydrogenase (Mdh) (Figure 1.2). The utility of ATP-futile cycles is not fully understood, but the dissipation of excess ATP may be necessary for metabolic control and energy homeostasis (Katz and Rognstad, 1978; Dauner *et al.*, 2001b).

Cell respiration

B. subtilis generates between 0.5 and 1 ATP per mole NADH, which corresponds to a maximal P-to-O ratio of 1 (Sauer and Bailey, 1999; Zamboni and Sauer, 2003). Under aerobic conditions, the terminal electron acceptor is oxygen (von Wachenfeldt and Hederstedt, 2003). Under anaerobic conditions, *B. subtilis* is still able to grow by respiration with nitrate as electron acceptor or fermentatively, resulting in formation of various anaerobic fermentation byproducts (Nakano *et al.*, 1997; Cruz Ramos *et al.*, 2000).

Catabolite repression and global regulators of carbon and nitrogen metabolism

During evolution, bacteria developed mechanisms that enable selective uptake and degradation of different carbon sources. In the presence of a preferred carbon source, genes encoding for metabolism of other carbon substrates are not expressed. This mechanism is called 'carbon catabolite repression' (Singh *et al.*, 2008). In *B. subtilis*, several specific and global regulators are in charge to maintain an optimal flux distribution in central metabolism depending on the environmental conditions. Carbon catabolite control protein A (CcpA) is responsible for repression of hundreds of catabolic genes, when sufficient amounts of glucose are available (Sonenshein, 2007). The gluconeogenic genes *pckA* and *gapB* are additionally controlled by another carbon catabolite control protein, CcpN (Servant *et al.*, 2005). Transcription of several TCA cycle enzymes, namely citrate synthase (CitZ), aconitase (CitB) and isocitrate dehydrogenase (Icd), is controlled by CcpC. Genes encoding for these enzymes are also under regulation of CcpA and are furthermore controlled by the global regulator CodY (Sonenshein, 2007), altogether resulting in a complex regulatory network. As for CcpA and CodY, the cell senses intracellular levels of key metabolites such as fructose 1,6-

bisphosphate, branched-chain amino acids and GTP. Similar control mechanisms can be found in nitrogen metabolism as well (Fisher, 1999; Commichau *et al.*, 2006). TnrA, the global regulatory protein of nitrogen metabolism, senses the glutamine level, which is the preferred nitrogen source for *Bacillus* (Fisher, 1999). It activates operons that are responsible for the uptake of ammonium and the utilization of other nitrogen sources, when glutamine is not available.

1.3 Osmoregulation in *Bacillus subtilis*

In its environment, the soil-inhabiting bacterium *B. subtilis* is permanently exposed to fluctuations in the concentration of solutes as a consequence of raining and desiccation phases across the upper soil layers. This leads to substantial changes in external osmolarity caused by all kinds of compounds, such as ions and organic solutes. The cell may dehydrate under hypertonic conditions or burst under hypotonic conditions due to the semi-permeable cytoplasmic membrane. Also during industrial fermentation processes, production organisms are confronted with high substrate and salt concentrations in the growth medium, accumulating product titers and gradients thereof. Knowing the impact of osmotic shifts on cell physiology, regulatory network operation and production performance is thus of great importance for the design of a cell factory and the associated bioprocess.

Cellular response to osmotic stress

When *B. subtilis* is exposed to an upshift in osmotic pressure, it uses a two-step strategy to counteract dehydration of the cytosol (plasmolysis) and loss of cellular functioning (Kempf and Bremer, 1998), especially respiration, membrane processes and cell proliferation (Figure 1.3). Since dehydration occurs within seconds and the cell has to maintain its turgor pressure, *Bacillus* instantly imports potassium from its environment via two K⁺ transport systems with different affinity (Whatmore *et al.*, 1990): KtrAB (high-affinity) and KtrCD (low-affinity) (Figure 1.3). Hereby, intracellular potassium levels increase up to three fold compared to basal levels of 300 mM (Whatmore *et al.*, 1990; Holtmann *et al.*, 2003), depending on the strength of the osmotic stress. High concentrations of potassium ions, however, interfere with many cellular processes and become thus toxic for the cell. Consequently, *B. subtilis* accumulates compatible solutes, which are highly water-soluble without net charge and do not impair with cellular physiology (Kempf and Bremer, 1998).

Rapid solute release via mechanosensitive channels (Msc) serves as rescue valve in case of a down-shift in osmolarity (Hoffmann *et al.*, 2008).

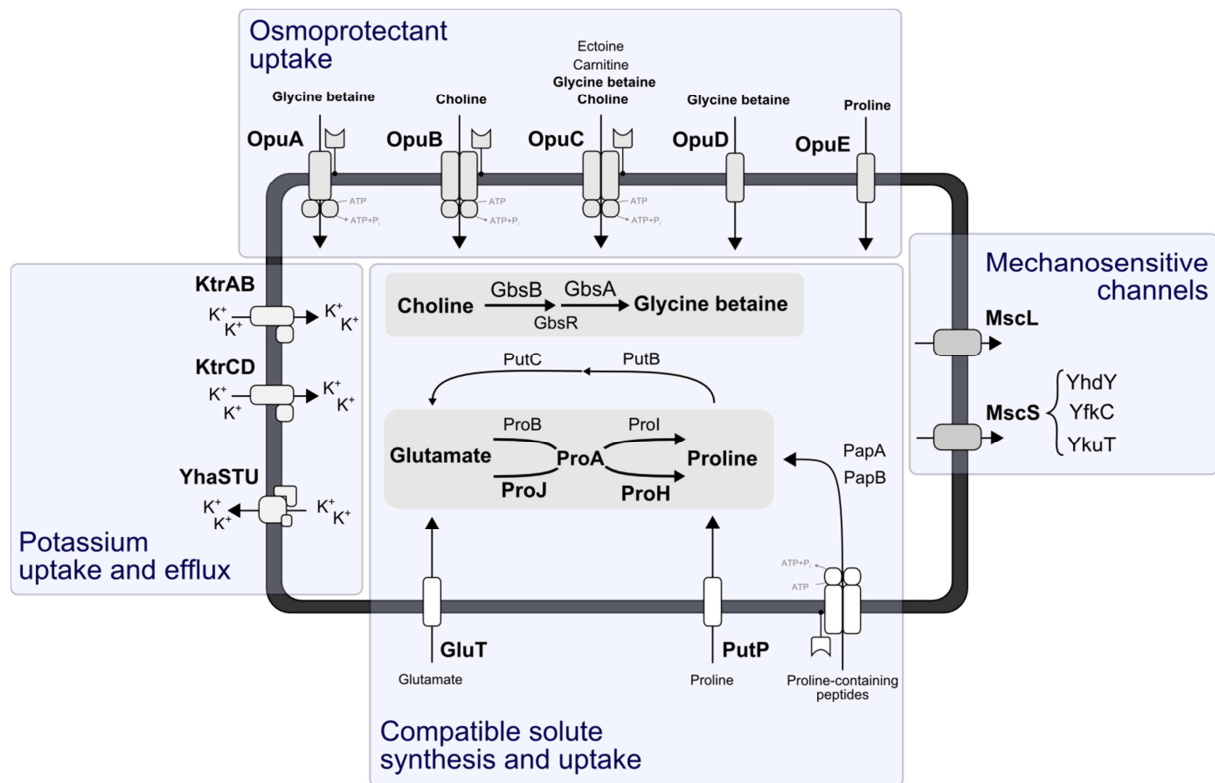


Figure 1.3: Overall cellular response of *B. subtilis* to cope with osmotic stress.

De novo synthesis and uptake of compatible solutes

Compatible solutes are termed 'chemical chaperones', since they are able to stabilize the structure of proteins, i.e. they exclude solutes from the hydration shell around the protein because of unfavorable interactions with the protein surface (Arakawa and Timasheff, 1985). By minimizing the volume, from which the solutes have to be excluded, the protein is stabilized in its native form, since it has a smaller surface than the denatured form. This phenomenon is called 'preferential exclusion' (Arakawa and Timasheff, 1985). Compatible solutes are either synthesized *de novo* or are taken up from the environment as osmoprotectants.

The only compatible solute that *B. subtilis* can synthesize *de novo* is the amino acid proline. In addition to an anabolic route via glutamate 5-kinase (ProB), glutamate 5-semialdehyde dehydrogenase (ProA) and pyrroline 5-carboxylate reductase (ProI), *B. subtilis* possesses a second, osmosensitive route via ProJ (orthologous to ProB), ProA and ProH (orthologous to

Pro1) for proline biosynthesis (Brill *et al.*, 2011). Only ProA is commonly used by both routes. The accumulated proline level correlates linearly with the osmotic burden.

Another, even more effective osmolyte is the methylamine glycine betaine (Hoffmann *et al.*, 2013). In *B. subtilis* it can be synthesized only when the precursor choline is exogenously provided (Kempf and Bremer, 1998). Uptake of usable osmoprotectants from the environment can occur via five compound-specific osmoprotectant uptake systems (OpuA to OpuE, Figure 1.3). Among them are three ATP binding cassette transporters (OpuA to OpuC). Glycine betaine can be imported via three high-affinity and osmotically inducible transport systems (OpuA, OpuC and OpuD) underlining the special importance of this osmoprotectant for *B. subtilis* (Hoffmann *et al.*, 2013). During fine-tuning of the intracellular pool, OpuE, a solute symporter, additionally recaptures continuously released proline. All Opu systems are induced in cells grown at high salinity. Additionally, the proline precursor glutamate, proline itself or proline-containing peptides can be imported via specific transport systems (Hoffmann *et al.*, 2013; Zaprasis *et al.*, 2013).

In general, alterations in osmolarity do not only influence metabolic processes, but rather affect the overall cell physiology including the activation of a general stress response mediated via the transcription factor σ_B (Hecker and Völker, 2001; Höper *et al.*, 2006; Hahne *et al.*, 2010), a high-salinity induced iron limitation (Hoffmann *et al.*, 2002; Höper *et al.*, 2006), an altered cell envelope composition (López *et al.*, 1998; López *et al.*, 2006), synthesis of degradative enzymes and expression of genetic competence (Kunst and Rapoport, 1995; Dartois *et al.*, 1998), an impeded sporulation (Ruzal *et al.*, 1998; Ruzal and Sanchez-Rivas, 1998), a repression of chemotaxis and cell motility genes (Steil *et al.*, 2003), as well as an impact on the supercoiling behavior of DNA (Krispin and Allmansberger, 1995; Alice and Sanchez-Rivas, 1997).

Industrial interest in the production of compatible solutes

Over the past decades, increasing knowledge about osmotic stress responses and concomitant release of compatible solutes in halotolerant and halophilic microorganisms, initiated the development of industrial bioprocesses for their commercial production (Sauer and Galinski, 1998; Schubert *et al.*, 2007; Pastor *et al.*, 2010; Becker *et al.*, 2013). The obtained products find broad applications in pharmaceutical, nutritional and cosmetic industries (Roberts, 2005; Lentzen and Schwarz, 2006; Pastor *et al.*, 2010).

1.4 Metabolic flux analysis and its use in combination with other omics methodologies

Metabolic flux analysis using ^{13}C -labeled tracer substrates

Metabolic flux analysis is about the quantification of intracellular fluxes, i.e. *in vivo* reaction rates through different pathways within the intact living cell. Hereby, levels of substrates, cofactors, effectors, or regulators determine the *in vivo* flux through a particular enzyme as systems property. This differs in most cases dramatically from estimates of the *in vitro* activity, for which cells are disrupted so that enzymes are withdrawn from their physiological environment and analyzed under artificial assay conditions. In practice, flux analysis typically focuses on the 50-100 reactions of central carbon metabolism which have particular relevance in systems biology and biotechnology since they catalyze the major carbon flow and match with the reactions involved in biosynthesis of most industrial products (Sauer, 2006).

Initially, flux studies recruited measured extracellular fluxes, i.e. substrate uptake or product secretion, and biosynthetic requirements entered into assumed stoichiometric reaction networks to derive certain intracellular fluxes (Wiechert, 2001). These pioneering studies provided first valuable insights into microbial metabolism on the flux level, but relied on uncertain assumptions, simplifications, and constraints such as balances of reduction equivalents or energy stoichiometry which unfortunately determine the actual flux result quite significantly (Wittmann, 2002). Moreover, important fine structures such as parallel, cyclic or reversible reactions which play an important role in microorganisms were not accessible (Krömer *et al.*, 2004; Sauer and Eikmanns, 2005). In recent years, flux analysis has been extended by the integration of ^{13}C labeling information from stable isotope experiments overcoming previous limitations. In these studies, ^{13}C -labeled tracer substrates are fed to the examined cells until the ^{13}C label has propagated through the metabolic network into metabolic products. Their isotope labeling pattern depends on the particular flux distribution and thus provides a sensitive 'fingerprint' to calculate metabolic *in vivo* fluxes. By means of mass spectrometry (MS) or nuclear magnetic resonance (NMR), the labeling pattern can be quantified (Wittmann and Heinzle, 1999; Christensen and Nielsen, 1999; Dauner *et al.*, 2001a). For flux calculation, the measured ^{13}C labeling data, biosynthetic requirements, and

extracellular fluxes are integrated with a computer model which is an *in silico* representation of the biochemical network investigated. The model contains all relevant reactions of carbon core metabolism and the corresponding carbon atom transition between the involved metabolites. The basic workflow of the resulting comprehensive strategy, comprising experimental and computational steps, is given in Figure 1.4.

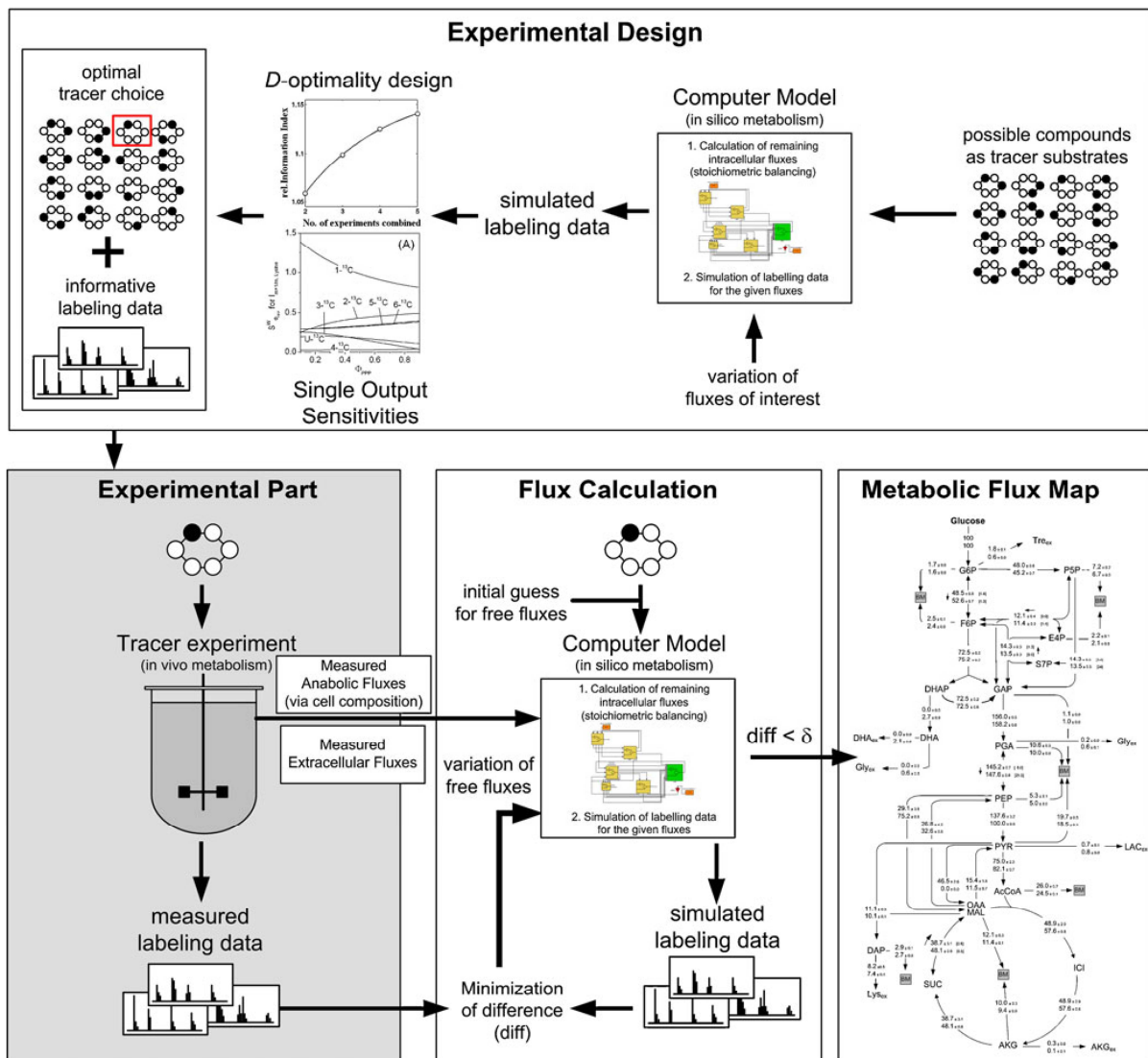


Figure 1.4: Schematic work flow for ^{13}C metabolic flux analysis comprising (i) experimental design to identify optimal substrates for a given flux problem, (ii) isotope tracer experiments with measurement of ^{13}C labeling patterns by mass spectrometry together with extracellular fluxes and biosynthetic requirements, and (iii) computational calculation of fluxes with models as *in silico* representation of the studied network. This basic concept is typically applied for routine quantification of steady-state fluxes. It can be varied in several aspects depending on the focus of the flux study.

Metabolic flux analysis as outlined below has evolved into an advanced approach to assess steady-state fluxes of microbial cells (Sauer, 2006). Inherently, fluxomics is laborious and requires a broad spectrum of quite diverse experimental and computational expertise, which is not easily brought together. Accordingly, and in contrast to other omics technologies, only a few leading laboratories have so far significantly contributed to its development and application.

Most common metabolic flux studies use mass spectrometric ^{13}C labeling analysis of about 10-15 amino acids obtained from hydrolyzed cell protein (Christensen and Nielsen, 1999; Dauner and Sauer, 2000). They contain rich information for flux estimation, since they reflect the carbon backbone of eight key intermediates from different parts of central carbon metabolism (Table 1.1) (Szyperski, 1995). The most popular technique for amino acid labeling analysis today is gas chromatography mass spectrometry (GC-MS), since this approach requires only about 1 mg of cells, allows an excellent separation of the analytes within only about 20-30 min, and provides high precision data on mass isotopologue distribution with measurement errors below 0.5 % (Wittmann, 2007). Initially developed and applied mainly in the field of biomedicine (Lapidot and Nissim, 1980; Nissim *et al.*, 1981; Tsalikian *et al.*, 1984; Nissim and Lapidot, 1986), GC-MS-based metabolic flux approaches have been substantially extended and optimized, and emerged as a key technology in metabolic physiology and biotechnology (Christensen and Nielsen, 2000; Kelleher, 2001; Wiechert, 2001; Wittmann, 2002; Des Rosiers *et al.*, 2004; Des Rosiers and Chatham, 2005).

For flux calculation, computer-based models of the investigated metabolic network are usually utilized to globally fit the unknown flux parameters combining isotopomer and metabolite balancing (Wittmann, 2007). Applying an optimization algorithm the deviation of the labeling data between computer model and experiment is minimized by iterative variation of the free fluxes until the flux distribution is identified. In combination with experimentally determined extracellular fluxes, absolute carbon fluxes throughout the network are derived. In recent years, general modeling frameworks have been developed for a general and systematic description of carbon transfer. The most efficient approach with regard to simulation speed uses elementary metabolite units (EMUs, Figure 1.5) (Antoniewicz *et al.*, 2007a). In this work the software tool OpenFlux using the EMU approach is used (Quek *et al.*, 2009).

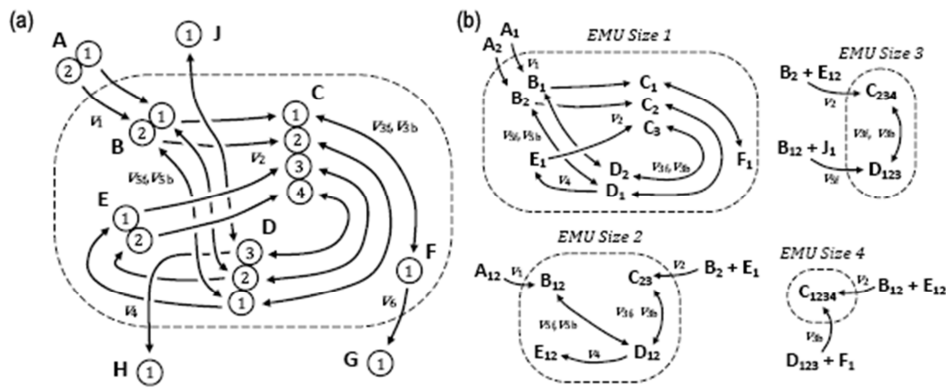


Figure 1.5: Atom transition in a common reaction network (a) and decomposition into smaller sub-networks (b), each containing equally sized elementary metabolite units (EMUs). EMUs are distinct subsets of a molecule's atoms, whereas the EMU size indicates the number of atoms included in the EMU (Antoniewicz *et al.*, 2007a).

Metabolic fluxes in *Bacillus subtilis*

First studies on metabolic fluxes in *B. subtilis* in continuous and batch culture were conducted in the mid-90s, based on growth parameters and stoichiometric balance equations in central carbon metabolism (Goel *et al.*, 1993; Sauer *et al.*, 1996). As stoichiometric metabolic flux analysis suffers from above mentioned shortcomings (Wiechert, 2001), future works relied on the use of ^{13}C -tracer-based experiments in combination with NMR and MS technology. A main driver for the continuous research interest marked the establishment of *B. subtilis* as potent host organism for the production of riboflavin (vitamin B2) (Perkins and Pero, 1993). In the following years, numerous publications shed light on growth energetics and cellular metabolism of various *Bacillus* strains under a broad spectrum of growth conditions. This included the development of a growth rate-dependent stoichiometric biomass composition for wild-type *B. subtilis* (Dauner and Sauer, 2001). Additionally, metabolic flux studies examined biological phenomena such as nutrient limitation (Dauner *et al.*, 2001a; Dauner *et al.*, 2001b; Rühl *et al.*, 2012), availability of different carbon sources (Dauner *et al.*, 2002; Schilling *et al.*, 2007; Kleijn *et al.*, 2010; Chubukov *et al.*, 2013), growth under riboflavin production conditions (Rühl *et al.*, 2010; Zamboni *et al.*, 2005) and maintenance metabolism (Zamboni *et al.*, 2003; Zamboni and Sauer, 2003; Tännler *et al.*, 2008). A large-scale metabolic flux study of 137 *B. subtilis* knockout mutants revealed its general network rigidity and metabolic robustness (Fischer and Sauer, 2005). Obviously, cells tend to maintain a standby mode in anticipation of changing environmental conditions. Schilling *et al.* investigated the cellular response of *B. subtilis* to the availability of organic

acids on transcriptome, metabolome and fluxome level (Schilling *et al.*, 2007). This identified a mismatch between changes in gene expression and corresponding flux, meaning that transcriptional regulation is not sufficient to account for metabolic adaptation. Chubukov *et al.* draw a similar conclusion after comparing the *in vivo* pathway activity and corresponding enzyme changes in *B. subtilis* grown on eight different carbon sources (Chubukov *et al.*, 2013). In addition to the above mentioned works, some studies focused on the characterization of other important *Bacillus* species like *Bacillus clausii* (Christiansen *et al.*, 2002), *Bacillus megaterium* (Fürch *et al.*, 2007; Fürch *et al.*, 2007), *Bacillus licheniformis*, *Bacillus amyloliquefaciens* and *Bacillus pumilis* (Tännler *et al.*, 2008).

Towards systems-level understanding of metabolism – the multi-omics approach

Systems biology is the integration and application of mathematics, engineering and bioinformatics for the quantitative analysis of biological systems (Chong and Ray, 2002; Sauer *et al.*, 2007). As a single analytical omics platform (e.g. transcriptomics, proteomics, metabolomics or fluxomics) does not always provide enough information to understand the behavior of a cellular system, multi-omics approaches are required to draw a more precise picture of the underlying metabolic and regulatory networks. Omics approaches are mainly data-driven, holistic and top-down. Hereby, metabolic fluxes through central carbon metabolism are of pivotal importance for systems level understanding as they fundamentally represent the cellular phenotype as integrated output of its molecular entities, i.e. transcripts, proteins and metabolites (Figure 1.6).

Most multi-omics studies to date combine the most frequently used tools for transcriptomics and proteomics in order to obtain complementary coverage of metabolism, perform cross-validation, or obtain novel biological insights into post-transcriptional regulation mechanisms (Zhang *et al.*, 2010). Flux analysis of microbial cells is a rather advanced and routine method in itself, but has not been used as broadly as genomics, transcriptomics, and proteomics which have advanced into widely applied commercially available technologies. The analysis of the metabolome is not as mature and yet not fully comprehensive, which is inherently caused by the different chemical nature, high turnover rate, and large concentration difference of the analytes (Zhang *et al.*, 2010), and persisting difficulties with appropriate sampling and cell quenching hampering quantitative metabolomics (Bolten *et al.*, 2007). This is one explanation

for the tremendous difference of several orders of magnitude to which extent the different omics technologies are applied today (Figure 1.7).

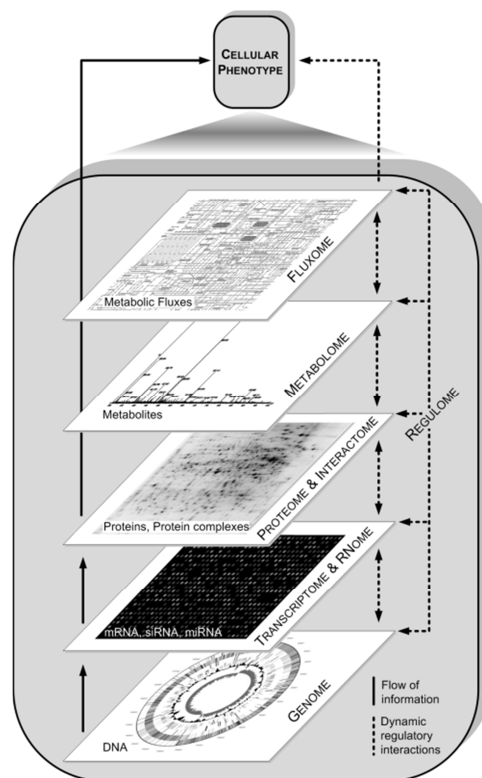


Figure 1.6: Architecture and interactions among and within the different functional layers in a cellular system. Solid lines, flow of information; dashed lines, regulatory interactions between molecular species.

It appears obvious that in many cases, the interaction between components of the network involved cannot be understood without knowledge on *in vivo* flux. To unravel and quantify the different layers of control, superimposing the flux network, the flux state has to be linked to the set of cellular components, i.e. genes, transcripts, proteins, and metabolites. The integration of ^{13}C fluxomics in multi-omics experiments, however, has special requirements. Care has to be taken concerning the label introduced in ^{13}C fluxomics experiments which typically interferes with conventional MS-based technologies for identification and quantification of proteins as well as metabolites. In such cases, a parallelized setup is needed. The isotope labeling experiments for fluxome analysis have to be conducted under identical conditions in parallel to those for other omics analyses, including a thorough validation of key physiological parameters such as substrate uptake, growth, product formation, respiration, or intracellular fingerprints which are not affected by the ^{13}C label (Krömer *et al.*,

2004). This might include additional controls via intracellular metabolites, accessible with enzyme assays or by HPLC, as well as transcription profiling, which are not biased by the presence of label. In addition, financial constraints have to be considered with respect to the high price of ^{13}C substrates, typically demanding for small cultivation volume.

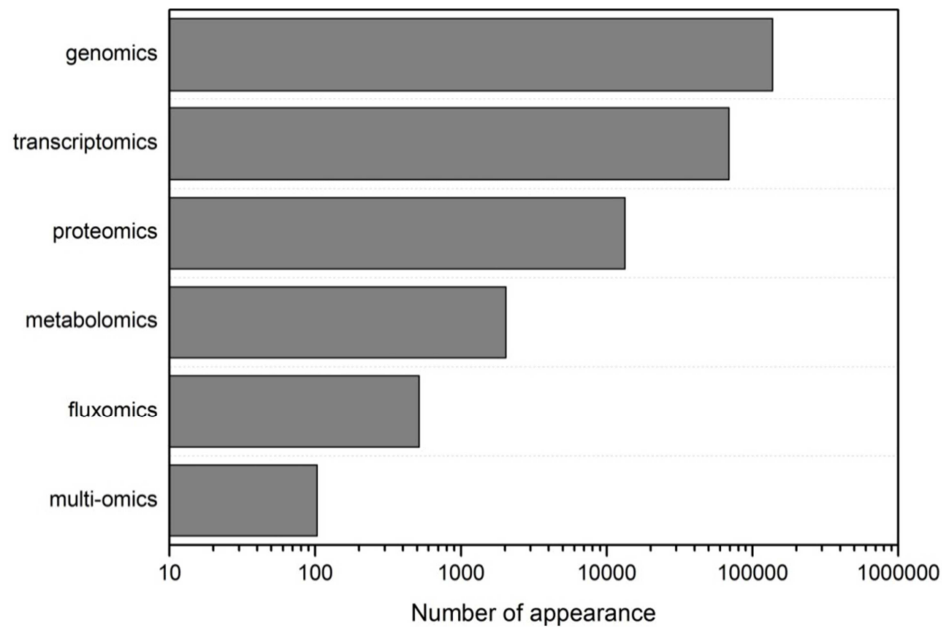


Figure 1.7: Frequency of the use of the terms 'genomics', 'transcriptomics', 'proteomics', 'metabolomics', 'fluxomics' and 'multi-omics' in scientific publications. Since the terms are not always used in the relevant studies, the search additionally included related terms to represent the corresponding field e.g. 'sequencing', 'gene expression', 'intracellular metabolite', 'flux analysis' or 'omics approach'. The number of appearance was extracted from the PubMed database (February, 2014).

The resulting picture immediately indicates that only a small set of multi-omics studies so far includes fluxes – and thus allows to really bridging cellular components with network function, which is a key goal of systems biology and systems metabolic engineering. In this context, systems metabolic engineering describes the application of systems biological approaches for the development of efficient cell factories and sustainable bioprocesses for the production of bulk and fine chemicals, biofuels, polymers and pharmaceuticals (Lee *et al.*, 2005; Mukhopadhyay *et al.*, 2008; Kuhn *et al.*, 2010). Out of the few studies performed to date, most investigated biotechnologically relevant microorganisms, underlining systems metabolic engineering as one of the major drivers (Table 1.2).

Table 1.2: Selected multi-omics studies of the last decade.

Organism	Integrated analytical platforms				Reference
	Transcriptomics	Proteomics	Metabolomics	Fluxomics	
<i>Bacillus subtilis</i>	x		x	x	Schilling <i>et al.</i> , 2007
	x		x	x	Chubukov <i>et al.</i> , 2013
	x	x	x	x	Kohlstedt <i>et al.</i> , 2014
<i>Corynebacterium glutamicum</i>	x		x	x	Krömer <i>et al.</i> , 2004
<i>Escherichia coli</i>	x	x		x	Shimizu <i>et al.</i> , 2004
	x			x	Fong <i>et al.</i> , 2005
	x			x	Hua <i>et al.</i> , 2007
	x	x	x	x	Ishii <i>et al.</i> , 2007
			x	x	Wittmann <i>et al.</i> , 2007
	x		x	x	Nakahigashi <i>et al.</i> , 2009
<i>Mycoplasma pneumoniae</i>	x	x	x	x	Kühner <i>et al.</i> , 2009, Güell <i>et al.</i> , 2009, Yus <i>et al.</i> , 2009
	x		x	x	Moxley <i>et al.</i> , 2009
	x		x	x	Borodina <i>et al.</i> , 2008

The increasing need for flux studies as key technology in future systems biology and systems metabolic engineering will clearly intensify efforts to apply and extend this technology. Concerning the integration with other omics approaches, promising future developments comprise the coupling of dynamic ^{13}C labeling experiments with metabolomics (Nöh *et al.*, 2007; Antoniewicz, 2013). Increasing metabolite coverage in metabolomics provides direct access to labeling patterns of many more pathway intermediates than routinely available, greatly extending the resolution power of flux studies. Global multi-omics studies will require intelligent software tools that extract true novel biology out of the expected massive data sets. Current developments of statistical methods such as unsupervised learning, correlation network analysis, pattern recognition, or principal component analysis as well as dynamic Bayesian networks, or dynamic control theory appear quite useful, but will surely not suffice to fully unravel the complexity of the studied systems. Here, further exploration of novel concepts and integration of the heterogeneous data sets is still needed.

The study of cells under conditions different from routine chemostat or balanced batch conditions will require development of novel approaches, including specific strategies for labeling input, cultivation, labeling analysis, and modeling. First interesting examples extend flux analysis to previously inaccessible conditions. This comprises the quantification of flux dynamics in non-stationary systems (Antoniewicz *et al.*, 2007b), or of fluxes in non-growing cells (Yang *et al.* 2005; Yang *et al.* 2006; Rühl *et al.*, 2012). An interesting concept for flux analysis in large scale, involving precise labeling quantification at low enrichment by GC-IR-MS (gas chromatography isotope ratio mass spectrometry) (Yuan *et al.*, 2010) opens the possibility to perform flux studies in real case production processes. The coming years will hopefully see more conceptual extension of flux analysis so that it becomes applicable to the level of single cells towards unraveling of population heterogeneity, as well as to the flux cross-talk within consortia of different cell types, the dominating form of microbial life – both promising fascinating novel biology and useful information towards superior biocatalysts.

A multi-omics study on the osmostress response in *Bacillus subtilis*

Previous profiling studies on the osmotic stress response of *B. subtilis* mostly involved a single analytical platform (Hoffmann *et al.*, 2002; Steil *et al.*, 2003; Höper *et al.*, 2006). Recently, Hahne and co-workers combined modern transcriptome and proteome analysis to examine the global cellular stress response to a sudden osmotic up-shock (Hahne *et al.*, 2010). However, an integration of functional network operation (the fluxome) with the cellular components is needed to obtain a deeper systems-level understanding of *B. subtilis*' adaptation to salt stress. Furthermore, the long-term adaptation under nutrient limitation and the impact of available osmoprotectants are of outmost interest. Although the technical development of analytical methods in the recent years provides an excellent basis, no such systems-level studies have been performed so far.

2 Materials and Methods

2.1 Strain

In the present work a tryptophan-prototroph derivative of the wild-type *Bacillus subtilis* 168 was used. *Bacillus subtilis* BSB1 (168 Trp⁺) was constructed within the BaSysBio consortium by transformation of strain 168 *trpC2* using chromosomal DNA from strain 1012 *leuA8 metB5* (Saito *et al.*, 1979; Nicolas *et al.*, 2012). For maintenance, cells were grown on LB medium and stored in 15 % (v/v) glycerol at -80°C. Cryostocks were then used to grow single colonies on LB-agar plates.

2.2 Chemicals

Bacto™ Tryptone and yeast extract were obtained from BD Biosciences (Heidelberg, Germany). All other chemicals and solvents for media preparation, sampling and analytical purposes were purchased from Sigma-Aldrich (St. Louis, USA) and Merck (Darmstadt, Germany), respectively, and were of analytical grade. Silylation reagents for gas chromatography (e.g. MBDSTFA and MSTFA) were obtained from Macherey-Nagel (Düren, Germany). Labeled glucose (99 % purity) was obtained from Euriso-top (Saarbrücken, Germany) and Sigma-Aldrich (Darmstadt, Germany). Ultrapure water (resistivity >18.2 MΩ at 25 °C) was produced using a Milli-Q Integral Water Purification System (Millipore, Merck KGaA, Darmstadt, Germany).

2.3 Media

LB medium consisted of 10 g L⁻¹ tryptone, 10 g L⁻¹ NaCl and 5 g L⁻¹ yeast extract. For solid medium 15 g L⁻¹ agar was added. Main cultivations were performed in modified M9 minimal medium with glucose as sole carbon source at 5 g L⁻¹ (batch culture) and 1 g L⁻¹ (carbon-limited chemostat), respectively. The medium further contained 8.5 g L⁻¹ Na₂HPO₄·2H₂O, 3 g L⁻¹ KH₂PO₄, 1 g L⁻¹ NH₄Cl, 0.5 g L⁻¹ NaCl, 246 mg L⁻¹ MgSO₄·7H₂O, 30 mg L⁻¹ 3,4-dihydroxybenzoic acid, 14.7 mg L⁻¹ CaCl₂·2H₂O, 13.5 mg L⁻¹ FeCl₃·6H₂O and 10 mL of a trace element solution with the following components: 0.17 g L⁻¹ ZnCl₂, 0.1 g L⁻¹

MnCl₂·4H₂O, 0.06 mg L⁻¹ CoCl₂·6H₂O, 0.06 mg L⁻¹ Na₂MoO₄·2H₂O and 0.043 g L⁻¹ CuCl₂·2H₂O. The medium was supplemented with 70.13 g L⁻¹ NaCl (1.2 M, corresponding to an osmolality of 2,560 mosm kg⁻¹) with or without 117.15 mg L⁻¹ glycine betaine (1 mM) to mimic osmotic stress and osmoprotection under carbon limitation, respectively. In order to investigate the impact of nitrogen-limitation on the adaptation to different kinds of osmotic stress, cells were grown in nitrogen-limited chemostats. Here, the NH₄Cl concentration was reduced to 0.2 g L⁻¹, whereas the glucose concentration was increased to 3 g L⁻¹ to guarantee carbon excess. To compare salt-induced ionic stress with sugar-induced non-ionic osmotic stress, the minimal medium was supplemented with 40.09 g L⁻¹ NaCl (0.69 M) and an iso-osmolar glucose concentration of 250 g L⁻¹ (1.39 M). For metabolic flux analysis, naturally labeled glucose was replaced by 99 % [1-¹³C] glucose. In case of high-glucose cultivation, the labeled fraction was reduced to 10 % for cost reasons.

2.4 Cultivation

All cultivations were conducted at 37 °C. First, cells from glycerol stocks were incubated overnight on LB agar. Single colonies were then grown for 2 hours in LB medium (10 mL in baffled 100 mL shake flasks) on a rotary shaker (230 rpm, 5 cm shaking diameter, Multitron, Infors AG, Bottmingen, Switzerland), harvested by centrifugation (5 min, 8,500 x *g*, Biofuge Stratos, Heraeus, Hanau, Germany), washed with 0.9 % NaCl and used to inoculate a second pre-culture in M9 medium (50 mL in baffled 500 mL shake flasks, 230 rpm). Washed cells, harvested in the mid-exponential growth phase, served as inoculum for further investigation.

Cultivation in microtiter plates

For screening purposes, cells were grown in duplicates in 48-well FlowerPlates (m2p labs, Baesweiler, Germany) in a BioLector system (DASGIP, Jülich, Germany). Wells were each filled with 1 mL M9 minimal medium, supplemented with varying levels of NaCl (0 to 1.6 M), glycine betaine (0.01 to 10 mM) and glucose (5 to 300 g L⁻¹), respectively, resulting in different growth conditions with varied osmotic stress and osmoprotection potential. Cell growth was monitored online as optical density at 620 nm (OD₆₂₀) at a shaking speed of 1,000 rpm and a humidity of 95 %.

Cultivation in shake flasks

Cultivations in shake flasks were performed in quadruplicates on a rotary shaker (230 rpm, 5 cm shaking diameter, Multitron, Infors AG, Bottmingen, Switzerland). One of the replicates contained the tracer substrate [1-¹³C] glucose instead of naturally labeled glucose. The initial cell concentration was kept below an OD₆₀₀ of 0.05 so that the influence of naturally labeled biomass was negligible for later flux estimations (Wittmann and Heinzle, 2005).

Chemostat cultivation in bioreactors

Continuous cultivation under carbon and nitrogen limitation, respectively, was performed at a fixed dilution rate of 0.1 h⁻¹ in a parallelized 1 L bioreactor system with a working volume of 300 mL, kept at an aeration rate of 0.5 vvm and a stirrer speed of 1,000 rpm (DASGIP, Jülich, Germany). Culture settings were controlled at 37 °C and pH 7.1, respectively. The feed medium was pumped into the reactor at a pump rate of 30 mL h⁻¹ from independent reservoirs, while culture broth was continuously removed from the reactor through a pipe, adjusted to the initial fill level (Figure 2.1). Foam formation was prevented using sterile-filtered Ucolub (FRAGOL, Mülheim, Germany). For each condition, four biological replicates were conducted in parallel. One of these contained the isotopic tracer medium for ¹³C metabolic flux analysis. Reactors were connected to a mass spectrometer (Pfeiffer Vacuum, Aslar, Germany) for exhaust gas analysis. The cultures were operated until metabolic and isotopic steady state was reached, i.e. after at least five volume changes. Then, cells were harvested for parallel analysis of transcriptome, metabolome, proteome, and fluxome, respectively.

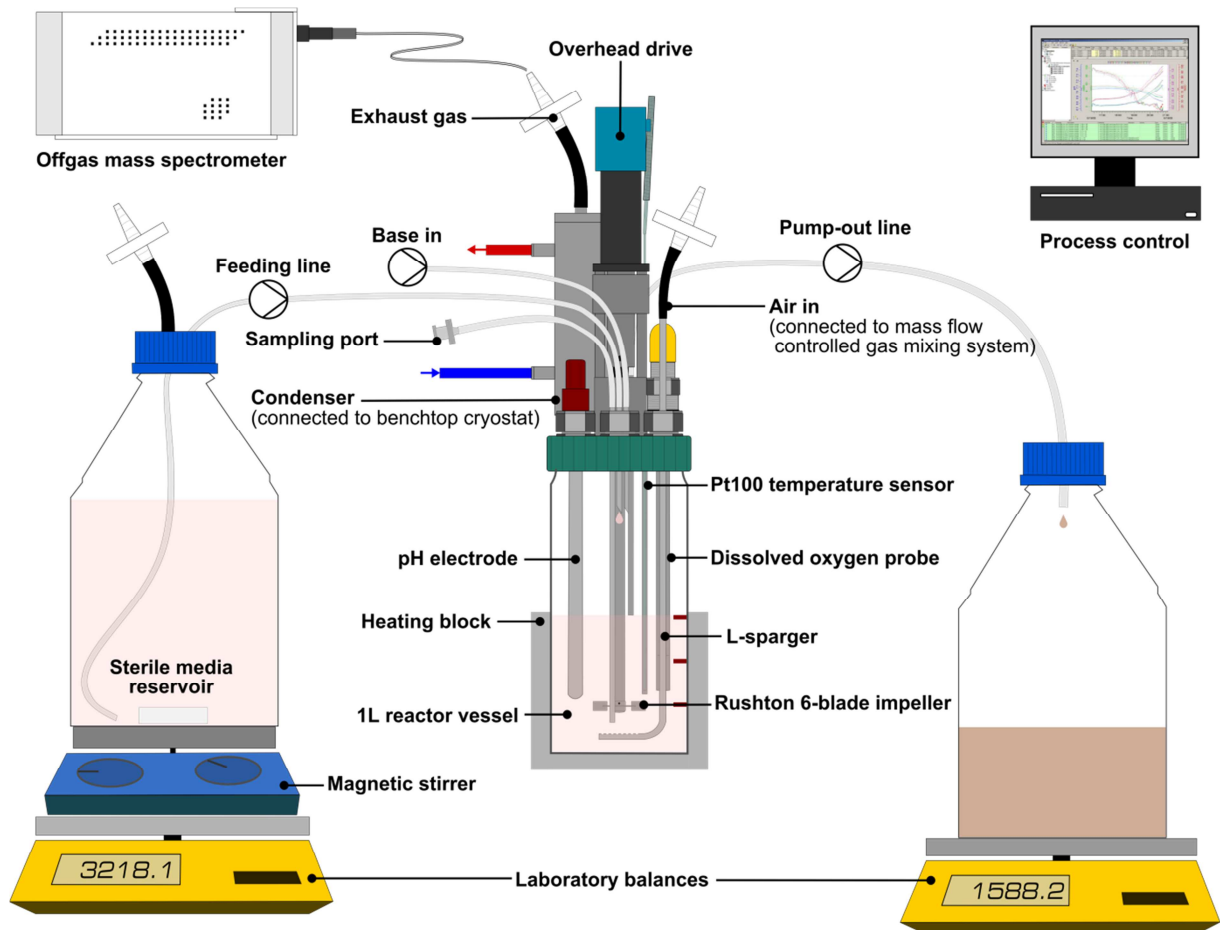


Figure 2.1: Experimental setup for systems biology analysis of *B. subtilis* in chemostat. Totally four reactors were conducted in parallel, including one replicate with $[1-^{13}\text{C}]$ glucose. The growth rate of 0.1 h^{-1} was controlled by a fixed feed pump rate and continuous removal of culture broth, thus keeping the reactor volume constant at 300 mL. The mode of operation was regularly checked via weighing of the remaining feed and collected culture broth, kept on analytical balances.

2.5 Analytical techniques

Determination of cell concentration

Optical density and dry cell weight

Cell concentration was monitored as optical density at 600 nm (OD_{600}) (Biochrom Libra Instruments, Cambridge, UK). Samples were diluted on an analytical balance (Sartorius BP211D, Göttingen, Germany) to values below 0.3, and measured in duplicate against blank medium as reference.

In addition, dry cell weight (DCW) was determined after harvesting 25 mL of culture broth by filtration ($0.2 \mu\text{m}$ pore size, RC membrane filters, Sartorius, Göttingen, Germany), including

one washing step with NaCl solutions that had an ionic strength equal to that of the medium and one with deionized water. The cell dry mass was weighted after drying at 80 °C until constant weight.

OD₆₀₀ and DCW correlate with a mean coefficient of 0.268 g_{DCW} L⁻¹ (R² = 0.996) for a broad spectrum of growth conditions (Figure 2.2). Chemostat growth under nitrogen limitation with D = 0.1 h⁻¹, however, showed a somewhat lower correlation factor of 0.191 (R² = 0.99), which might be caused by cell morphology changes during prolonged cultivation in chemostat under nitrogen limitation (Čáslavská *et al.*, 1972; Pazlarova, 2010).

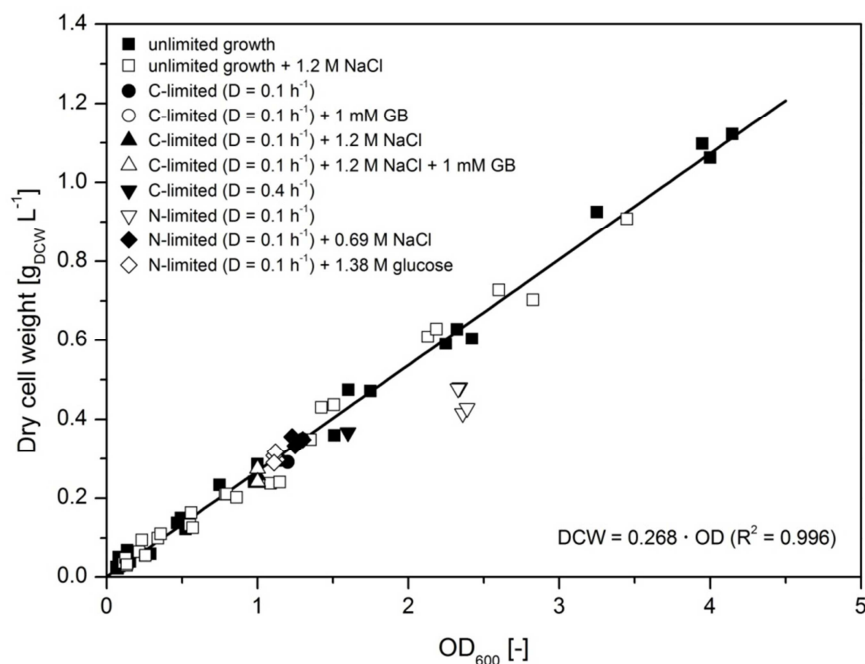


Figure 2.2: Correlation between optical density at 600 nm and dry cell weight (g L⁻¹) for *B. subtilis* BSB1. Correlation is similar with a factor of 0.268 under various growth conditions, except for growth under nitrogen-limitation (Čáslavská *et al.*, 1972; Pazlarova, 2010).

Colony forming units and spore frequency

In order to determine the sporulation rate in continuous culture, 100 µL of cell suspension was diluted stepwise (1:10) with M9 minimal medium to countable cell concentrations (10¹-10³). Then, 100 µL of the three highest dilutions were plated on LB agar and incubated for 12 h at 37 °C. The remaining volume was heated for 35 min at 85 °C to kill all vegetative cells. After the heat treatment, that only spores sustain, 100 µL of each dilution were again plated on LB agar and incubated for 12 h at 37 °C. Finally, colonies were counted and compared.

Elemental biomass composition

Elemental composition (C, H, N and S) of dried biomass pellets was determined by elemental analysis (Elementar Analysensysteme GmbH, Hanau, Germany).

Transcriptomics

The preparation of RNA and DNA microarray analysis was carried out by Praveen Kumar Sappa at the Interfaculty Institute of Genetics and Functional Genomics at the University of Greifswald (Nicolas *et al.*, 2012).

Isolation of RNA

Shortly, total RNA was isolated with a method described previously (Eymann *et al.*, 2002) with some modifications. Bacterial cells were harvested by centrifugation for 5 min at 4 °C after addition of ½ volume of frozen killing buffer (20 mM Tris/HCl [pH 7.5], 5 mM MgCl₂, 20 mM NaN₃) to the culture sample. After discarding the supernatant, cell pellets were frozen in liquid nitrogen and stored at -80 °C. For mechanical disruption, the pellets were re-suspended in 200 µL of ice-cold killing buffer, immediately dropped into a Teflon disruption vessel (pre-cooled and filled with liquid nitrogen), and then disrupted in a Mikro-Dismembrator S (Sartorius, Göttingen, Germany) (2 min at 2,600 rpm). The resulting frozen powder was resuspended in 4 mL of pre-warmed lysis solution (4 M guanidine thiocyanate, 25 mM sodium acetate [pH 5.2], 0.5 % *N*-laurylsarcosinate [w/v], 50 °C) by repeated pipetting. Afterwards, 1 mL aliquots of the lysate were transferred to microcentrifuge tubes and immediately frozen in liquid nitrogen. Total RNA was isolated by acid-phenol extraction. The samples were extracted twice with an equal volume of acid phenol/chloroform/isoamyl alcohol (25:24:1, [pH 4.5]) and once with chloroform/isoamyl alcohol (24:1). After adding ¹/₁₀ volume of 3 M sodium acetate (pH 5.2), RNA was precipitated with isopropanol, washed with 70 % ethanol and dissolved in 100 µL of RNase free water. For transcriptome analysis, 35 µg RNA were DNase-treated using the RNase-Free DNase Set (Qiagen, Venlo, Netherlands) and purified using the RNA Clean-Up and Concentration Micro Kit (Norgen Biotek, Thorold, Canada). The RNA concentration was measured using a Nanodrop (Peqlab Biotechnologie GmbH, Erlangen, Germany); the quality of the RNA preparations was assessed by means of the Agilent 2100 Bioanalyzer according to the manufacturer's instructions. For two-color hybridizations, reference pools containing equal amounts of RNA from samples of different

conditions were prepared. 'Pool 1' contained RNA from all carbon-limited chemostat experiments and was used for the investigation of salt stress and osmoprotection (Chapter 3.3), whereas 'Pool 2' additionally contained RNA from all nitrogen-limited samples (Chapter 3.4).

DNA microarray analysis and data processing

For DNA microarray analysis, synthesis and purification of fluorescently labeled cDNA was carried out according to (Charbonnier *et al.*, 2005) with minor modifications. For this purpose, 10 µg of total RNA was mixed with random primers (Promega, Madison, USA) and spike-ins (Two-Color RNA Spike-In Kit, Agilent Technologies, Santa Clara, USA). The RNA-primer mixture was incubated at 70 °C for 10 min followed by 5 min incubation on ice. Then, the following reagents were added: 10 µL of 5x First Strand Buffer (Invitrogen, Carlsbad, USA), 5 µL of 0.1 M DTT (Invitrogen, Carlsbad, USA), 0.5 µL of a dNTP mix (10 mM dATP, dGTP, and dTTP, 2.5 mM dCTP), 1.25 µL of Cy3-dCTP or Cy5-dCTP (GE Healthcare, Little Chalfont, UK) and 2 µL of SuperScript II reverse transcriptase (Invitrogen, Carlsbad, USA). The reaction mixture was incubated at 42 °C for 60 min and then heated to 70 °C for 10 min. After 5 min on ice, the RNA was degraded by incubation with two units of RNaseH (Invitrogen, Carlsbad, USA) at room temperature for 30 min. Labeled cDNA was then purified using the CyScribe GFX Purification Kit (GE Healthcare, Little Chalfont, UK). The individual samples were labeled with Cy5, whereas the reference pool was labeled with Cy3. 500 ng of Cy5-labeled cDNA and 500 ng of Cy3-labeled cDNA were hybridized together to the microarray following Agilent's hybridization, washing and scanning protocol (Two-Color Microarray-based Gene Expression Analysis, version 5.5). Data were extracted and processed using the Feature Extraction software (version 9.5, Agilent Technologies, Santa Clara, USA). For each gene on a microarray, the error-weighted average of the log ratio values of the individual probes was calculated using the Rosetta Resolver software (version 7.2.1, Rosetta Biosoftware, Seattle, USA). As the analysis was performed by hybridizing the individual samples against a common reference, the ratio values represent relative gene expression levels at a given time point. Microarray data for carbon-limited chemostat experiments have been deposited in the NCBI's Gene Expression Omnibus (GEO) database and are accessible through GEO Series accession no. GSE53333. Data from nitrogen-limited cells follow.

Proteomics

Protein extraction and absolute protein quantification was performed by Praveen Kumar Sappa at the Interfaculty Institute of Genetics and Functional Genomics at the University of Greifswald.

QconCATs

QconCATs (Quantification concatamers) are artificial proteins labeled with stable heavy isotopes that are an assembly of unique proteotypic peptides (Qpeptides) derived from multiple proteins of interest (Beynon *et al.*, 2005). The QConCAT-proteins used in this study covered enzymes of the central carbon metabolism including the glutamate and proline biosynthetic pathways of *B. subtilis*. The QconCAT was designed adhering to commonly accepted guidelines (Pratt *et al.*, 2006). Peptides with the potential post translational modifications were excluded from the design. Synthesis of the synthetic gene and labeling (^{13}C and ^{15}N) of the QconCAT-protein with heavy arginine and lysine and the subsequent purification were done by PolyQuant GmbH (Regensburg, Germany). For each protein three Qpeptides were designed, whereof at least two peptides (except for few proteins where single peptide based quantification was performed) were used for quantification.

Protein extraction and estimation

Protein extracts from frozen pellets were prepared and estimated as described previously (Starcher, 2001; Maaß *et al.*, 2011). In short, during the experiment an equivalent volume of 12.5 optical density units (OD units) of the bacterial culture was harvested by centrifugation at 13,200 x *g* for 10 min at 4 °C. The supernatant was discarded. After washing of the pellets with 2 mL of TE-buffer (20 mM Tris, 10 mM EDTA, pH 8) the pellets were stored at -80 °C. Frozen pellets were resuspended in 500 µL of ice cold TE-buffer and added to a prefilled 2 mL vial (Sarstedt) with 500 µL amount of unwashed glass beads (160 µm, Sigma Life sciences, St. Louis, USA). Cell disruption was performed by ribolyzing (FastPrep, Thermo Scientific, Waltham, USA) for 30 s at 6.5 m s⁻¹ speed and then on ice for 5 min, this was repeated for two more times (repetition ensured the disruption efficiency to be 99-99.9 % complete) and centrifuged at 13,000 x *g* (10 min, 4 °C). Resultant supernatant was transferred to a new 1.5 mL microcentrifuge tube (carryover of glass beads is avoided) and centrifuged at

13,000 x *g* (30 min, 4 °C), this process was repeated once again to remove remains of glass beads and cell debris. Protein concentration of extracts was determined using a ninhydrin-based assay (Starcher, 2001). Briefly, 20 μL of crude protein extract was mixed with 20 μL 12 N HCl and incubated for 24 h at 100 °C. 400 μL of a 200-fold dilution of the hydrolyzed protein extract was added to 600 μL of freshly prepared ninhydrin-reagent. After 10 min incubation at 100 °C the extinction was measured at 575 nm. For every batch of samples a calibration curve using BSA (bovine serum albumin) ranging from 0.25 $\mu\text{g } \mu\text{L}^{-1}$ to 10 $\mu\text{g } \mu\text{L}^{-1}$ was prepared.

Purification and Digestion

In order to purify the protein extracts by in-gel digestion, 15 μg of protein lysate and a defined amount of QconCat was applied to a NuPAGE[®] Bis-Tris Gel 4-12 % (Life Technologies Corporation, Carlsbad, USA). Separation, staining and destaining was carried according to the manufacture guidelines except for the run time. The run was stopped exactly after 5 min which allowed the sample to be separated for 1 cm. Each lane was sliced into three pieces which were processed independently. The gel pieces were washed twice with 200 μL of 20 mM ammonium bicarbonate in 50 % (v/v) acetonitrile (ACN) for 30 min at 37 °C. Thereafter the gel pieces were dehydrated by two times washing with 200 μL of ACN for 15 min. Trypsin solution (20 ng μL^{-1} trypsin in 20 mM ammonium bicarbonate) was added until the gel pieces stopped swelling. Digestion was allowed to proceed for 16-18 h at 37 °C. The peptides were extracted from the gel pieces with 40 μL of 0.1 % (v/v) acetic acid by incubation in an ultrasonic bath for 30 min, followed by a second extraction with 40 μL of 50 % ACN in 0.05 % acetic acid. The peptide containing supernatants of each band were collected and pooled for each lane; excess liquid was removed by lyophilisation. The resulting peptide mixtures were resuspended in 100 μL of buffer A (0.1 % acetic acid, 2 % ACN) and purified using C₁₈-ZipTip columns (Millipore, Bedford, USA). 300 ng of the purified peptide mixture was used for subsequent MS analysis.

Liquid chromatography tandem-mass spectrometry analysis

Peptide separation was carried out using an Acelaim PepMap 100 column (C18, 3 mm, 100 Å, 15 cm bed length, Dionex), applying a binary gradient from 0 % to 40 % buffer B (100 % ACN (v/v), 0.1 % acetic acid (v/v)) in 70 min, and to 100 % B in additional 15 min at a

flow rate of 300 nL min⁻¹. LC-MS/MS analysis was performed on a triple quadrupole mass spectrometer (TSQ Vantage, Thermo Scientific, Waltham, USA) operated in nano-electrospray mode. For ionization 1,800 V of spray voltage and 250 °C capillary temperature were used. The resolution for both quadrupoles, i.e. for Q1 and Q3 was 0.7 Da (FWHM). The collision gas pressure of Q2 was set to 1.5 mTorr. Three product ions per peptide with highly ranked intensities were chosen for targeted analysis. Collision energy was optimized for each of the product ions belonging to the corresponding peptide using Skyline (MacCoss Lab, Washington, USA) (MacLean *et al.*, 2010a; MacLean *et al.*, 2010b). By combining the optimized collision energies and the recorded retention time for each target peptide a scheduled method was developed to measure all the peptides of interest in a single MS/MS analysis. TSQ Vantage was operated in SRM (single reaction monitoring) mode and data acquisition was done in scheduled SRM manner.

Data analysis

Two LC-MS/MS measurements were performed for each sample and the raw files were analyzed with the software Skyline 1.0 (MacCoss Lab, Washington, USA). Ratios of peak areas for endogenous light peptides to heavy Qpeptides were exported from Skyline. Based on the known amount of the spiked Qpeptides the endogenous light peptide concentrations were calculated. Peptides that exhibit missed cleavage and bad chromatographic properties were excluded from quantification of that corresponding protein.

Metabolomics

Extracellular substrate and products

During cultivation supernatant samples were taken for the determination of glucose consumption, and extracellular product formation. Glucose concentration was quantified by a Glucose Analyzer (YSI Life Sciences, Yellow Springs, USA). Organic acids and alcohols (citrate, 2-oxoglutarate, pyruvate, succinate, lactate, formate, acetate, acetoin, isobutyrate, ethanol, isovalerate) were quantified by HPLC equipped with a UV (210 nm) and an RI detector (Hitachi, Tokyo, Japan) using an Aminex HPX-87H column (Bio-Rad, Hercules, USA) at 45 °C. Isocratic elution with 12 mM H₂SO₄ (flow rate 0.5 mL min⁻¹) was used. A bicinchoninic acid-based protein assay kit (Thermo Fisher Scientific, Rockford, USA) was applied for the determination of total extracellular protein in culture supernatant. During nitrogen-limited

growth, ammonium was quantified by cation HPLC (Dionex ICS-2000 RFIC, Sunnyvale, USA) at 40 °C using 30 mM methanesulfonic acid at 0.5 mL min⁻¹ as eluent.

Intracellular amino acids

Intracellular amino acids were sampled and quantified as described previously (Bolten *et al.*, 2007). A volume of 2-4 mL of cell suspension was harvested via fast filtration (cellulose-nitrate, 0.2 µm pore size, 47 mm, Sartorius, Göttingen, Germany) and washed once with 10-15 mL of a NaCl solution that matched the ionic strength of the medium. Cell-containing filters were incubated (15 min, 100 °C) in caps containing 2 mL of 200 µM α-aminobutyric acid (ABU) as internal standard. Extracts were cooled on ice, transferred into 2 mL tubes and centrifuged (5 min, 13,200 x g, 4 °C) to remove all debris. Intracellular amino acids were then separated and quantified via HPLC (Agilent Technologies, Waldbronn, Germany) (Figure 2.3). Prior to injection analytes were derivatized using O-phthaldialdehyde (OPA) and 9-fluorenylmethylchloroformate (FMOC). In order to detect cysteine, mercaptopropionate (0.5 % in 0.5 M bicine [pH 9]) was used as reducing agent and sulfhydryl groups were blocked with iodacetic acid (50 mg mL⁻¹ in 0.5 M bicine [pH 9]) (Krömer *et al.*, 2005).

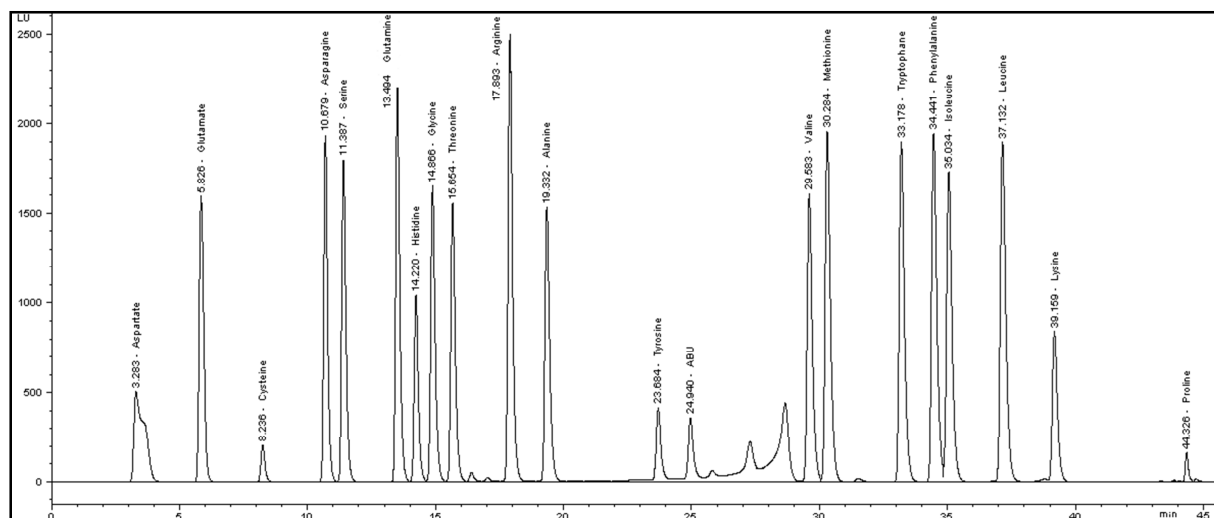


Figure 2.3: HPLC chromatogram of a standard mixture of proteinogenic amino acids after precolumn derivatization with O-phthaldialdehyde (OPA) and 9-fluorenylmethylchloroformate (FMOC). The concentration for all substances was 1 mM, except for tyrosine (0.2 mM). α-aminobutyrate (ABU) was used as internal standard.

Sampling and extraction of intracellular metabolites

Prior to filtration for intracellular metabolite sampling, the upper part of the filtration system (funnel, filter base) was cooled to $-20\text{ }^{\circ}\text{C}$ for 10 min. For intracellular metabolome analysis of *B. subtilis* the fast filtration sampling method (Meyer *et al.*, 2010) was extended by the addition of a liquid nitrogen cooling step to arrest metabolism immediately after cell sampling and before filtration. For this purpose, 10-15 OD units of the main culture were poured into a 50 mL falcon tube and cooled with liquid nitrogen for 10 s (sample temperature after cooling $9\pm 2\text{ }^{\circ}\text{C}$). The falcon tube was dipped periodically in and out of the N_2 and shaken carefully in between to avoid freezing of the sample. Subsequently the cooled culture was filtered (pore size $0.45\text{ }\mu\text{m}$, 47 mm, S-Pak[®] filters, Millipore, Schwalbach, Germany) and cells were quenched in 60 % ethanol (w/v, $< 4\text{ }^{\circ}\text{C}$) and liquid nitrogen. The 60 % ethanolic quenching and extraction solution was pre-cooled before sampling at $-20\text{ }^{\circ}\text{C}$ for 30 min. The frozen samples were stored at $-80\text{ }^{\circ}\text{C}$ until further treatment. For metabolite extraction and cell disruption, samples were thawed on ice ($\leq 6\text{ }^{\circ}\text{C}$) and the internal standards were added (20 nmol ribitol and norvaline for GC-MS and 2.5 nmol camphorsulfonic acid (CSA) for LC-MS analysis). Afterwards samples were vortexed and shaken 10 times alternately and centrifuged for 5 min at $4\text{ }^{\circ}\text{C}$ and $15,500 \times g$. The supernatant was transferred to a new falcon tube, while the pellet was once more extracted using cold double-distilled water. The supernatants were combined and restocked with double-distilled water to a final organic solution concentration of 10 % and stored at $-80\text{ }^{\circ}\text{C}$ prior to lyophilization at $-54\text{ }^{\circ}\text{C}$ and 0.52 mbar (CHRIST Alpha 1-4, Martin Christ Gefriertrocknungsanlagen, Osterode, Germany).

Mass-spectrometry- and NMR-based metabolite quantification was performed by Hanna Meyer from the Institute of Biochemistry at the University of Greifswald (Meyer *et al.* 2013).

Nucleotides, nucleosides, sugar-phosphates and cofactors

Ion-pairing (IP) LC-MS measurement was performed using an Agilent HPLC System (1100 series, Agilent Technologies, Santa Clara, USA) coupled to a Bruker micrOTOF mass spectrometer (Bruker Daltonics, Bremen, Germany) as described by (Liebeke *et al.*, 2010). The Agilent HPLC System was equipped with a quaternary pump, an online degasser, and an autosampler. Completely lyophilized samples were dissolved in $100\text{ }\mu\text{L}$ double-distilled water and centrifuged for 2 min ($15,500 \times g$, $4\text{ }^{\circ}\text{C}$) to remove cell debris. Supernatants were

transferred into glass vials with micro inserts for small volume injections. A volume of 25 μL of sample was injected for IP-LC-MS analysis. Chromatographic separation was performed using an RP- C_{18} AppliChrom OTU LipoMare[®] column (3.5 μm , 150 x 4.6 mm, AppliChrom, Oranienburg, Germany) with a C_{18} SecurityGuard Cartridge[®] precolumn (Phenomenex, Aschaffenburg, Germany). The gradient flow rate was 0.4 mL min^{-1} and the total data acquisition runtime was 40 min. The mobile phase was A: 5 % methanol and 95 % water, containing 10 mM tributylamine as ion-pairing reagent and 15 mM acetic acid for pH adjustment to pH 4.9, and B: 100 % methanol. The gradient elution started with 100 % A for 2 min, 0-31 % B in 2 min, 31-50 % B in 18.5 min, 50-60 % B in 2.5 min, 60-100 % B in 1 min, hold 100 % B for 7 min, 100-0 % B in 1 min, and hold 10 min at 0 % B. A Bruker micrOTOF (Bruker Daltonik, Bremen, Germany) mass spectrometer was operating in ESI negative mode using a mass range from 50 to 3,000 m/z . For the MS source parameters a dry N_2 flow rate of 8.0 L min^{-1} , a dry temperature of 180 $^{\circ}\text{C}$, a nebulizer pressure of 1.6 bar, a capillary voltage of 4,000 V and a capillary exit of -150 V were used. Further the skimmer 1 was set to -50 V, the hexapole 1 to -25 V and the hexapole 2 to -24 V. The transfer time was 50 μs and pre-pulse storage was 8.0 μs . Reference masses of the Agilent 'ESI-tune mix' for electro spray applications in negative mode were used for automated m/z calibration in each chromatographic run. Metabolite quantification was done via measurement of standard calibration solutions from 0.005 mM to 1,000 mM. The integrated mass area was related to the internal standard CSA and a polynomial regression of degree 2 with a $1/x$ weighting was used as calibration equation using the Quantanalysis software (Bruker Daltonics, Billerica, USA).

Organic acids, sugars, nucleobases, intermediates from glycolysis and TCA cycle

GC-MS analysis was performed using a DB-5ms (*id* 0.25 mm, *d_f* 0.25 μm , *l* 30 m, Agilent Technologies, Santa Clara, USA), an Agilent gas chromatograph (6890N, Agilent Technologies, Santa Clara, USA) and an Agilent quadrupole mass spectrometer (mass selective detector: MSD5973, Agilent Technologies, USA) as described previously (Liebeke *et al.*, 2008). Completely lyophilized samples were derivatized for 90 min at 37 $^{\circ}\text{C}$ with 60 μL *O*-methoxylamine (MeOX) containing 20 mg mL^{-1} pyridine, and 30 min at 37 $^{\circ}\text{C}$ with 120 μL *N*-methyl-*N*-trimethylsilyl-trifluoroacetamide (MSTFA, Chromatographie Service, Langerwehe, Germany). After centrifugation for 2 min at room temperature to remove cell debris, the

metabolite containing supernatant was transferred into GC vials prior to measurement as described previously (Liebeke *et al.*, 2008). Metabolite quantification was done by the ChomaTOF[®] (LECO, St. Joseph, USA) software. Peak areas of extracted ions were normalized to the area of the internal standard ribitol. For determination of the calibration equation, different concentrations of pure standards were measured and analyzed in the same manner. Dependent on the precision of the calibration equation, calibration was done via a polynomial regression of degree 1 or 2 and a 1/x weighting. The computed metabolite concentrations were further normalized to the sample volume and related to the respective cell dry weight.

Extracellular metabolites

Extracellular metabolome samples were obtained by rapid syringe filtration (0.2 μm pore size, Filtropur S[®], Sarstedt, Nümbrecht, Germany) of 2 ml cell culture. Samples were stored at -20 °C prior to ¹H-NMR analysis. 400 μL of the extracellular sample was buffered to pH 7.0 by addition of 200 μL of a sodium hydrogen phosphate buffer (0.2 M, pH 7.0, including 1 mM sodium 3-trimethylsilyl-[2,2,3,3-D₄]-1-propionic acid (TSP)) made up with 50 % D₂O to provide an NMR-lock signal (Liebeke *et al.*, 2011). Spectral referencing was done relative to 1 mM TSP in phosphate buffer. All NMR spectra were obtained at 600.27 MHz at a temperature of 310 K using a Bruker AVANCE-II 600 NMR (Bruker Biospin GmbH, Rheinstetten, Germany). A modified 1D-NOESY pulse sequence was used with pre-saturation on the residual HDO water signal during both the relaxation delay and the mixing time. A total of 64 free induction decays (FID scans) were collected using a spectral width of 30 ppm for a one-dimensional spectrum. Data analysis was implemented by AMIX[®] (Bruker Biospin GmbH, Rheinstetten, Germany). Metabolite signal integrals compared to the signal integral of the internal standard TSP was used for direct quantification.

¹³C Metabolic flux analysis

Cell pellets were washed and hydrolyzed with 6 M HCl for 24 h at 105 °C. The obtained hydrolysates were transferred to centrifugal filter tubes (0.22 μm pore size, Ultrafree-MC, Millipore, Schwalbach, Germany) and centrifuged (1 min, 12.000 x *g*) to remove cell debris. Clarified hydrolysates were then dried under a constant nitrogen stream for 30 min at room temperature. Afterwards, derivatization of the amino acids was carried out at

80 °C in 50 µL dimethylformamide containing 0.1 % pyridine and 50 µL *N*-methyl-*N*-tert-butyltrimethylsilyl-trifluoroacetamide (MBDSTFA, Macherey-Nagel, Düren, Germany) for 30 min. Derivatized amino acids were then separated by gas chromatography and analyzed on a quadrupole with electron impact ionization (GC 5975C and MSD 7890A, Agilent Technologies, Waldbronn, Germany) (Wittmann, 2002). Temperatures of front inlet, transfer line, ion source and quadrupole were 250 °C, 280 °C, 230 °C and 150 °C, respectively. Helium 5.0 was used as carrier gas at a flow rate of 1.7 mL min⁻¹. A sample volume of 1 µL was injected with split ratios between 1:10 and 1:30 and separated on a HP-5MS GC column (*id* 0.32 mm, *d_f* 0.25 µm, *l* 30 m, Agilent, Waldbronn, Germany) applying the oven temperature profile in Table 2.1.

Table 2.1: GC oven temperature profile for amino acid separation.

Time [min]	Temperature [°C]
0.0	120
2.0	120
12.0	200
24.5	325
27.0	325

In scan mode, the sample was checked for quality (retention time, peak symmetry, exclusion of isobaric overlays). For ¹³C labeling analysis, only a specific set of fragment ions (selective-ion-monitoring) was measured (Figure 2.4).

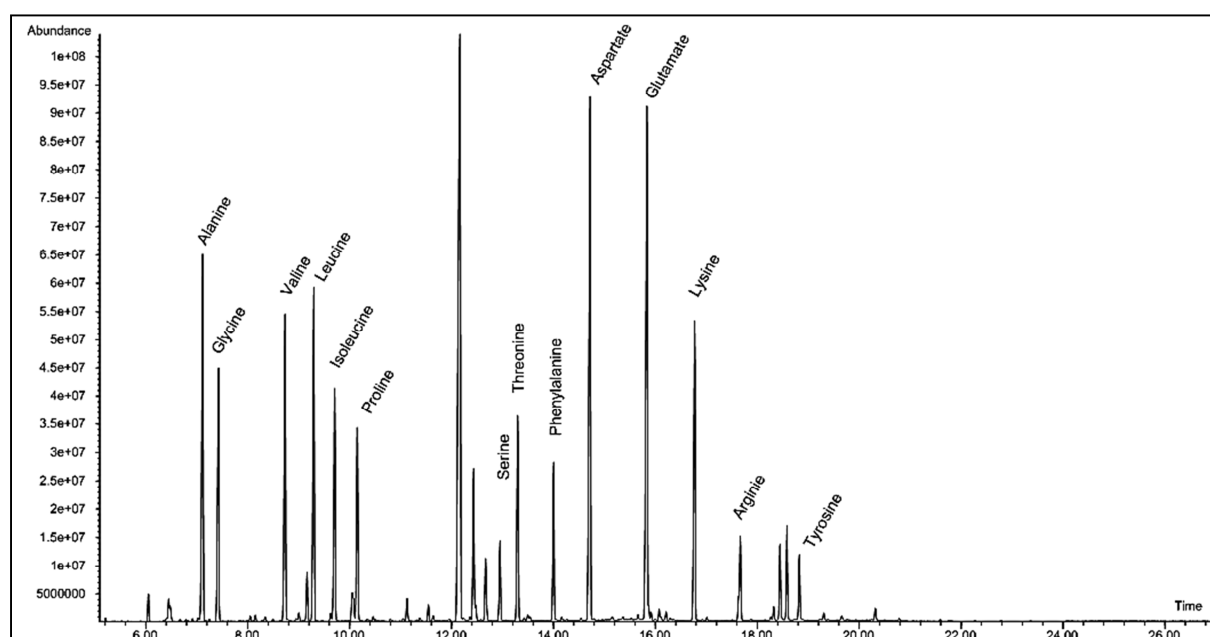


Figure 2.4: Total ion spectrum of a standard amino acid mixture as TBDMS derivates. Detection was performed in selective-ion-monitoring (SIM) mode.

All used fragment ions contained the complete carbon backbone of the corresponding amino acid ([M-57] fragment, Table 2.2).

Table 2.2: [M-57] fragment ions of proteinogenic amino acids as TBDMS derivates containing the complete carbon skeleton. M_0 corresponds to mass-to-charge ratio of the monoisotopic molecule ion.

Amino acid	M_0 [m/z]	Carbon skeleton
Alanine	260	C ₁ – C ₃
Glycine	246	C ₁ – C ₂
Valine	288	C ₁ – C ₅
Leucine	302	C ₁ – C ₆
Serine	390	C ₁ – C ₃
Threonine	404	C ₁ – C ₄
Phenylalanine	336	C ₁ – C ₉
Aspartate	418	C ₁ – C ₄
Glutamate	432	C ₁ – C ₅
Lysine	431	C ₁ – C ₆
Tyrosine	446	C ₁ – C ₉
Arginine	442	C ₁ – C ₆

The mass isotopomer distribution was then extracted from the mass spectra. Metabolic fluxes were then estimated using the open source software OpenFLUX (Quek *et al.*, 2009). The user-defined metabolic model is parsed into a MATLAB-readable model (Mathworks, Natick, USA). MATLAB subsequently estimates flux parameters using its non-linear constraint-based optimization function FMINCON, an iterative least-square algorithm. Starting with a random initial set of fluxes, the algorithm computes the remaining dependent fluxes via stoichiometric mass balances, estimates the resulting labeling patterns of all compounds in the metabolic network for the given fluxes and compares them with the experimental labeling information until an optimal fit is reached (Wittmann, 2007). Prior to modeling, mass distributions were corrected for naturally occurring isotopes (van Winden *et al.*, 2002) using a built-in extension of OpenFLUX. After flux parameter estimation, 90 % confidence intervals were determined in 50 iterations by a Monte-Carlo sensitivity analysis (Wittmann and Heinzle, 2002).

Enzyme activity assays

For enzyme activity measurements, *B. subtilis* BSB1 cells were grown in shake flasks in M9 minimal medium (37 °C, 230 rpm). During mid-exponential growth phase (about 3 (mg

protein) mL⁻¹), cells were harvested by centrifugation (5 min, 4 °C, 9,800 x *g*, Biofuge stratus, Heraeus, Hanau, Germany) and washed in disruption buffer. The cell pellet was then re-suspended in 2 mL buffer and transferred to lysis tubes (0.1 mm silica spheres, Lysing Matrix B, MP Biomedicals, Heidelberg, Germany). Cell disruption was performed with a ribolyser (FastPrep[®]-24, MP Biomedicals, Heidelberg, Germany) at 6 m s⁻¹ (3 x 40 s, 1 minute on ice in between). Crude cell extracts were obtained by centrifugation for 10 min at 13,200 x *g* and 4 °C (Centrifuge 5415R, Eppendorf, Hamburg, Germany). Protein concentration was determined photometrically (Libra, Biochrom, Cambridge, UK) using a bicinchoninic acid-based protein assay (BCA Protein Assay Kit, Thermo Scientific, Bonn, Germany) and BSA as calibration standard.

All activity measurements were performed in triplicates at 30 °C in a total reaction volume of 1 mL by monitoring the change in absorbance (SPECORD[®] 40, Analytik Jena, Jena, Germany). Specific enzyme activities are given in U mg⁻¹, corresponding to the conversion of 1 μmol of substrate per minute and milligram of total protein, and were calculated using the following equation:

$$\text{spec. Act.} \left[\frac{\text{U}}{\text{mg}} \right] = \frac{\text{change in absorbance} \left[\frac{1}{\text{s}} \right] \cdot 60 \left[\frac{\text{s}}{\text{min}} \right] \cdot 1000 \left[\frac{\mu\text{mol}}{\text{mmol}} \right]}{\text{protein concentration} \left[\frac{\text{mg}}{\text{L}} \right] \cdot \varepsilon \left[\frac{\text{L}}{\text{mmol} \cdot \text{cm}} \right] \cdot d \left[\text{cm} \right]} \quad (\text{Eq. 2.1})$$

Thereby, ε is the extinction coefficient of the monitored compound and d is the path length. The used extinction coefficients were 6.22 L mmol⁻¹ cm⁻¹ for NAD(P)H measured at 340 nm (Dominguez *et al.*, 1998) and 14.15 L mmol⁻¹ cm⁻¹ for 5-thio-2-nitrobenzoic acid (TNB) measured at 412 nm (Radmacher and Eggeling, 2007). Cell extract and substrate solution were provided separately in a 1.5 mL polystyrene cuvette (Brand, Wertheim, Germany) and were subjected to six different effector conditions. Therefore, the reaction mixture (containing reaction buffer, salts, cofactors, and coupling enzymes) and the effector mixture (containing varying potassium, proline and glycine betaine concentrations) were combined and quickly added to cell extract and substrate. Additionally, negative controls were carried out without substrate. Reaction and effector mix were pre-warmed to 30 °C. Substrate stock solutions were adjusted to the pH of the applied reaction buffer. When potassium was present in the reaction mixture (i.e. for glucose 6-phosphate dehydrogenase and malic enzyme), the potassium concentration in the respective effector mix was reduced to the appropriate level.

Glucose 6-phosphate dehydrogenase [EC 1.1.1.49] (Moritz et al., 2000)

The enzyme catalyzes the transformation of glucose 6-phosphate and NADP⁺ into 6-phosphogluconolactone and NADPH. Cells were disrupted in 100 mM Tris/HCl (pH 7.5), 10 mM MgCl₂ and 0.75 mM DTT. The reaction buffer consisted of 100 mM Tris/HCl (pH 7.8), 10 mM MgCl₂, 200 mM KCl and 1 mM NADP⁺. Activity was determined using 5 mM glucose 6-phosphate and 50 µL cell extract.

NADP⁺-dependent 6-phosphogluconate dehydrogenase [EC 1.1.1.44] (Moritz et al., 2000)

The enzyme converts 6-phosphogluconate and NADP⁺ into ribulose 5-phosphate, CO₂ and NADPH. Cell disruption was performed in 100 mM Tris/HCl (pH 7.5), 10 mM MgCl₂ and 0.75 mM DTT. The activity was measured in 100 mM Tris/HCl (pH 7.8) in the presence of 10 mM MgCl₂, 0.5 mM NADP⁺, 1 mM 6-phosphogluconate and 25 µL cell extract.

Phosphoglucoisomerase [EC 5.3.1.9] (Dominguez et al., 1998)

The isomerase forms fructose 6-phosphate from glucose 6-phosphate and vice versa. Cell disruption was performed in 100 mM Tris/HCl (pH 7.8) supplemented with 10 mM MgCl₂. The reaction was assayed providing 100 mM Tris/HCl, 10 mM MgCl₂, 0.5 mM NADP⁺ and 1.25 U glucose 6-phosphate dehydrogenase [EC 1.1.1.44] as coupling enzyme. The assay was performed at pH 7.8 with 4 mM fructose 6-phosphate and 20 µL cell extract.

Fructose 1,6-bisphosphate aldolase [EC 4.1.2.13] (Engels et al., 2008)

In this reaction, fructose 1,6-bisphosphate is cleaved into dihydroxyacetone phosphate and glyceraldehyde 3-phosphate. The disruption buffer contained 100 mM Tris/HCl (pH 7.5) and 10 mM MgCl₂. The assay mixture contained 100 mM Tris/HCl (pH 7.4), 10 mM MgCl₂, 0.15 mM NADH, 1.75 U glycerol 3-phosphate dehydrogenase [EC 1.1.5.3] and 0.025 U triosephosphate isomerase [EC 5.3.1.1] as coupling enzymes, 2 mM fructose 1,6-bisphosphate as substrate and 50 µL cell extract.

Pyruvate kinase [EC 2.7.1.40] (Netzer et al., 2004)

Pyruvate kinase catalyzes the transformation of phosphoenolpyruvate and ADP to pyruvate and ATP. Cells were mechanically disrupted in 100 mM Tris/HCl (pH 7.5) and 10 mM MgCl₂. Pyruvate kinase activity was measured at pH 7.0 with 100 mM Tris/HCl, 15 mM MgCl₂,

1 mM ADP, 0.25 mM NADH, 12 mM phosphoenolpyruvate and 20 μ L cell extract using 5.5 U of lactate dehydrogenase [EC 1.1.1.27] as coupling enzyme.

Citrate synthase [EC 2.3.3.1] (Radmacher and Eggeling, 2007)

The enzyme catalyzes the condensation of acetyl-CoA and oxaloacetate to citrate. The enzymatic reaction can be monitored by the reaction of coenzyme A with 5,5'-dithiobis-(2-nitrobenzoic acid) (DTNB). Cells were disrupted in 100 mM Tris/HCl (pH 7.5) with 10 mM $MgCl_2$. The reaction mixture contained 50 mM Tris/HCl (pH 7.5), 0.1 mM DTNB, 0.15 mM acetyl-CoA, 0.25 mM oxaloacetate and 10 μ L crude cell extract.

Isocitrate dehydrogenase [EC 1.1.1.42] (Becker et al., 2009)

The enzyme cleaves isocitrate and $NADP^+$ into 2-oxoglutarate, CO_2 and NADPH. Cell disruption was performed in 100 mM Tris/HCl (pH 7.8) supplemented with 10 mM $MgCl_2$. The enzyme activity was measured at pH 7.8 with 100 mM Tris/HCl, 10 mM $MgCl_2$, 0.5 mM $NADP^+$, 1 mM isocitrate and 25 μ L cell extract.

Malate dehydrogenase [EC 1.1.1.37] (Yoshida, 1965)

Malate dehydrogenase catalyzes the interconversion of malate and oxaloacetate. The disruption of cells was conducted in buffer containing 100 mM Tris/HCl (pH 7.5), 10 mM $MgCl_2$ and 0.75 DTT. The assay mixture for malate oxidation contained 100 mM Tris/HCl, 10 mM $MgCl_2$, 0.5 mM NAD^+ , 7.5 mM malate and 25 μ L cell extract, and was performed at pH 8.8.

Fructose 1,6-bisphosphatase [EC 3.1.3.11] (Dominguez et al., 1998)

The gluconeogenic reaction transforms fructose 1,6-bisphosphate into fructose 6-phosphate. The used cell disruption buffer contained 100 mM Tris/HCl at pH 7.8 and 10 mM $MgCl_2$. The specific enzyme activity was measured in the above buffer, additionally containing 0.5 mM $NADP^+$, 5 mM fructose 1,6-bisphosphate, 1 U glucose 6-phosphate dehydrogenase [EC 1.1.1.49] and 2 U phosphoglucosomerase [EC 5.3.1.9] as coupling enzymes, and 50 μ L crude cell extract, respectively.

NADP⁺-dependent malic enzyme [1.1.1.38] (Lerondel et al., 2006)

The disruption buffer for the determination of malic enzyme activity contained 100 mM Tris/HCl (pH 7.8) and 200 mM KCl. Activity at pH 8.0 was measured in reaction buffer containing 50 mM Tris/HCl, 10 mM MgCl₂, 10 mM MnCl₂, 10 mM mercaptoethanol, 2.5 mM NADP⁺, 40 mM malate and 50 µL cell extract.

2.6 Determination of rates and yields

Physiological parameters were determined during steady state after at least 5 volume changes after start of the continuous mode. Since the dilution rate D [h⁻¹] and thus the growth rate μ [h⁻¹] are constant under these conditions, biomass and product yields were determined from the differences of the corresponding concentrations in the feed medium and the culture supernatant, respectively.

$$Y_{X/S} = \frac{X}{S_0 - S} \cdot M_{Glc} \quad (\text{Eq. 2.2})$$

$$Y_{P/S} = \frac{P}{S_0 - S} \cdot M_{Glc} \quad (\text{Eq. 2.3})$$

with

- X – Biomass concentration at steady-state [g_{DCW} L⁻¹],
- P – Product concentration in the supernatant at steady-state [mmol L⁻¹],
- S_0 – Substrate concentration in the feed [g L⁻¹],
- S – Residual steady-state substrate concentration [g L⁻¹],
- M_{Glc} – Molar mass of glucose [g mol⁻¹].

The corresponding specific substrate consumption q_S and product formation rates q_P were calculated as follows:

$$q_S = \frac{D}{Y_{X/S}} \cdot 1000 \quad (\text{Eq. 2.4})$$

$$q_P = \frac{P \cdot D}{X} \quad (\text{Eq. 2.5})$$

The specific carbon dioxide formation rate was calculated using inert gas balancing (Eq. 2.6).

$$q_{CO_2} = \frac{F_{air}}{V_m \cdot V_R \cdot X} \cdot \left(\frac{x_{CO_2,in}}{100} - \frac{x_{CO_2,out}}{100} \cdot \frac{x_{N_2,in}}{x_{N_2,out}} \right) \quad (\text{Eq. 2.6})$$

with F_{air} – Gas flow rate [sL h⁻¹],
 V_m – Molar volume of the gas at standard temperature and pressure [L mol⁻¹],
 V_R – Reactor volume [L],
 X – Biomass concentration [g L⁻¹],
 $x_{CO_2,in}, x_{CO_2,out}$ – Relative mass fraction of CO₂ at the reactor in- and outlet [%],
 $x_{N_2,in}, x_{N_2,out}$ – Relative mass fraction of N₂ at the reactor in- and outlet [%].

For shake flask cultivations without measurement data on CO₂ formation, the specific formation rate q_{CO_2} was calculated from the obtained metabolic flux data by considering all CO₂-releasing and -consuming reactions in carbon core metabolism and the CO₂ generation for anabolic purposes (Klein *et al.*, 2013).

2.7 Multi-omics data integration and visualization

Selected multi-omics data sets were integrated and visualized as biochemical pathway maps created with ProMeTra (Bielefeld, Germany) (Neuweger *et al.*, 2009). For flux visualization, the open source tool VANTED (Junker *et al.*, 2006) including the FluxMap add-on (Rohn *et al.*, 2012) was used (Gatersleben, Germany). Hierarchical clustering, principle component analysis, Student's t-tests and canonical correlation analysis were performed with R (R Core Team, 2013) including the additional packages FactoMineR (Lê *et al.*, 2008) and mixOmics (Lê Cao *et al.*, 2009). Venn diagrams were created using the R package venneuler (Wilkinson, 2011).

2.8 Experimental workflow

The final workflow of the multi-omics chemostat experiments is depicted in Figure 2.5. All cellular species (transcripts, proteins, intra- and extracellular metabolites) were sampled at steady state in biological (n = 3-4) and technical replicates (n = 2-3). Sampling was performed according to well-established standard operating procedures that have been developed in each involved laboratory (Meyer *et al.*, 2010; Meyer *et al.*, 2013; Bolten *et al.*, 2007; Bolten and Wittmann, 2008). Subsequently, samples were pretreated and analyzed for

gene expression (Eymann *et al.*, 2002; Charbonnier *et al.*, 2005), protein abundance (Starcher, 2001; Beynon *et al.*, 2005; Pratt *et al.*, 2006; Maaß *et al.*, 2011), metabolite concentrations (Liebeke *et al.*, 2008; Liebeke *et al.*, 2010; Liebeke *et al.*, 2011; Meyer *et al.*, 2013) and ^{13}C labeling pattern (Wittmann, 2002; Wittmann, 2007). Finally, data from each analytical platform were analyzed statistically and integrated with each other. Applying ^{13}C metabolic flux analysis yielded *in vivo* reaction rates and thus served as integrated cellular response of *B. subtilis* to the different treatments.

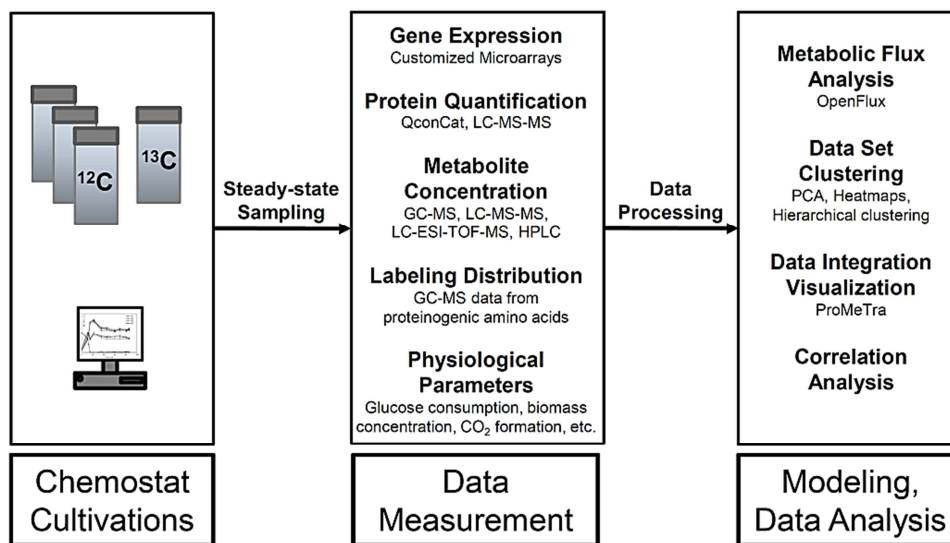


Figure 2.5: Schematic three-phase workflow of the chemostat study.

3 Results and Discussion

3.1 First insights into cellular metabolism of *B. subtilis* BSB1

Impact of NaCl, glucose and glycine betaine on *B. subtilis*' growth behavior

In high-salinity studies, ionic osmotic stress is usually mimicked through addition of NaCl (Steil *et al.*, 2003; Höper *et al.*, 2006; Hahne *et al.*, 2010). Non-ionic osmotic stress is generally induced by high-soluble sugars or sugar alcohols, such as sucrose, lactose, glycerol, sorbitol or mannitol (Kuhlmann and Bremer, 2002; Shabala *et al.*, 2009; Hoffmann *et al.*, 2013). After an initial screening for adequate stressors this study used glucose as non-ionic osmotic stress inducer.

Increasing concentrations of NaCl and glucose have a tremendous impact on the maximum growth rate of moderately halotolerant *B. subtilis* grown in microtiter plates (Figure 3.1). Thereby, cell growth is similarly affected by ionic and non-ionic osmotic stress. At concentrations higher than 1.2 M NaCl and 1.67 M glucose (300 g L⁻¹), respectively, no cell growth was observed during a cultivation time of 60 hours. The osmotic burden had an even more pronounced effect on the length of the initial lag phase (Figure 3.1). The lag phase increased from 2 h in the absence of an osmotic stressor up to more than 2 days at the highest tolerable NaCl concentration. A similar trend was observable in shake flasks and at bioreactor scale, however, shorter lag phases and higher specific growth rates were observed. When glycine betaine was added, lag phases became significantly shorter and the original growth rate was partially restored (Figure 3.1). For instance, the two-day lag phase in the presence of 1.2 M NaCl decreased to about 12 hours, when 0.1 mM glycine betaine was supplemented to the medium. This is likely supported by the fact that the cell does not depend on *de novo* synthesis of the osmoprotectant proline, but rather assimilates the externally supplied glycine betaine, and is therefore able to counteract the osmotic stress more quickly. In addition to sole osmotic stress, imposed by high glucose concentrations, also the increased medium viscosity and thus limitations in oxygen transport become more important.

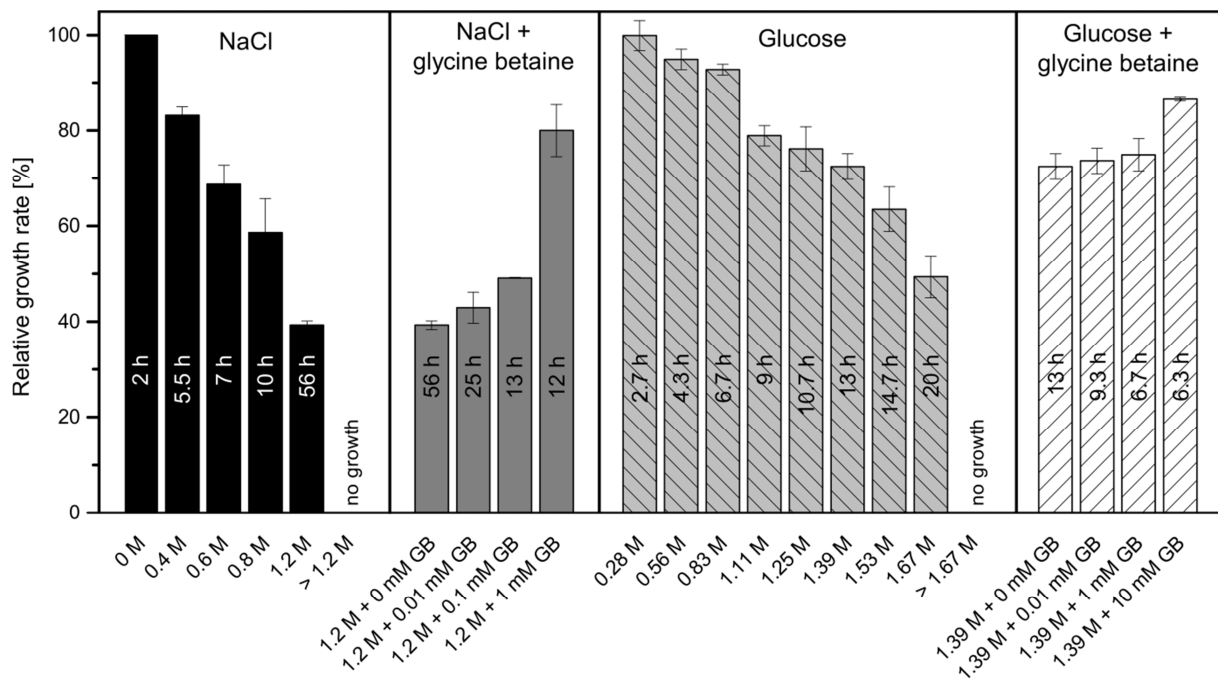


Figure 3.1: Impact of different NaCl and glucose concentrations on specific growth rate μ_{\max} and lag phase duration of *B. subtilis* BSB1 growing on glucose in M9 minimal medium with and without glycine betaine. Cultivation was performed in a 48 well microtiter flowerplate at 37 °C and a shaking frequency of 1,000 rpm. Optical density was monitored online at 620 nm and the specific growth rate was determined from at least 6 data points in exponential growth phase. A relative growth rate of 100 % corresponds to a $\mu_{\max} = 0.74 \text{ h}^{-1}$. Condition-dependent approximate lag phase durations are displayed vertically. In order to compare ionic and non-ionic stress, the used sugar has to be sufficiently soluble to mimic the same osmolarity as the corresponding salt. With respect to a reasonable experimentation under high-sugar stress, stable isotopes of the chosen compound have to be commercially available and affordable.

Cell physiology and metabolic flux distribution under different stress conditions

The initial effector screening (Figure 3.1) and knowledge from previous studies on the osmoprotection response in *B. subtilis* (Hoffmann *et al.*, 2002; Höper *et al.*, 2006; Hahne *et al.*, 2010; Brill *et al.*, 2011) suggested three test conditions for further investigations: a non-stressed reference, a stress condition at the maximal tolerable salt concentration of 1.2 M NaCl, and an osmoprotection condition in which salt-stressed cells were additionally supplemented with 1 mM glycine betaine. The three conditions were first tested in a shake flask setup. Obtained physiological data can be found in Table 3.1.

Table 3.1: Physiological data of *B. subtilis* BSB1 grown in shake flask on M9 minimal medium under non-stressed (reference) and salt-stressed conditions (salt stress, 1.2 M NaCl). For osmoprotection, salt-stressed cells were additionally supplemented with 1 mM of glycine betaine. Data were obtained from at least 6 biological replicates.

Condition	Growth rate [h ⁻¹]	Biomass yield [g _{dcw} mol ⁻¹]	Glucose uptake rate [mmol g _{dcw} ⁻¹ h ⁻¹]	Acetate production [mmol g _{dcw} ⁻¹ h ⁻¹]	Pyruvate production [mmol g _{dcw} ⁻¹ h ⁻¹]	Acetoin production [mmol g _{dcw} ⁻¹ h ⁻¹]	CO₂ formation^a [mmol g _{dcw} ⁻¹ h ⁻¹]
Reference	0.72 ± 0.01	66.59 ± 2.87	10.81 ± 0.51	4.93 ± 0.57	0.38 ± 0.19	< 0.01	23.99 ± 1.26
Salt stress	0.23 ± 0.01	55.81 ± 3.48	4.06 ± 0.37	0.72 ± 0.14	0.09 ± 0.03	0.05 ± 0.03	10.10 ± 0.36
Osmoprotection	0.29 ± 0.01	44.70 ± 2.38	6.41 ± 0.39	2.31 ± 0.42	0.80 ± 0.19	1.19 ± 0.23	12.24 ± 1.53

^a Specific CO₂ formation rate was calculated from flux data considering all CO₂-releasing and -consuming reactions in carbon core metabolism and CO₂ generation during biomass formation (Klein *et al.*, 2013).

The cell physiology differs strongly between the three conditions in terms of biomass yield, metabolite spectrum and CO₂ formation. Specific growth rate and glucose consumption drop to about one third in salt-stressed cells compared to reference values, and are partially restored upon addition of glycine betaine. This is in agreement with microtiter plate cultivations (Figure 3.1).

Parallel labeling experiments, using [1-¹³C] glucose, [1,2-¹³C₂] glucose and a 50:50 mixture of naturally labeled and fully labeled glucose (U¹³C), were conducted to screen for adequate ¹³C tracers and to access the intracellular flux distribution under these conditions. The predefined biochemical network (Appendix Table 6.1) and measured intra- and extracellular metabolite formation rates (Table 3.1) served as input for the metabolic flux analysis. To begin with, the previously published stoichiometric growth model for wild-type *B. subtilis* created by Dauner and Sauer (Dauner and Sauer, 2001) was used to estimate the anabolic precursor demand for biomass formation under each condition as function of the corresponding growth rate. The resulting flux distribution is shown in Figure 3.2.

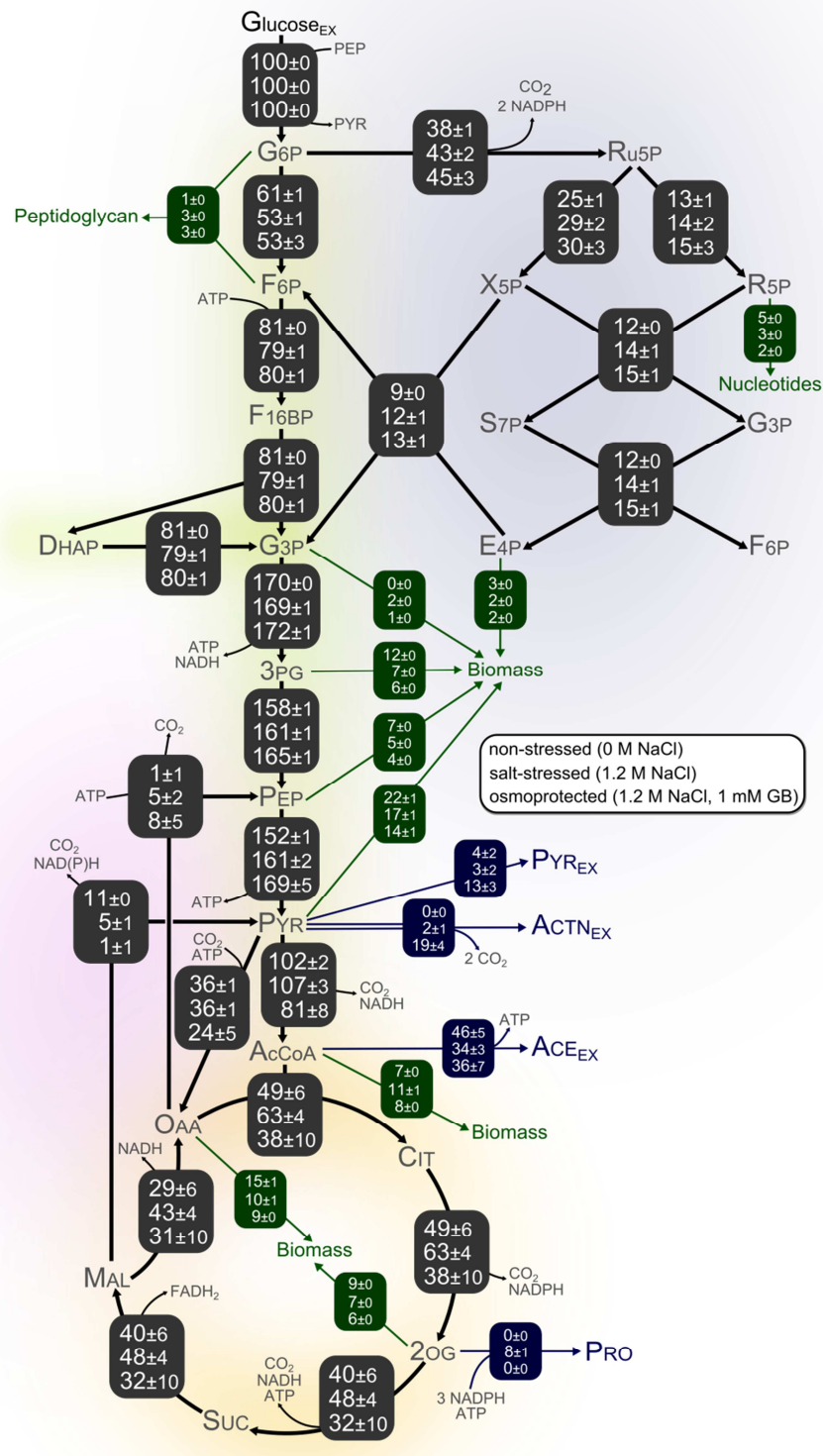


Figure 3.2: Metabolic flux distribution in *B. subtilis* BSB1 grown in shake flasks on M9 minimal medium. The data (from top to bottom) display a non-stressed reference compared to salt-stressed (1.2 M NaCl) and osmoprotected cells. For osmoprotection salt-stressed cells were additionally supplemented with 1 mM of the osmoprotectant glycine betaine. The reaction network comprises osmosensitive proline synthesis (PRO), extracellular by-product formation (PYR, pyruvate; ACTN, acetoin; ACE, acetate) and anabolic fluxes into biomass. Fluxes are given as relative values (in %) normalized to the glucose uptake rate (Table 3.1).

The presence of salt triggered an increased carbon flux towards the osmoprotectant proline. About 8 % of total carbon was channeled into this biosynthetic pathway. This coincided with a reduced flux into overflow metabolism and an increased flux towards the TCA cycle, providing more 2-oxoglutarate, the precursor of glutamate and proline. The synthesis of proline from 2-oxoglutarate consumes 3 moles of NADPH. An important physiological aspect is the question, whether the cell can provide sufficient amounts of the cofactor NADPH to meet its anabolic needs. In central carbon metabolism the cell possesses three key reactions to provide NADPH: the oxidative pentose phosphate pathway, isocitrate dehydrogenase and an NADP⁺-dependent malic enzyme. The cofactor demand results from the biomass composition under a certain condition. In addition to intracellular amino acids, like glutamate or proline, main NADPH consumers are proteins and lipids. Under all tested conditions, production and demand were balanced. In the presence of salt, cofactor production is even higher caused by higher fluxes through isocitrate dehydrogenase and the oxidative part of the PP pathway (Figure 3.3).

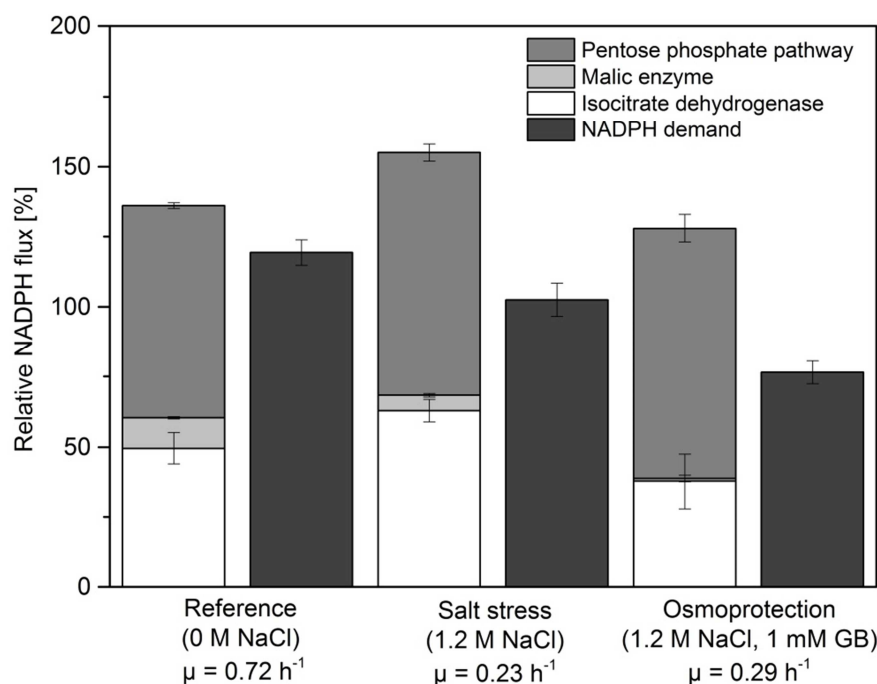


Figure 3.3: Comparison of NADPH formation and demand in non-stressed, salt-stressed and osmoprotected cells.

When glycine betaine was supplemented, osmosensitive proline synthesis is prevented. Additionally, overflow metabolism was significantly increased. In total, about 70 % of consumed carbon was directly drained into synthesis of pyruvate, acetate and acetoin, resulting in a reduced TCA cycle flux and a lower anaplerosis via pyruvate carboxylase.

Despite a decreased requirement for NADPH, PP pathway flux was still as high as in salt-stressed cells. However, when salt was present in the medium, the cell produced the cofactor above its actual demand (Figure 3.3). At that point it is not possible to distinguish whether the observed flux alterations were exclusively salt-stress related or influenced by the different growth physiology (Table 3.1).

Serine biosynthesis pathway is strongly affected by salt-stress

It should be mentioned that the labeling pattern of serine was quite different in salt-stressed cells compared to non-stressed cells, whereas the mass isotopomer distribution of the remaining amino acids was rather similar. This effect only occurred, when glucose tracers other than single labeled $[1-^{13}\text{C}]$ were used (Figure 3.4).

The altered mass isotopomer distribution might be caused by induction of an alternative biosynthesis pathway for this particular amino acid at high-salinity, e.g. via a threonine degradative pathway. Under normal growth conditions, serine is exclusively derived from 3-phosphoglycerate (Figure 1.1). Additionally considering serine synthesis via threonine dehydrogenase (Tdh), 2-amino-3-ketobutyrate CoA ligase (Kbl) and the glycine cleavage system (GcvTHP) led to a much better fit of experimental and simulated labeling data (not shown).

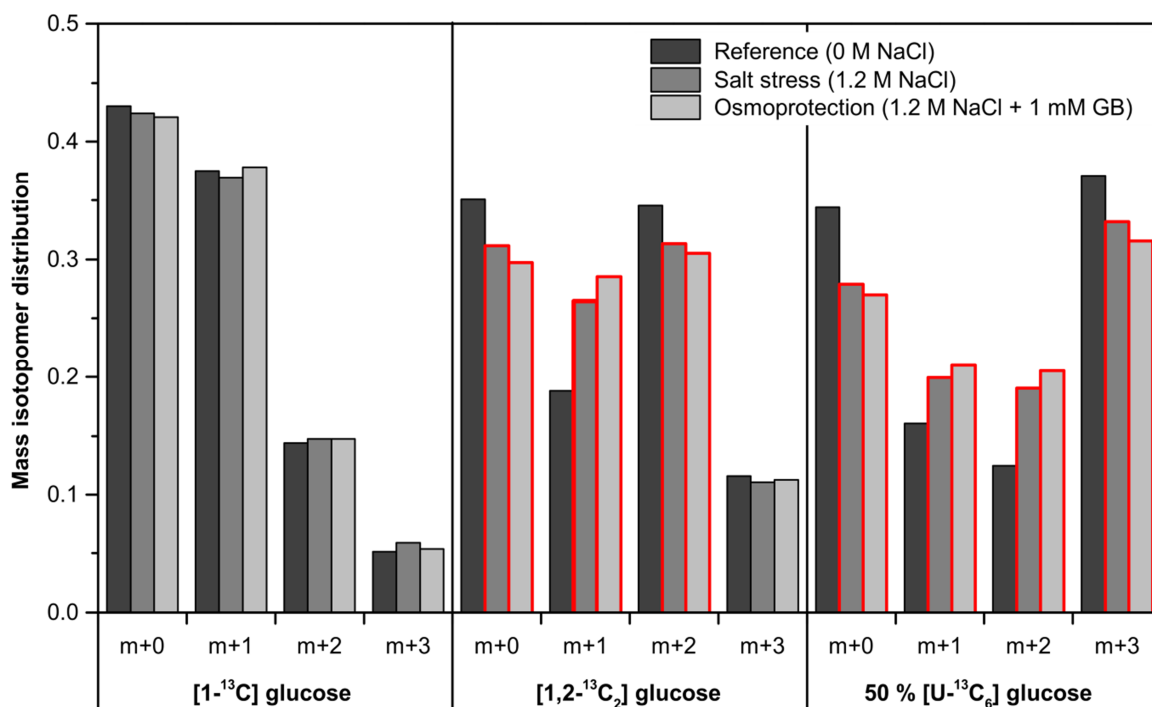


Figure 3.4: Altered labeling pattern of serine (m/z 390, C_1-C_3) in salt-stressed cells.

Indeed, expression of the glycine cleavage system (*gcvTP*) is about four-fold induced on the transcript and protein level both in shake flask and chemostat cultivations in the presence of salt (data obtained in this study, tiling array data from Nicolas *et al.* 2012 and personal communication with Praveen K Sappa). However, expression of *tdh* and *kbl*, the proposed remaining pathway genes, is about three-fold repressed in salt-stressed cells grown in chemostat. Altogether, the exact pathway remains unclear and needs further attention.

Cell physiology and metabolic flux distribution at different growth rates

Global analysis of regulatory functionality requires a carefully defined and controlled cell physiology. Obviously, shake flask and batch cultures have their limitations in terms of growth dynamics and process control. To elucidate the systems-wide response of *B. subtilis* on all accessible functional levels, the experimental workflow had to be developed into a multi-omics approach, allowing precise process control, larger volumes and fast sampling of all cellular species at metabolic steady-state. In order to overcome the above mentioned limitations, cells are preferably grown in a chemostat (Hoskisson, 2005). This mode of operation offers additional advantages as secondary growth effects are removed and reproducibility and accuracy of omics data are increased (ter Linde *et al.*, 1999; Piper *et al.*, 2002; Kolkman *et al.*, 2005). The growth rate-dependent effects emerge from different growth rate management, and are often masking real physiological changes (Hoskisson, 2005; Goelzer and Fromion, 2011). This can be avoided by imposing the same growth rate to all conditions.

A newly developed experimental workflow (Figure 2.5) was initially tested in a batch and two chemostat cultivations at different growth rates. Cultivations were performed in quadruplicates including one reactor supplemented with [1-¹³C] instead of naturally labeled glucose. The tracer provided sufficient overall resolution ability for the metabolic network (Fischer *et al.*, 2004; Metallo *et al.*, 2009), although fluxes around the PEP-PYR-OAA node exhibit somewhat larger confidence intervals (Dauner *et al.*, 2001a). In this phase of the study all sample protocols and analytical procedures were validated and growth rate-related data on the transcriptome, proteome, metabolome and fluxome level were collected. Table 3.2 summarizes the physiological outcome of the experiments.

Table 3.2: Physiological data of *B. subtilis* BSB1 grown in M9 minimal medium at different growth rates.

Growth rate [h ⁻¹]	Biomass yield [g _{glc} mol ⁻¹]	Glucose uptake rate [mmol g _{DCW} ⁻¹ h ⁻¹]	Acetate production [mmol g _{DCW} ⁻¹ h ⁻¹]	Pyruvate production [mmol g _{DCW} ⁻¹ h ⁻¹]	CO₂ formation [mmol g _{DCW} ⁻¹ h ⁻¹]	Carbon recovery [%]
0.83 ± 0.04 ^a	72.6 ± 6.9	11.54 ± 0.94	5.71 ± 0.95	0.39 ± 0.06	20.5 ± 1.3	96.7 ± 3.8
0.41 ± 0.01 ^b	59.9 ± 2.2	6.79 ± 0.38	0.13 ± 0.02	0.01 ± 0.00	15.2 ± 0.3	101.5 ± 7.2
0.10 ± 0.00 ^b	55.6 ± 5.8	1.82 ± 0.18	0.02 ± 0.01	< 0.01	6.7 ± 0.2	98.3 ± 6.5

^a Cells were grown exponentially; ^b Cells were grown in carbon-limited chemostat at the corresponding dilution rate.

The imposed growth rate strongly influenced the cell physiology. Carbon limitation prevented the formation of significant amounts of overflow metabolites as observed in batch culture. Biomass yield, glucose consumption and CO₂ production decrease with the growth rate.

The concept of maintenance as introduced by Pirt describes a linear relationship between growth rate and specific glucose uptake rate (Pirt, 1965):

$$q_{glc} = \frac{\mu}{Y_{glc}^{max}} + m_{glc} \quad (\text{Eq. 2.7})$$

Hereby, the maintenance coefficient m_{glc} describes the non-growth associated substrate demand for cell maintenance, e.g. shifts in metabolic pathways, cell motility, proofreading, synthesis and turnover of macromolecules such as enzymes and RNA or defense against various stresses. It can be determined by extrapolating the linear fit between glucose uptake and the growth rate (Figure 3.5). The obtained maintenance coefficient of 0.44 ± 0.09 mmol g_{DCW}⁻¹ h⁻¹ for unstressed cells compares favorably to previously reported values for various *Bacillus* species (Sauer *et al.*, 1996; Tännler *et al.*, 2008). It follows from Figure 3.5: the slower the growth rate imposed, the higher the relative carbon fraction attributed to cell maintenance.

From the reactor supplemented with [1-¹³C] glucose, cell pellets were harvested and the labeling pattern of 12 proteinogenic amino acids was extracted. Together with a mathematical representation of the *B. subtilis* central carbon metabolism (Appendix Table 6.1) and collected kinetic data (Table 3.2), *in vivo* pathway activity was quantified. Anabolic precursor demand was calculated from an adjusted biomass model. Therefore, the growth rate-dependent biomass composition published by Dauner and Sauer (Dauner and Sauer, 2001) was updated for this purpose (see Chapter 3.2 'Prerequisites', Appendix Table 6.2).

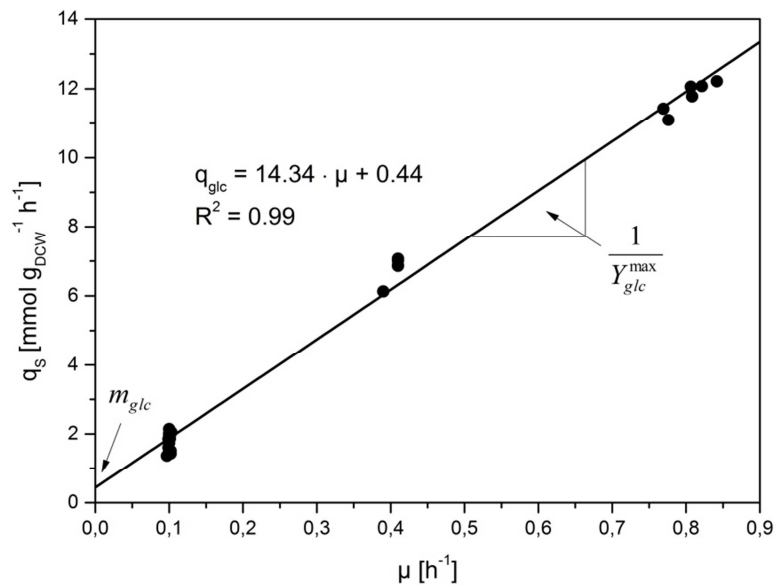


Figure 3.5: Specific glucose uptake rate q_s as function of growth rate μ ($n=30$). Intercept between ordinate and the linear regression represents the maintenance coefficient m_{glc} (0.44 ± 0.09 mmol $g_{DCW}^{-1} h^{-1}$).

The resulting flux distributions for different growth rates are depicted in Figure 3.6. The obtained flux profiles were in good agreement with previously published studies using *B. subtilis* under similar growth conditions (Sauer *et al.*, 1997; Dauner *et al.*, 2001a; Schilling *et al.*, 2007; Tännler *et al.*, 2008). *B. subtilis* recruited both glucose metabolizing pathways – glycolysis and the PP pathway – simultaneously with a ratio of about 2:1. Under exponential growth conditions, the cell transformed up to 50 % of the consumed glucose into acetate and thus generates one mole of ATP per mole acetate via substrate phosphorylation. When glucose was limiting, carbon is nearly completely metabolized via the TCA cycle and energy was mainly generated through oxidative phosphorylation. A high anaplerotic flux through PEP carboxykinase replenished the TCA cycle with OAA. Under all conditions, a significant carbon fraction was channeled back from TCA cycle via gluconeogenic PEP carboxykinase and malic enzyme, thus constituting ATP futile cycles (Figure 3.6) (Sauer and Eikmanns, 2005). Such futile cycles partially contribute to the cellular energy balance by fine-tuning the intracellular ATP level (Dauner *et al.*, 2002).

The NADPH demand for biomass formation depends on the biomass composition and increases with the growth rate (Figure 3.6) (Tännler *et al.*, 2008). However, cofactor production inferred from the flux data were even higher at lower dilution rates, leading to a drastic apparent excess of NADPH. When cells grew exponentially, demand and supply were balanced (Figure 3.3). The apparent imbalance between demand and production in slow-growing cells has already been observed previously (Sauer *et al.*, 1997; Dauner *et al.*, 2002; Tännler *et al.*, 2008; Fuhrer and Sauer, 2009; Rühl *et al.*, 2012). Accordingly, *B. subtilis* exhibits a small but significant *in vitro* transhydrogenase activity that may play a role in redox balancing by transferring electrons from excess NADPH to NAD^+ (Dauner and Sauer, 2001; Fuhrer and Sauer, 2009). In addition, dehydrogenases in the oxidative part of PP pathway are not 100 % specific for NADP^+ (Fuhrer and Sauer, 2009). Rühl *et al.* proposed several transhydrogenation cycles that are active in resting *Bacillus* cells and that are probably involved in maintaining redox homeostasis (Rühl *et al.*, 2012). Thus, transhydrogenation may be realized by the simultaneous operation of NADPH- and NAD^+ -dependent isoenzymes, like the malic enzymes YtsJ and MalS and the glyceraldehyde 3-phosphate dehydrogenases GapB and GapA, respectively. Also other mechanisms, like additional biosynthesis-degradation cycles, the NADPH consumption for the detoxification of reactive oxygen species or keeping a certain cofactor amount for potential changes in nutrient supply, may be involved (Rühl *et al.*, 2012).

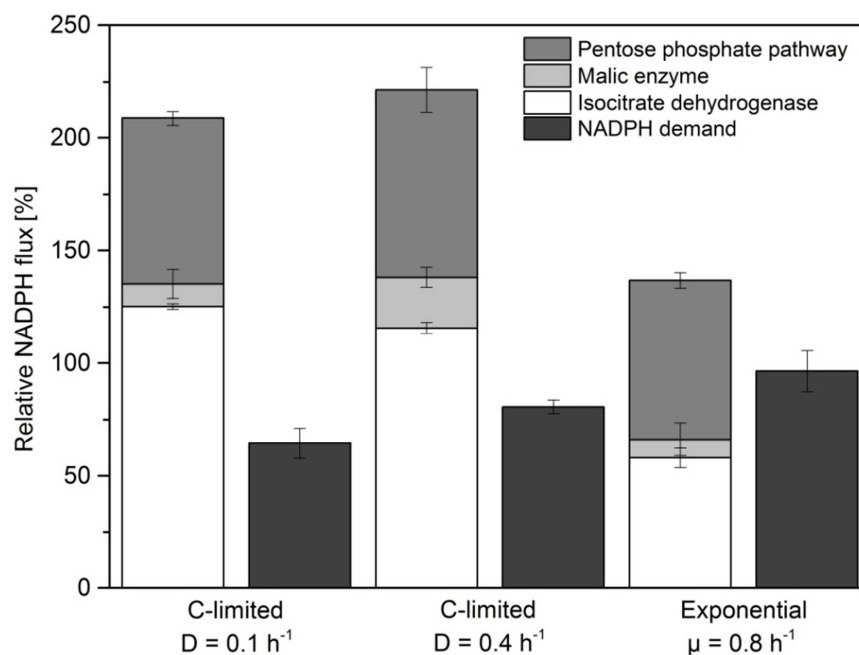


Figure 3.7: Comparison of NADPH formation and demand during glucose-limited and exponential growth.

The results above indicate a strong influence of the growth rate on the overall cell physiology (Table 3.2, Figure 3.6 and Figure 3.7). Also on the proteome and metabolome level, as well as in gene expression, significant differences between the compared growth rates could be observed as revealed by principal component analysis of the raw data sets (Figure 3.8).

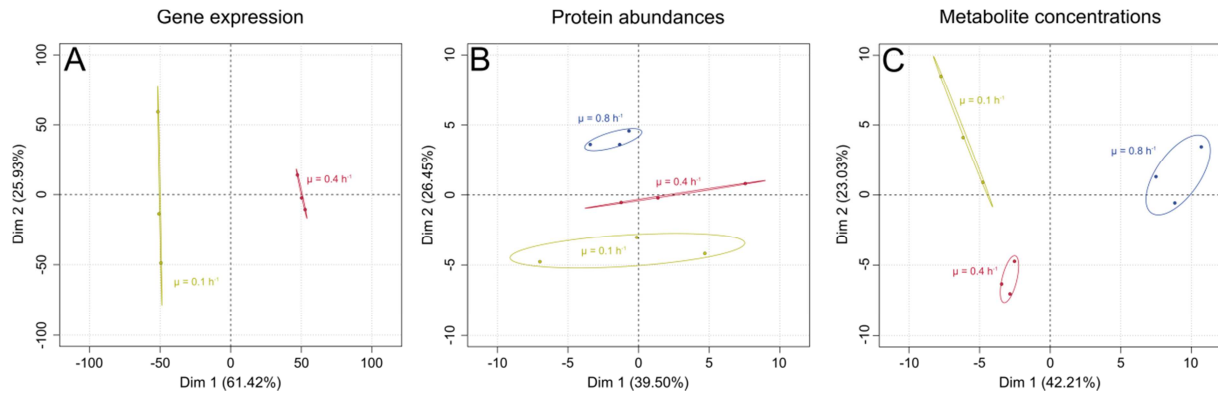


Figure 3.8: Principal component analysis plots of generated data sets. **(A)** Gene expression data from 4105 genes obtained by microarray analysis; **(B)** Protein abundance of 41 central carbon metabolism enzymes comprising glycolysis, TCA cycle, gluconeogenesis, glutamine, glutamate and proline synthesis; **(C)** Concentrations of 106 intra- and extracellular metabolites. Each replicate of a condition is represented by one data point. Clustering replicates are surrounded by 95 % confidence ellipses. No microarray analysis was performed for exponential growth.

In order to avoid this problem and to allow for an unbiased interpretation of the data, the dilution rate for all further chemostat experiments was set to 0.1 h^{-1} , a value considerably below the maximum growth rate under severe salt stress (Table 3.1). Furthermore, the highest tolerable concentration of NaCl (1.2 M) and the most effective glycine betaine concentration under high-salinity (1 mM) were chosen to study the effects of salt stress and osmoprotection under simultaneous nutrient limitation in continuous culture (Figure 3.1). For comparison of ionic and non-ionic osmotic stress, induced by NaCl and glucose, respectively, iso-osmolar concentrations of 0.69 M NaCl and 1.39 M glucose were chosen. As glucose would be available in excess under high-glucose conditions, chemostat experiments were conducted under nitrogen limitation and were compared to a reference cultivation without additional salt or glucose.

3.2 Systems biology setup for multi-omics analysis

Chapter 3.1 gave first insights in the physiology of *B. subtilis* and indicated the influence of nutrient supply and osmotic stress on the *in vivo* flux activity in central carbon metabolism. The outcome is a well-proven experimental and analytical setup, as well as the definition of process parameters and stressor concentrations for the following systems-level investigation. The results presented in Chapter 3.3 and 3.4 are the outcome of an extensive data mining process and are visualized in a comprehensive manner. During cultivation and prior to a detailed analysis of the generated multi-omics data sets, pre-defined quality criteria were met. The below described measures are essential to assure data validity and reliability of the drawn biological conclusions. This theoretical section is decoupled from the following results section (Chapter 3.3 and 3.4), in order to facilitate the reading and comprehension of the study outcome, without being distracted by experimental and analytical details regarding the origin of the presented data.

Defining data quality criteria

Metabolic and isotopic steady-state

A prerequisite for this study is a well-established cellular steady-state prior to sampling. Metabolic steady-state of cells was verified by a stable optical density, constant CO₂ offgas readings and an invariant residual glucose level and extracellular product formation (as exemplified for continuous growth under carbon limitation, salt stress and osmoprotection in Figure 3.9).

As acetate and pyruvate were always detectable in the culture broth, they served as key metabolites for steady-state monitoring. Under nitrogen-limitation, residual ammonium concentrations were additionally monitored. When all criteria were fulfilled, all four reactors were sampled successively.

Intracellular non-stationarity can be identified by changes in the labeling pattern over time. Only when the obtained mass isotopomer distributions are stable over a certain time (e.g. 20 h as in Figure 3.10), isotopic steady-state is certainly reached.

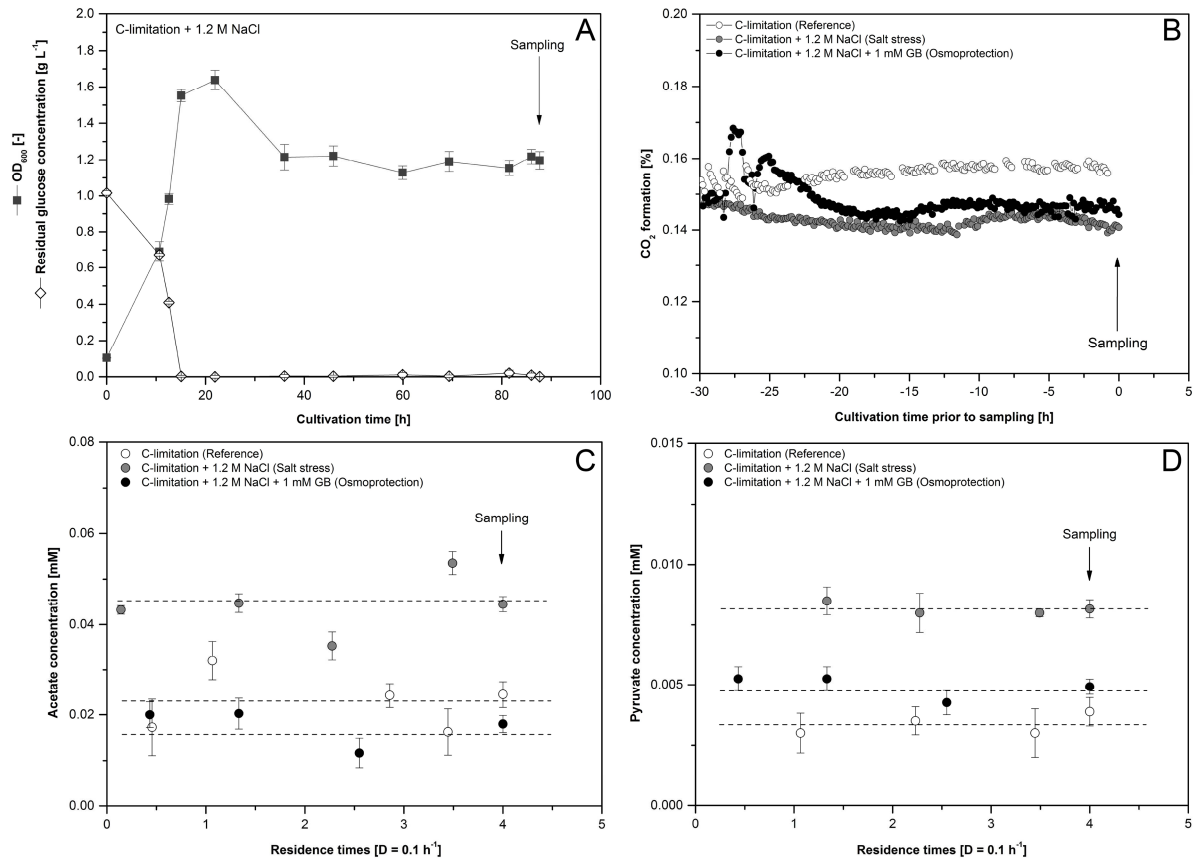


Figure 3.9: Monitoring steady-state in (A) optical density, residual glucose levels (B), CO₂ offgas readings, and extracellular (C) acetate and (D) pyruvate concentrations prior to sampling during continuous cultivation. Exemplary data originates from carbon-limited cultivations of *B. subtilis* BSB1 in M9 medium ($D = 0.1 \text{ h}^{-1}$) under non-stressed reference) and salt-stressed conditions (1.2 M NaCl). For osmoprotection salt-stressed cells were additionally supplemented with 1 mM of glycine betaine.

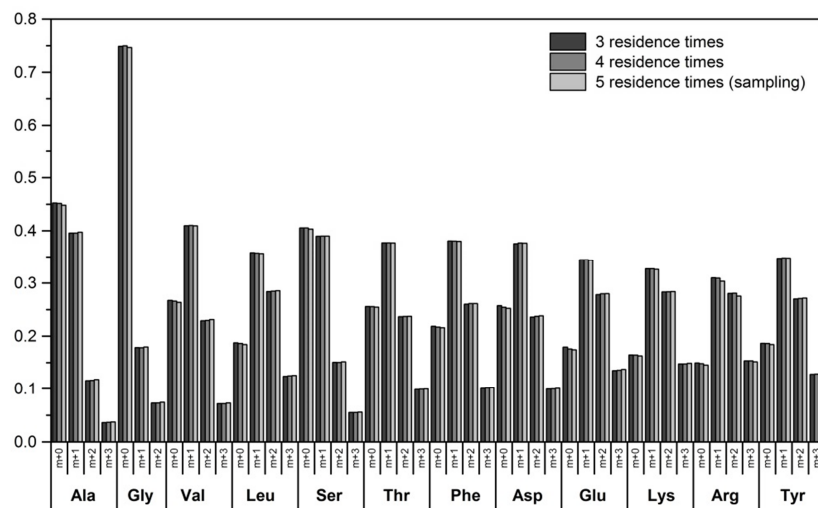


Figure 3.10: Isotopic steady-state in amino acid labeling over two residence times prior to fluxome sampling exemplified for continuous cultivation under nitrogen-limitation ($D = 0.1 \text{ h}^{-1}$).

Carbon fate and recovery

The entire carbon contained in the input substrate is converted by the cell and can be recovered in four different fractions: non-consumed glucose, cellular biomass, extracellular metabolites and proteins, and carbon dioxide in the offgas. A closed carbon balance serves as indicator for a robust analytical setup and meaningful results. In order to validate the consistency of the recorded physiological data, carbon balances for all conditions were calculated, considering the assimilated substrate carbon and the produced carbon (Eq. 3.1).

$$C_{rec} [\%] = \frac{x_{C,X} \cdot X \cdot D + x_{C,S} \cdot S \cdot D + \sum_{i=1}^n (x_{C,P_i} \cdot M_{P_i} \cdot P_i) \cdot D + x_{C,CO_2} \cdot q_{CO_2} \cdot M_{CO_2} \cdot X}{x_{C,S} \cdot S_0 \cdot D} \cdot 100 \quad (\text{Eq. 3.1})$$

with $x_{C,X}, x_{C,S}, x_{C,P_i}, x_{C,CO_2}$ – Relative mass fraction of carbon in biomass, substrate, extracellular products and CO₂

X – Biomass concentration [g_{DCW} L⁻¹],

D – Dilution rate [h⁻¹],

S – Substrate concentration in the feed [g L⁻¹],

M_{P_i} – Molar mass of extracellular product [g mmol⁻¹]

P_i – Concentration of extracellular product i in the supernatant [mmol L⁻¹],

q_{CO_2} – Specific CO₂ formation rate [mmol g_{DCW}⁻¹ h⁻¹],

M_{CO_2} – Molar mass of CO₂ [g mol⁻¹],

S_0 – Residual steady-state substrate concentration [g L⁻¹].

Closed carbon balances, as indicated by a carbon recovery of over 97 % for all tested conditions, confirmed that all major products were analytically covered. Figure 3.11 additionally shows the carbon fate for all conducted bioreactor cultivations. The majority of the assimilated substrate was converted to CO₂, followed by biomass formation. In continuous culture only a minor carbon fraction was channeled into the synthesis of organic acids, mainly acetate and pyruvate (about 1-5 %). In cultivations where carbon was the limited nutrient, significant amounts of extracellular protein were found. Probably, the cell secretes several degradative enzymes (e.g. glucanases, proteases, and nucleases) in order to extend its carbon substrate spectrum (Stülke and Hillen, 2000).

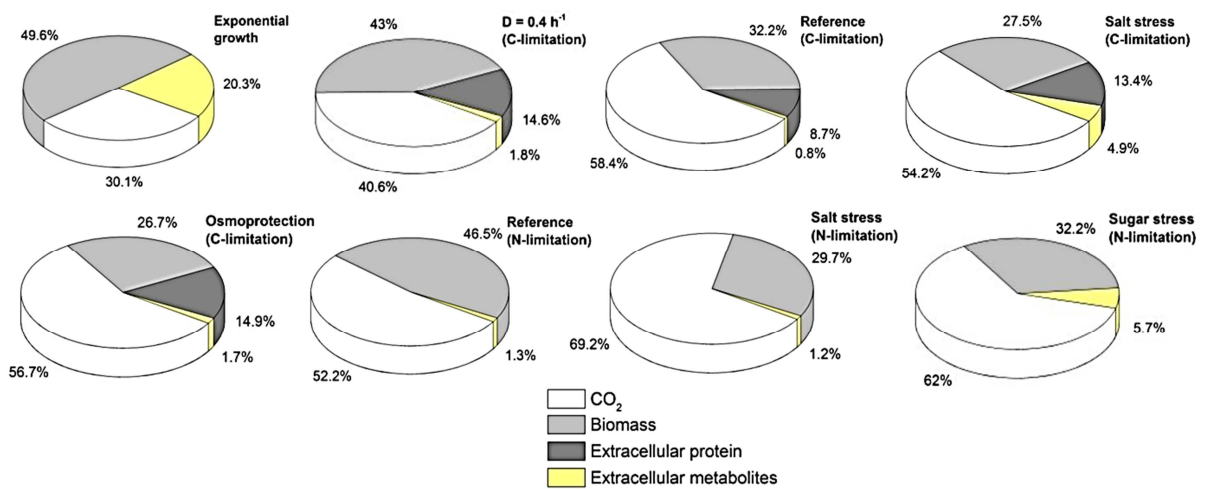


Figure 3.11: Substrate carbon fate into biomass, extracellular metabolites and protein, and CO₂ under various growth conditions.

Data accuracy, reproducibility and PCA discrimination

Prior to a more detailed inspection, the transcriptome, proteome and the metabolome data sets were statistically evaluated by principal component analysis (Figure 3.12). The individual replicates for each condition nicely clustered together within 95 % confidence ellipses, which further confirmed a high data quality. In contrast, stressed and non-stressed cells could be clearly distinguished. It was interesting to note that the osmoprotectant glycine betaine did not restore the characteristics of the non-stressed cells under carbon-limitation, as one might have expected. The formed cluster even did not locate between the two extremes, but rather represented a completely new and independent metabolic state. Also high-salinity and high-sugar stressed cells could clearly be distinguished, indicating different cellular mechanisms to cope with ionic and non-ionic stress of the same osmolarity.

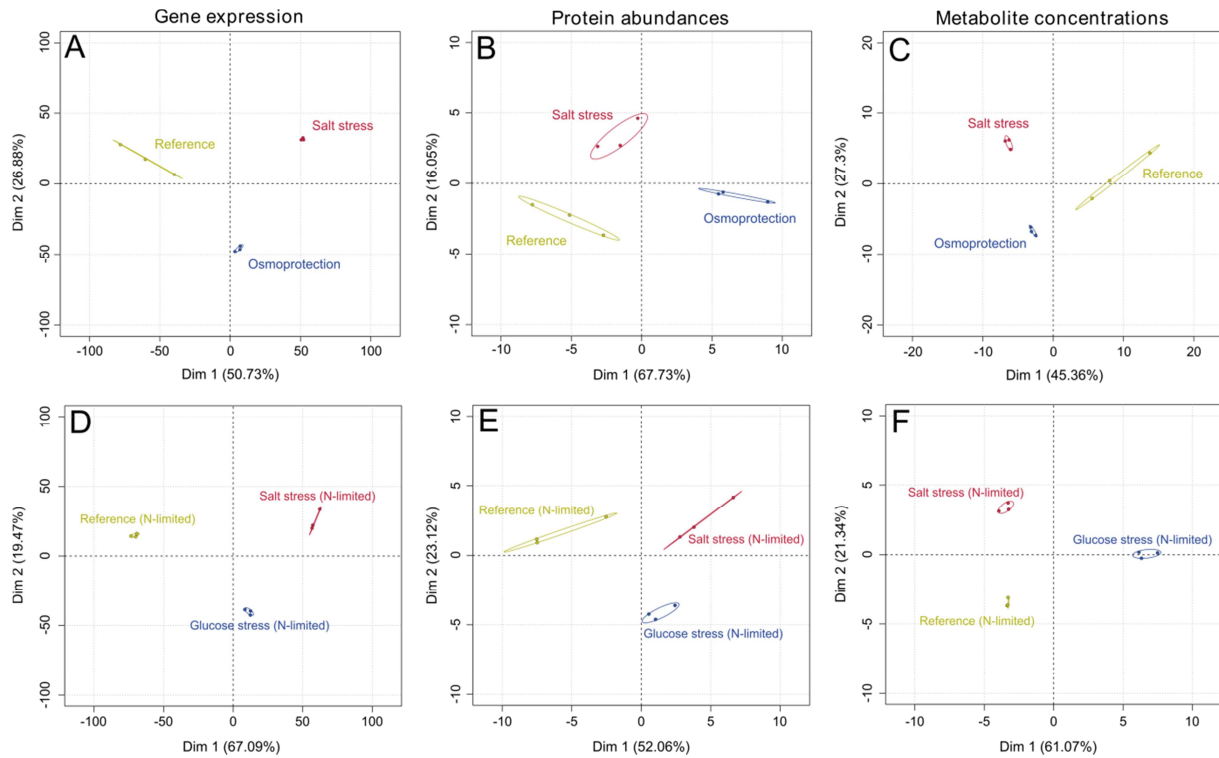


Figure 3.12: Principal component analysis plots of generated data sets. **(A-C)** Gene expression data from microarray analysis, Protein abundance of central carbon metabolism enzymes and metabolite concentrations in carbon-limited cultivations; **(D-F)** Corresponding data obtained from nitrogen-limited cultivations. Each replicate of a condition is represented by one data point. Clustering replicates are surrounded by 95 % confidence ellipses.

Validation of metabolome data – the adenylate energy charge

A fundamental determinant of cellular physiology is the energetic state, which can be quantified by the ratio between energy rich and energy poor adenylate nucleotides, referred to as the adenylate energy charge (AEC) (Atkinson, 1968). The AEC is in the range of 0.8 to 0.95 for growing cells and can be inferior in stressed, nutrient limited and engineered organisms (Thomas and Dawson, 1977; Kayser *et al.*, 2005; Bolten *et al.*, 2007; Boer *et al.*, 2010). In order to confirm the validity of the intracellular metabolome data, the AEC was calculated by the following equation:

$$AEC = \frac{[ATP] + 0.5 \cdot [ADP]}{[ATP] + [ADP] + [AMP]} \quad (\text{Eq. 3.2})$$

As the determined AEC was above 0.8 in all conditions (except for a slightly lower value of 0.75 in cells under osmoprotection), the collected metabolome data build a trustworthy representation of *B. subtilis*' *in vivo* situation under the here studied conditions.

Prerequisites for ^{13}C metabolic flux analysis

Condition-dependent macromolecular cell composition and reaction model

Macromolecular cell composition was reconstructed from previous biomass models for *B. subtilis* (Dauner and Sauer, 2001; Dauner *et al.*, 2001b; Oh *et al.*, 2007), yielding building block requirements of anabolic precursor metabolites (G6P, F6P, R5P, E4P, GAP, 3PG, PEP, PYR, AcCoA, 2OG, OAA) (Appendix Table 6.2).

Corrections include new findings in *B. subtilis*' lipid, lipoteichoic acid and fatty acid composition (Matsumoto *et al.*, 1998; de Mendoza *et al.*, 2003). The cell composition further considered the potential influence of salt adaptation of *Bacillus* to high salinity, particularly cellular changes in protein and ion content, intracellular amino acid pools quantified in this study, as well as variations in cell wall fraction and composition under osmotic stress. López *et al.* observed an increase in cardiolipin content, an altered ratio of glyco- to phospholipids, as well as differences in fatty acid composition under salt stress (López *et al.*, 1998; López *et al.* 2006; Dartois *et al.*, 1998).

The used biochemical network comprised 97 stoichiometric balance equations for pathways of central carbon metabolism including fluxes into biomass formation, metabolite export and precursor-amino acid relationships (Appendix Table 6.1). Reaction reversibilities were chosen according to (Dauner and Sauer, 2001).

Quality of the fit

The set of intracellular fluxes that gave the minimum deviation between experimental and simulated labeling patterns was taken as the best estimate for the intracellular flux distribution (Figure 3.13). Identical flux distributions were obtained with multiple initialization values for the free flux parameters, suggesting that global minima were identified in all examined cases. Obviously, a high level of agreement between experimentally determined and calculated labeling patterns, which differed on average by only about 1 %, was achieved (Appendix Table 6.3 and Table 6.4).

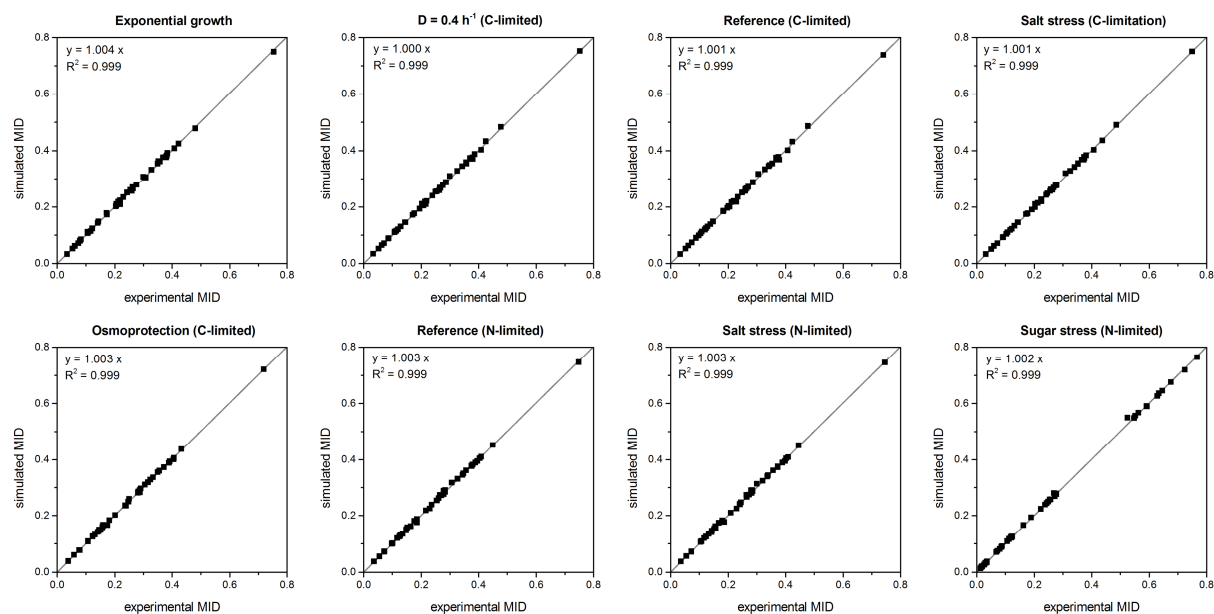


Figure 3.13: Optimal correlation of simulated and experimental mass isotopomer fractions of amino acids obtained from cell hydrolysates of *B. subtilis* BSB1 cultivated under different growth conditions using $[1-^{13}\text{C}]$ glucose as single tracer.

3.3 Adaptation of *Bacillus subtilis* carbon core metabolism to simultaneous nutrient limitation and osmotic challenge

Permanently fluctuating environmental conditions force biological systems to be highly adaptive and to remain in a vigilant state for upcoming changes. Cellular stress responses are complex and comprehend extensive interconnected transcriptomic, enzymatic and metabolic adjustments. One of the aims of systems biology is to delineate the functionality of regulatory mechanisms and cellular networks during those adaptation processes. The gram-positive soil bacterium *B. subtilis* is known for its capability to cope with drought and high salt concentrations in its environment. Besides, several *Bacillus* species are used in industrial bioprocesses for the production of technical enzymes, antibiotics, polymers, vitamins and organic acids, where it comes to a strong hyperosmotic burden for the cell, due to high substrate and salt concentrations as well as increasing product titers. These challenges require dynamic adjustments in gene expression, enzyme activity and metabolic fluxes to maintain survival, growth and adaptability of the cell. In nature and in most industrial fermentation processes, cells have to deal permanently with unfavourable low-growth conditions, that is why *B. subtilis*' long-term adaptation mechanisms are of special interest. In the present study, the global response of *B. subtilis* cells to salt stress and its recovery by the osmoprotectant glycine betaine (Boch *et al.*, 1994) was assessed at the level of protein and gene expression, and integrated with a detailed quantitative analysis of specific metabolic pathways.

Physiological adaptation to carbon-limited growth under salt stress and osmoprotection by glycine betaine

Salt stress somewhat decreased the biomass yield, which, however, was partially restored by the addition of glycine betaine (Table 3.3). In the presence of high salt, cells produced slightly more CO₂ and secreted trace amounts of leucine and valine. However, extracellular metabolite formation was generally weak under all conditions.

Table 3.3: Physiological data and carbon balance for *B. subtilis* BSB1 during chemostat growth on M9 minimal medium without further addition (reference), supplemented with 1.2 M NaCl (salt stress), and supplemented with 1.2 M NaCl and 1 mM glycine betaine (osmoprotection). The data comprise biomass yield ($Y_{X/S}$), specific rates for glucose uptake (q_S) and extracellular product formation (n=4).

	Unit	Reference	Salt stress	Osmoprotection
$Y_{X/S}$	$g_{DCW} mol^{-1}$	55.6 ± 5.8	44.1 ± 2.4	48.7 ± 3.2
q_S	$mmol g_{DCW}^{-1} h^{-1}$	1.8 ± 0.2	2.3 ± 0.1	2.1 ± 0.1
q_{CO_2}	$mmol g_{DCW}^{-1} h^{-1}$	6.7 ± 0.2	7.3 ± 0.3	7.6 ± 0.1
$q_{acetate}$	$\mu mol g_{DCW}^{-1} h^{-1}$	10.9 ± 1.1	12.0 ± 1.8	15.5 ± 3.3
$q_{pyruvate}$	$\mu mol g_{DCW}^{-1} h^{-1}$	1.3 ± 0.3	3.7 ± 0.3	1.5 ± 0.5
$q_{succinate}$	$\mu mol g_{DCW}^{-1} h^{-1}$	0.6 ± 0.2	1.1 ± 0.3	< 0.1
$q_{lactate}$	$\mu mol g_{DCW}^{-1} h^{-1}$	6.8 ± 1.4	< 0.1	< 0.1
$q_{oxoglutarate}$	$\mu mol g_{DCW}^{-1} h^{-1}$	< 0.1	6.7 ± 1.1	7.0 ± 2.0
$q_{isobutyrate}$	$\mu mol g_{DCW}^{-1} h^{-1}$	3.0 ± 1.2	29.2 ± 4.8	10.4 ± 2.6
$q_{isovalerate}$	$\mu mol g_{DCW}^{-1} h^{-1}$	3.4 ± 1.5	11.0 ± 2.0	9.4 ± 1.8
q_{valine}	$\mu mol g_{DCW}^{-1} h^{-1}$	< 0.1	36.7 ± 6.9	< 0.1
$q_{leucine}$	$\mu mol g_{DCW}^{-1} h^{-1}$	< 0.1	21.6 ± 2.8	< 0.1
$q_{protein}$	$mg g_{DCW}^{-1} h^{-1}$	26.6 ± 3.6	47.9 ± 2.6	53.2 ± 1.8
C recovery^a	%	98.3 ± 6.5	98.6 ± 6.8	101.4 ± 4.6

^a Estimation of the carbon balance considered measured carbon content of the biomass, which was 44.3 ± 0.1 (reference), 44.2 ± 1.0 (salt-stress) and 42.9 ± 0.9 % (osmoprotection). To account for the extracellular protein, a relative fraction of 53.5 % carbon was deduced from the protein composition of *B. subtilis* (Sauer *et al.*, 1996). The residual glucose level in the medium did not differ between the conditions ($25 \pm 9 \mu M$).

Stress response during carbon-limited growth is modulated by compatible solutes

The only compatible solute that *B. subtilis* can synthesize *de novo* is the amino acid proline (Whatmore *et al.*, 1990; Brill *et al.*, 2011). In this multi-omics analysis, the increased formation of proline at high osmolarity was reflected by the accumulation of mRNAs and proteins of the osmostress-responsive ProJ-ProA-ProH route (Figure 3.14).

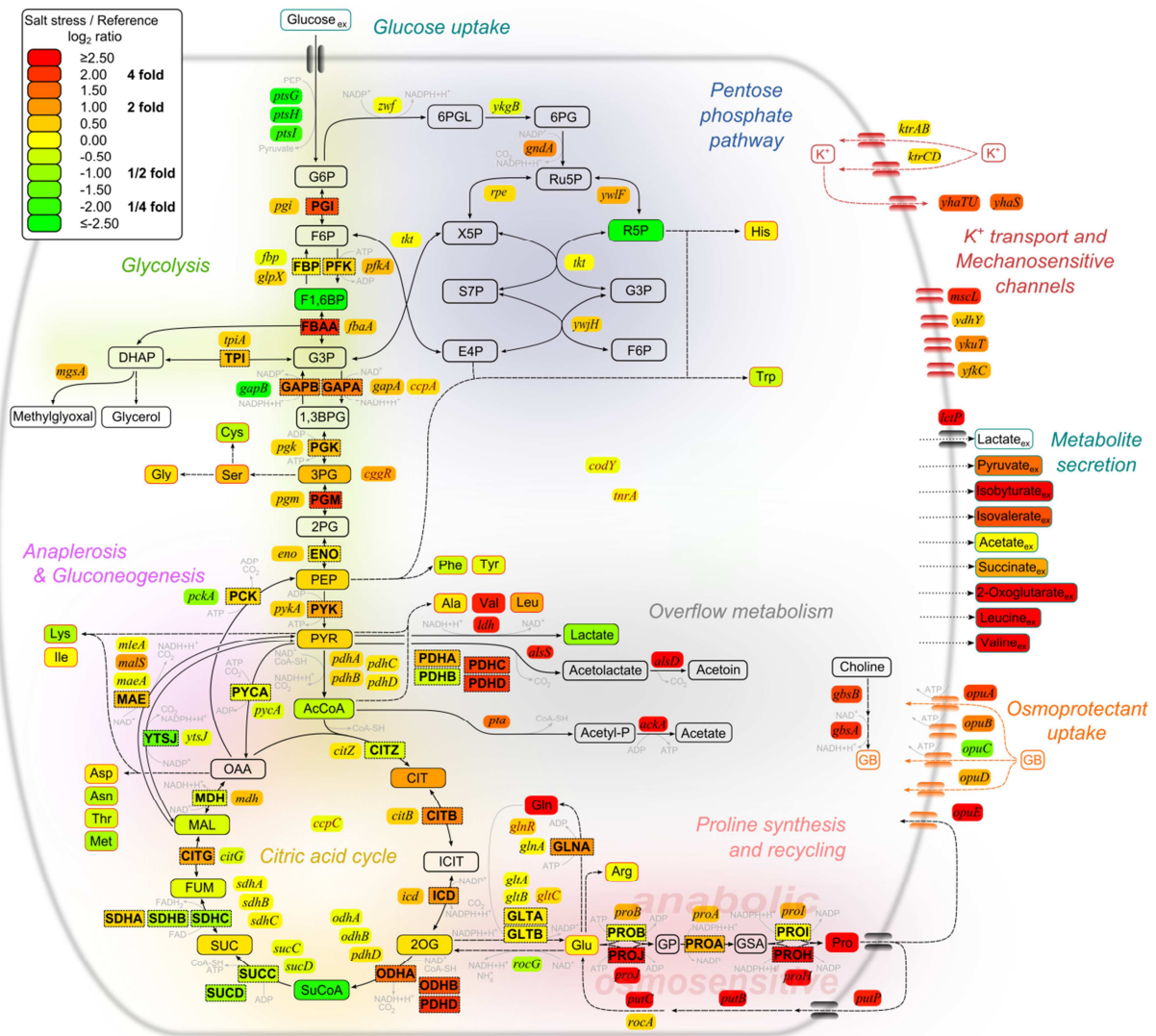


Figure 3.14: Integrated view of relative transcript, protein and metabolite concentrations in *B. subtilis*. Shown are changes in salt-stressed cells (in the presence of 1.2 M NaCl) compared to control conditions without additional salt. The data format is as follows: gene expression, italics; protein abundances, dashed rectangles; metabolite pools, rounded rectangles.

In particular, the amount of the *proH-proJ* mRNA was increased about seven-fold under osmotic stress conditions; and a corresponding up-regulation in the amounts of the ProH and ProJ enzymes was observed. In contrast, the cellular level of the ProA protein remained almost unchanged; a finding that is fully in agreement with the observation that *proA* transcription is not osmotically inducible (Brill *et al.*, 2011). Interestingly, the genes coding for catabolic proline uptake and breakdown, namely *putC*, *putB* and *putP*, were also activated. This suggests a cyclic pathway with simultaneous synthesis and degradation of proline, potentially involved in fine-tuning of the proline pool as osmoprotectant and as nitrogen and carbon source under the nutrient limiting conditions in the chemostat which relieves

catabolite repression (Singh *et al.*, 2008). It might also result from leakage of proline from the salt stressed cells thus ensuing PutR-mediated induction of the *putBCP* operon (Hoffmann *et al.*, 2012; Moses *et al.*, 2012). The expression of the glutamate synthase complex (GltAB) slightly decreased in the presence of high salt, despite the increased requirement to produce the proline precursor glutamate. This coincided with a repression of glutamate dehydrogenase gene *rocG* and a two-fold increase of glutamate regenerating GlnA, possibly acting as a driving force towards proline.

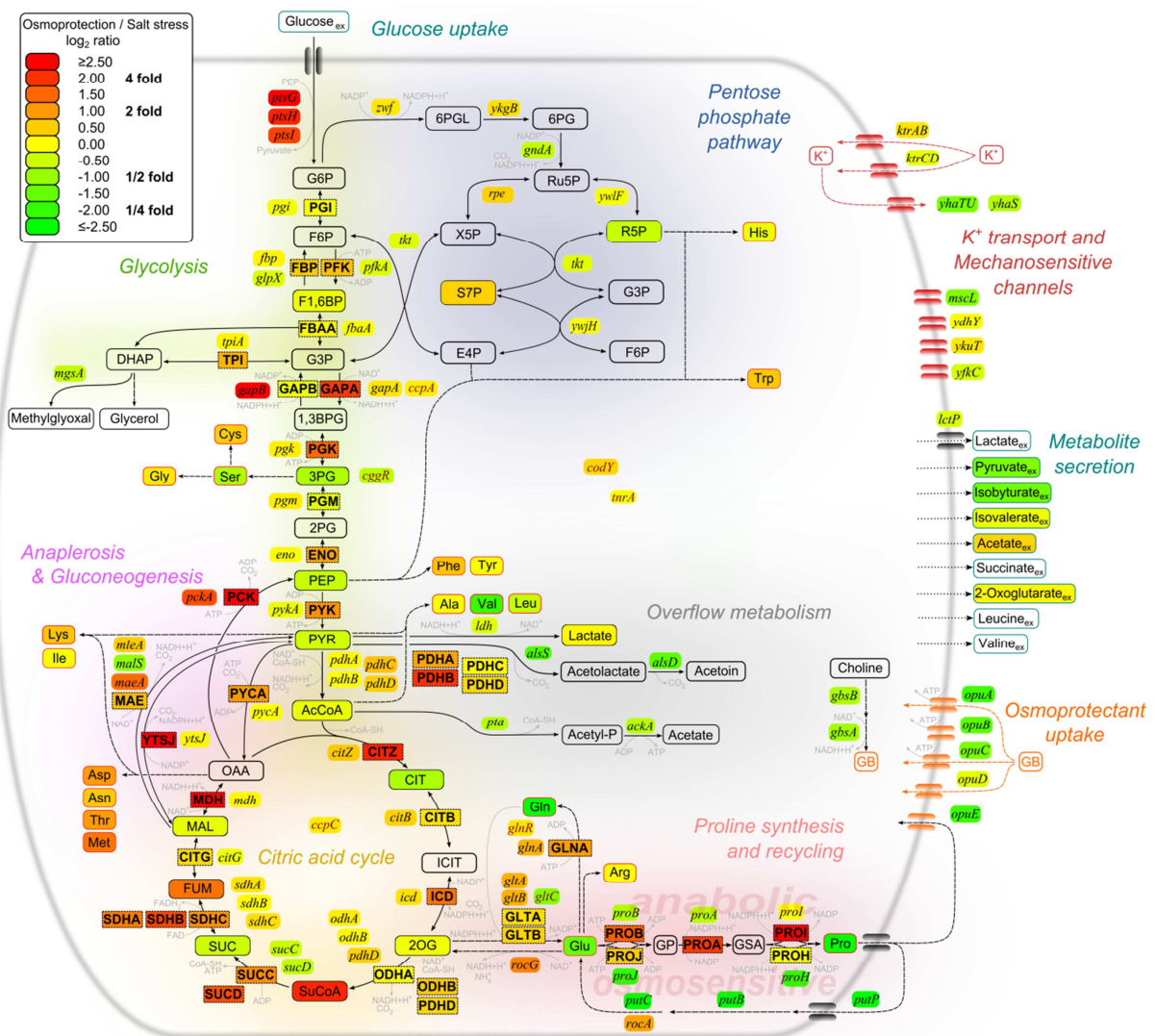


Figure 3.15: Integrated view of relative transcript, protein and metabolite concentrations in *B. subtilis*. Shown are changes in protected salt-stressed cells (in the presence of 1.2 M NaCl and 1 mM glycine betaine) compared to salt-stressed cells (without glycine betaine). The data format is as follows: gene expression, italics; protein abundances, dashed rectangles; metabolite pools, rounded rectangles.

Both enzymes, glutamine synthetase and glutamate synthase, form the so-called GS-GOGAT cycle that regulates assimilation and utilization of nitrogen (Gunka and Commichau, 2012). In the presence of externally provided glycine betaine, expression of the osmostress-responsive proline biosynthesis pathway was significantly reduced but still occurred above the level observed under reference conditions (Figure 3.15). This observation is in excellent agreement with the recently reported finely tuned repressing effect of glycine betaine on the cellular proline pool (Hoffmann *et al.*, 2013).

Selected flux switch points enable homeostasis in the carbon core network

The intracellular flux distribution of *B. subtilis* was quantified by a comprehensive approach, which integrated experimental data on growth stoichiometry (Table 3.3), cellular composition, corrected to reflect the impact of salt (Appendix Table 6.2), and ^{13}C labeling patterns of proteinogenic amino acids (Table 2.2 and Appendix Table 6.3) together with metabolite and isotopomer balancing. Under all tested conditions, *B. subtilis* recruited both, glycolysis and PP pathway, for the metabolization of glucose (Figure 3.16). Hereby, the PP pathway flux exceeded the anabolic requirement for intermediates from this pathway, so that a substantial fraction of carbon was channelled back into the lower glycolytic chain. Anaplerotic pyruvate carboxylase fuelled the TCA cycle with a flux of 45 %. Despite the growth on glucose, significant fluxes through gluconeogenic PEP carboxykinase and the malic enzyme(s) were detected. Simultaneous operation of PEP carboxykinase, pyruvate kinase and pyruvate carboxylase constitute an ATP-dissipating cycle with the net loss of one mole ATP per turn (Sauer and Eikmanns, 2005). In general, these fluxes around the PEP-PYR-OAA node contribute to the supply of energy and reducing power (NADPH) for biosynthetic reactions. Carbon flux through the TCA cycle was rather high, due to the lack of significant overflow metabolism known from unlimited growth that otherwise might have channelled carbon to acetate, lactate and acetoin. Overall, fluxes agreed rather well with recent estimates under similar conditions (Dauner *et al.*, 2001a; Tännler *et al.*, 2008). Figure 3.16 and Figure 3.17A highlight the flux response of *B. subtilis* to the imposed salt stress. Remarkably, cells were able to maintain overall fluxes throughout the core network, by specifically adjusting the split ratio at two distinct nodes.

Most pronounced, the flux at the level of 2-oxoglutarate was redirected from cyclic operation of the TCA cycle towards enhanced synthesis of glutamate, glutamine, and particularly proline to cope with the osmotic burden. The glutamate pool remained constant at about $700 \mu\text{mol g}_{\text{DCW}}^{-1}$. The related amino acids glutamine and proline show much smaller concentrations of 30 and $60 \mu\text{mol g}_{\text{DCW}}^{-1}$, respectively. Under salt stress, however, intracellular concentrations of glutamine and proline were 15- and 20-fold increased.

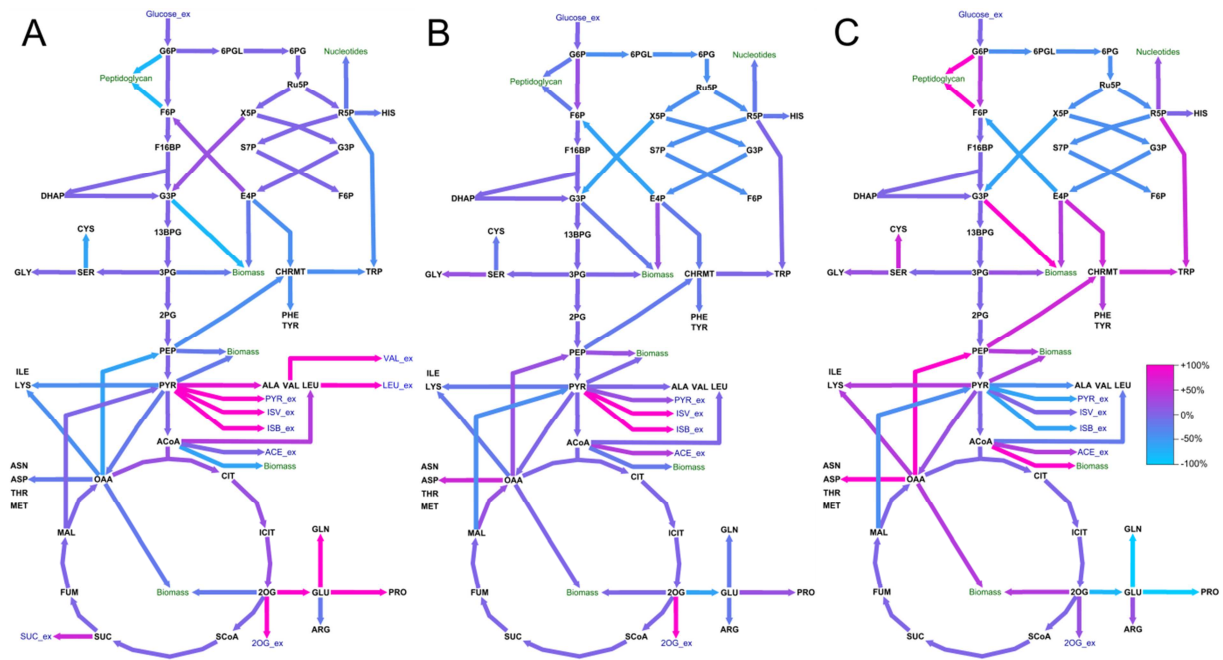


Figure 3.17: Carbon core metabolism largely maintains flux homeostasis. **(A)** Flux change in percent in salt-stressed cells (1.2 M NaCl) compared to non-stressed cells; **(B)** Flux change in percent in osmoprotected cells (1.2 M NaCl, 1 mM glycine betaine) compared to non-stressed cells; **(C)** Flux change in percent in osmoprotected cells compared to non-protected cells. Arrow colors indicate positive (fuchsia) and negative (cyan) flux changes. Unchanged fluxes are given as violet arrows. Non-standard abbreviations for metabolites: ACE, acetate; ACoA, acetyl-coenzyme A; CHRMT, chorismate; CIT, citrate; DHAP, dihydroxyacetone phosphate; E4P, erythrose 4-phosphate; F6P, fructose 6-phosphate; F16BP, fructose 1,6-bisphosphate; FUM, fumarate; G6P, glucose 6-phosphate; G3P, glyceraldehyde 3-phosphate; 13BPG, 1,3-bisphosphoglycerate; 2PG, 2-phosphoglycerate; 3PG, 3-phosphoglycerate; ISB, isobutyrate; ICIT, isocitrate; ISV, isovalerate; LAC, lactate; MAL, malate; OAA, oxaloacetate; 2OG, 2-oxoglutarate; 6PG, 6-phosphogluconate; 6PGL, 6-phosphogluconolactone; PEP, phosphoenolpyruvate; PYR, pyruvate; R5P, ribose 5-phosphate; Ru5P, ribulose 5-phosphate; S7P, sedoheptulose 7-phosphate; SUC, succinate; SCoA, succinyl-coenzyme A; X5P, xylulose 5-phosphate. Amino acids are abbreviated according to the standard three letter code.

Secondly, fluxes at the pyruvate node partly switched from anaplerosis to increased

intracellular levels of the branched chain amino acids valine and leucine and branched chain keto acids derived from them (Figure 3.14, Figure 3.16 and Figure 3.17A). The remaining flux network revealed only slight changes.

Flux changes at the 2-oxoglutarate and pyruvate nodes were not observed, when glycine betaine was added to salt-stressed cells (Figure 3.17B). Again, the cell recruited selected switch points in the metabolic network to balance overall flux. Particularly, flux towards glutamate-based amino acids and pyruvate-based metabolites and consequently intra- and extracellular levels of these compounds and their precursors were reduced in comparison with salt stressed cells (Figure 3.15, Figure 3.16 and Figure 3.17C). Importantly, the PP pathway flux also decreased under conditions of osmoprotection by glycine betaine, an observation that is in excellent agreement with a reduced demand for *de novo* synthesis of the osmoprotectant proline and also a three-fold decreased intracellular glutamate pool. *B. subtilis* was able to maintain its metabolic machinery, even under extremely changed environmental conditions. By holding up flux homeostasis through large parts of the metabolic network, cells maintained their high-energy status under salt stress and osmoprotection conditions, as compared with reference cells (Table 3.4).

Table 3.4: Intracellular levels of nucleotides for non-stressed, salt-stressed and osmoprotected *B. subtilis* cells, grown in chemostat cultures at 0.1 h^{-1} ($n=3$). The energy level is expressed by the adenylate energy charge (AEC) (Atkinson, 1968).

	Unit	Reference	Salt stress	Osmoprotection
AMP	$\mu\text{mol g}_{\text{DCW}}^{-1}$	1.9 ± 0.5	1.5 ± 1.4	1.2 ± 0.5
ADP	$\mu\text{mol g}_{\text{DCW}}^{-1}$	4.1 ± 0.6	5.8 ± 3.3	2.8 ± 0.3
ATP	$\mu\text{mol g}_{\text{DCW}}^{-1}$	19.2 ± 2.3	17.4 ± 6.8	6.3 ± 1.4
GTP	$\mu\text{mol g}_{\text{DCW}}^{-1}$	5.2 ± 2.5	1.7 ± 0.4	1.4 ± 0.3
AEC		0.84 ± 0.03	0.83 ± 0.04	0.75 ± 0.02

Flux homeostasis recruits distinct transcriptional rearrangements in core metabolic pathways

Hierarchical cluster analysis of expression patterns for genes of carbon core and proline metabolism revealed pronounced responses (Figure 3.18). Salt stress stimulated expression of genes physiologically connected with overflow pathways for the production of

acetoin, acetate and lactate. These changes were reversed under conditions of cellular osmoprotection by glycine betaine (Figure 3.18). In agreement with the increased demand for proline in salt-stressed cells, virtually all genes of the TCA cycle down to the 2-oxoglutarate node were slightly induced, whereas the downstream part of the TCA cycle was not activated. This observation is in full agreement with previous data derived from a proteome and transcriptome analysis of severely salt-shocked cells (Höper *et al.*, 2006; Hahne *et al.*, 2010). The genes *gndA* and *mals* encoding gluconate 6-phosphate dehydrogenase and a decarboxylating malic enzyme, respectively, were up-regulated under salt stress. Both are involved in intracellular balancing of NADPH (Rühl *et al.*, 2012). In contrast, expression of the two gluconeogenic enzymes, PEP carboxykinase (*pckA*) and NADP⁺-dependent malic enzyme (*ytsJ*) was repressed at high-salt. Overall, gene expression changes indicated concerted activation of the full biosynthetic chain from glucose 6-phosphate, the entry point of the substrate glucose into cellular metabolism, to synthesis of proline: hence, adjustments in metabolism across multiple pathways occur. It is interesting to note that the underlying change in gene expression comprised co-regulated modules (Figure 3.18). These modules mainly contained genes from pyruvate-based overflow metabolism and osmostress adaptive proline synthesis (Figure 3.18, cluster a), ammonium metabolism and TCA cycle (Figure 3.18, cluster b), glutamate and glutamine synthesis (Figure 3.18, cluster c) and glycolysis (Figure 3.18, cluster d). Together, expression of these modules is adjusted in a way to (i) keep the core metabolic fluxes constant under the simultaneously imposed carbon limitation and salt stress, and (ii) provide the cell with the metabolic resources to synthesize the vast amounts of proline and its precursors required to protect it against the detrimental effects of high salinity.

Glycine betaine restores the expression of carbon core metabolic genes

Glycine betaine is a very effective osmoprotectant for *B. subtilis* with pronounced beneficial effects on cell growth (Boch *et al.*, 1994). Presence of externally provided glycine betaine reduces the need for proline at high salt concentration (Hoffmann *et al.*, 2013). Accordingly, the osmosensitive pathway towards proline was shut off under osmoprotection (Figure 3.15 and Figure 3.18). Furthermore, expression of genes constituting the carbon core metabolic network was restored to the levels, observed under reference conditions (i.e. in the absence of salt stress).

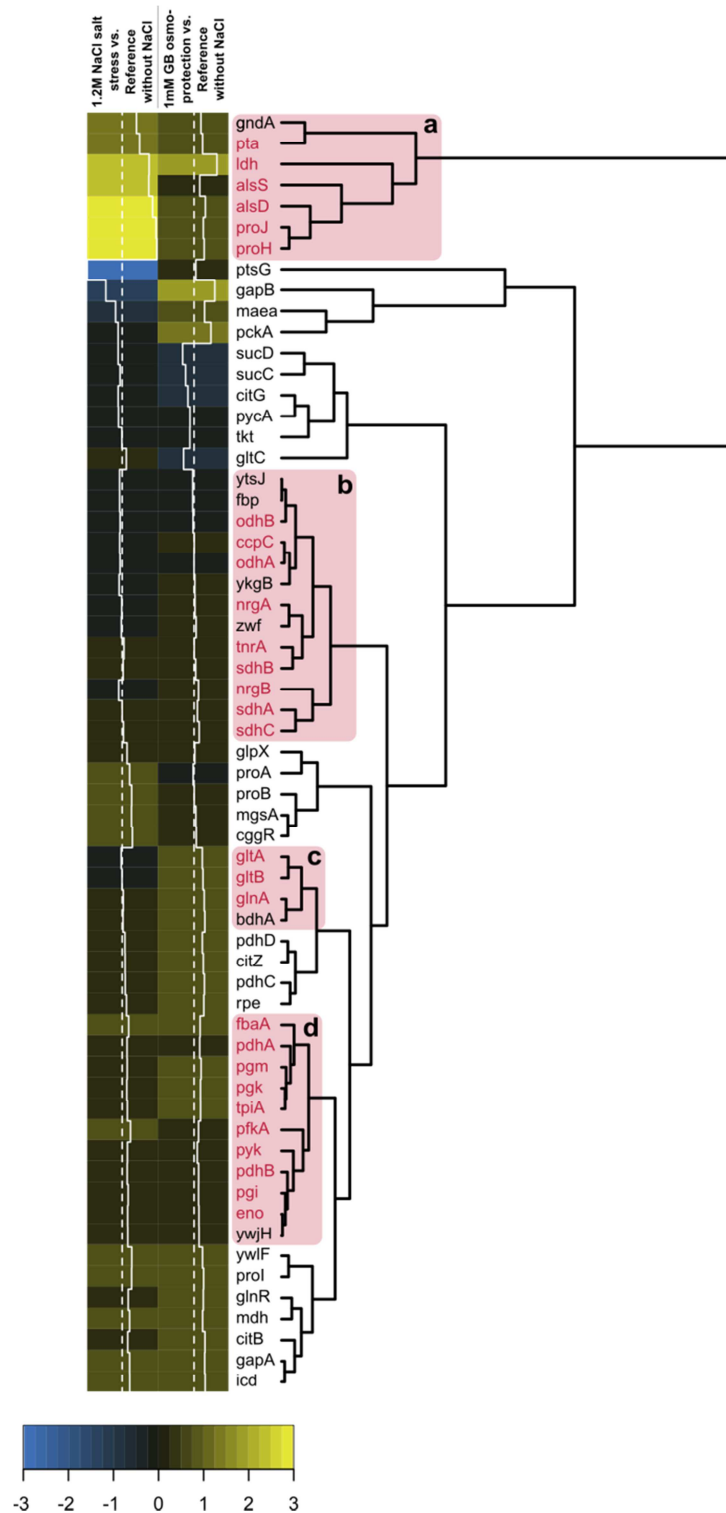


Figure 3.18: Hierarchical cluster analysis of gene expression of 61 genes in carbon core metabolism, glucose uptake, and glutamine, glutamate and proline metabolism, respectively (selected according to SubtiWiki database version 2013/2) (Mäder *et al.*, 2012). Four functional branches can be identified containing mainly (a) genes of osmosensitive proline synthesis, (b) genes belonging to ammonium metabolism and citric acid cycle, (c) genes involved in glutamate synthesis and (d) genes coding for glycolytic enzymes. Red coloration of gene names indicates functionally related genes within a cluster.

While expression levels of most of these genes were fully restored, reversion of the expression levels of few genes did not reach or exceed the reference levels (Figure 3.18). In particular, this was observed for genes of overflow metabolism and the gluconeogenic genes *pckA* and *gapB*, respectively. Apart from the restoration of gene expression of carbon core metabolism in the presence of glycine betaine, the overall transcriptional state of osmoprotected cells differed substantially from that of both reference and stressed cells (Figure 3.12).

Global gene expression changes are linked to salt stress and osmoprotection

Salt stress and osmoprotection of salt-stressed cells resulted in a variety of additional responses in gene expression beyond central carbon metabolism. Compared to non-stressed reference cells, 734 of the 4,105 analyzed genes were significantly induced at least two-fold at high osmolarity ($p < 0.05$, Student t-test, FDR corrected) (Figure 3.19, brown circle).

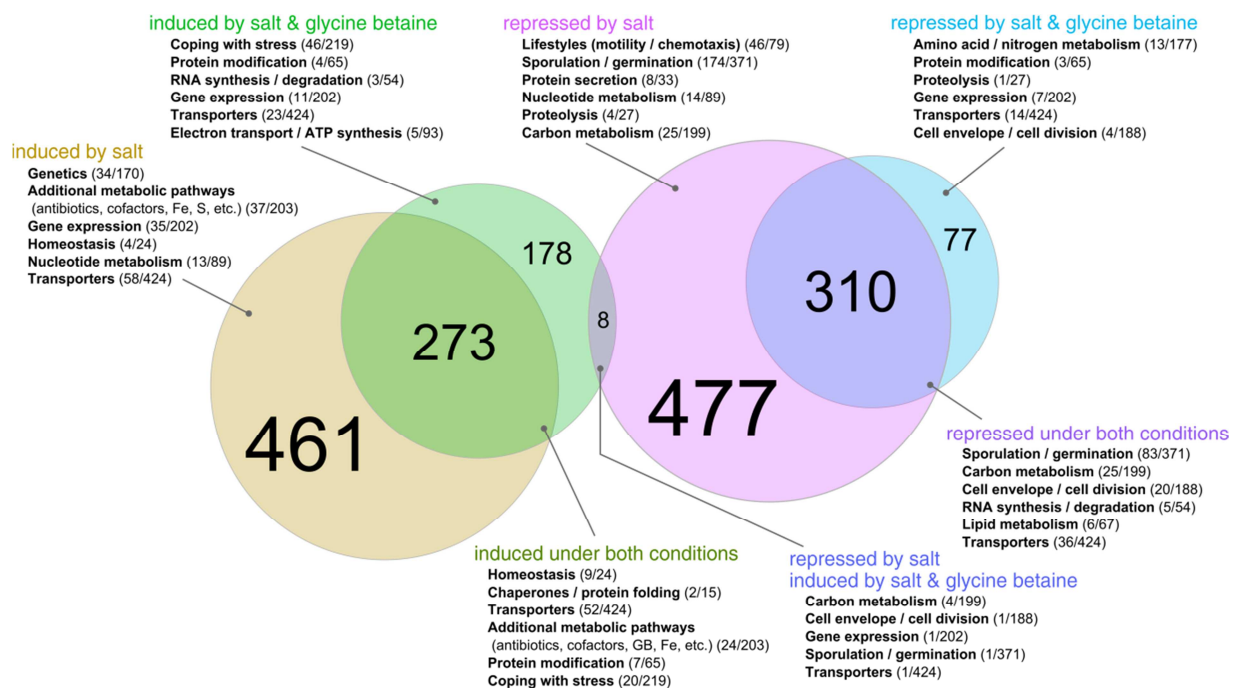


Figure 3.19: Effect of salt and glycine betaine on global gene expression in *B. subtilis* BSB1 under carbon limitation ($D = 0.1\text{h}^{-1}$). Shown genes are at least two-fold altered (Student t-test, $p < 0.05$, FDR corrected) compared to non-stressed cells. Overlapping areas in the Venn diagram represent genes, which are affected under both growth conditions (1.2 M NaCl; 1.2 M NaCl + 1 mM glycine betaine), whereas remaining circle areas are condition-specific. The most affected functional gene classes obtained from gene set enrichment analysis are listed for each subset. The functional categories were adopted from the SubtiWiki database (Version 2013/2) (Mäder *et al.*, 2012).

In addition to the effects on carbon core and proline metabolism, up-regulated genes included osmoprotectant uptake systems (*opuA*, *opuE*), genes involved in cell wall (*yqiHIK*, *cwlK*, *ltaS*, *yocH*, *ydjM*) (Steil *et al.*, 2003; Fischer and Bremer, 2012) and lipid metabolism (*ywpB*, *psd*) (López *et al.*, 1998; López *et al.*, 2002) as well as genes induced in response to salt stress-triggered iron limitation (Hoffmann *et al.*, 2002; Steil *et al.*, 2003) such as siderophore synthesis (*dhbABCEF*) and iron acquisition (*feuABC*, *fhuC*, *besA*). Additionally, higher expression levels were observed for genes involved in glycine betaine synthesis (*gbsAB*) (Nau-Wagner *et al.*, 2012), mechanosensitive channels (*mscL*, *ykuT*) (Hoffmann *et al.*, 2008; Hahne *et al.*, 2010), potassium efflux (*yhaSTU*) (Fujisawa *et al.*, 2007), sodium transport (*mrpABCDGEF*) (Kajiyama *et al.*, 2007) and synthesis of antimicrobial compounds (*srfA*, *sboA*, and *sunA* operons).

In agreement with known cellular responses to high osmolarity, a group of 795 genes that were repressed by salt (Figure 3.19, violet circle) comprised genes involved in cell wall and lipid metabolism (*lytF*, *lytD*, *fadM*, *ywjEF*, *acdA*, *des*), chemotaxis and motility (σ_D regulon) (Steil *et al.*, 2003) as well as genes encoding extracellular degradative enzymes (*wapA*, *epr*) (Dartois *et al.*, 1998; Steil *et al.*, 2003). *B. subtilis* genes, involved in biosynthesis of purines and in transport and salvage of purine bases are regulated in response to adenine levels by the PurR repressor (Weng *et al.*, 1995). Strikingly, 15 of these genes (*purE-D*, *xpt-pbux*, *pbuG*) are known to be regulated by a guanine-responsive riboswitch (G-box) (Mandal *et al.*, 2003). Most of them are down-regulated under high salt growth conditions.

B. subtilis is well-known for its ability to produce highly stress resistant endospores, a complex developmental program that is triggered by nutrient limitations (Piggot and Hilbert, 2004). In chemostat experiments, a large number of sporulation-related genes were among those genes that exhibited lower expression levels under high salt growth conditions. This is a reflection of the fact that a certain fraction of the *B. subtilis* cells in the chemostat cultures sporulated under reference, but not under salt-stress conditions, since sporulation is known to be blocked at an early stage at high salinity (Kunst and Rapoport, 1995; Ruzal *et al.*, 1998). The sporulation frequency in the non-salt-stressed chemostat cultures was roughly 10 %. Upon exposure to high salt cells seemingly reduced their potential to use alternative carbon sources, which is not a readily expected property of glucose-limited cells. The expression of genes encoding transporters and catabolic enzymes for various carbon substrates such as sugars, sugar alcohols, polysaccharides, amino sugars, organic acids and overflow

metabolites were down-regulated. Most probably, this is a reflection of the strong expression of a large part of the CcpA regulon in the 10 % of the population that undergoes sporulation under control conditions, because high expression of the same group of genes was seen in cells undergoing sporulation in Sterlini and Mandelstam medium (Nicolas *et al.*, 2012).

When glycine betaine was provided to salt-stressed cells, altogether 387 genes were significantly down-regulated, as compared to non-stressed cells (Figure 3.19, blue circle), including many genes that were induced at high osmolarity and for which this effect was partially or completely reversed in the presence of glycine betaine, like for example *opuE*, *yqilHK*, *cwlK*, *ydjM*, *ywpB*, *psd*, and *mscL*.

Genes, exclusively down-regulated by the presence of glycine betaine, are involved in synthesis of antibiotics (*ywfB*), modification and degradation of proteins (*ywlE*, *nprE*), metabolism of signaling nucleotides (*yuxH*), utilization of branched-chain keto acids (*buk*, *ptb*, *lpdV*, *bcd*), peptide and amino acid uptake (*alsT*, *appABCDF*, *ybaF*), DNA repair (*smf*), fatty acid biosynthesis (*fabHB*) and sulfonate uptake (*ssuBCD*).

On the other hand, 459 genes were significantly higher expressed under conditions of osmoprotection (Figure 3.19, green circle). Sixty percent of them are also induced in the absence of glycine betaine. The 186 genes exclusively up-regulated when glycine betaine is available include genes of cell wall (*lytAB*, *yrvJ*, *murD*) and lipid metabolism (*cypC*, *glpD*, *glpT*, *yhdN*), chemotaxis (*tlpA*), ribosome binding (*ytiA*), control of phosphorelay (*phrE*), iron uptake and Ca²⁺ export (*yhfQ*, *yfkE*), extended carbon metabolism (*mtlD*, *mmsA*, *yflS*, *citM*, *cysE*), nucleotide metabolism (*ydaK*, *cdd*) and synthesis of RNA chaperones (*cspD*).

It is interesting to note that there were eight genes that were down-regulated in the presence of salt, but were up-regulated when glycine betaine was provided. These genes are responsible for utilization and transport of acetoin (*acoR* regulon), glycerol 3-phosphate (*glpT*) and glucosamine (*gamA*). Besides, intracellular glucosamine was found solely in osmoprotected cells. Also within this group is *mgsR*, a gene coding for a transcriptional regulator of the σ_B regulon and *sivC*, coding for a sporulation inhibitor.

***B. subtilis* responds to osmotic stress and osmoprotection by adjustment of its bio-catalytic machinery**

As mentioned above, the gene expression in carbon core metabolism was mainly restored in the presence of glycine betaine. This, however, was not reflected at the protein and metabolite level (Figure 3.15, Appendix Figure 6.1). This supports the idea that not all physiological changes in a cell can be traced back to alterations in gene expression (Schilling *et al.*, 2007; Chubukov *et al.*, 2013). To further investigate the influence of salt stress and glycine betaine on cellular physiology under conditions of carbon limitation, we determined the absolute concentrations of 39 proteins and protein complex subunits of central carbon metabolism and of the proline synthesis pathway using the QconCAT technology.

Generally, the proteins differed quite substantially in their intracellular abundance. Citrate synthetase (CitZ), isocitrate dehydrogenase (Icd), malate dehydrogenase (Mdh) and glutamine synthetase (GlnA) were among the most abundant proteins of carbon core metabolism under all conditions. The three TCA cycle enzymes indeed form a protein complex that may be involved in substrate channeling through this pathway (Meyer *et al.*, 2011; Bartholomae *et al.*, 2013). Concerning the enzymes of proline synthesis, the dual-function enzyme ProA showed a higher abundance than all other proteins of this biosynthetic pathway under all conditions.

The salt stress had a pronounced effect on the protein level, far beyond that what was expected from simple inspection of the transcriptome data. The presence of 1.2 M NaCl increased the intracellular level of most measured proteins (Figure 3.20). This included mainly enzymes of glycolysis and TCA cycle down to the node of 2-oxoglutarate, such as phosphoglucoisomerase (Pgi), phosphoglycerate mutase (Pgm), fructose 1,6-bisphosphate aldolase (FbaA), glyceraldehyde 3-phosphate dehydrogenase (GapA), pyruvate dehydrogenase subunits (PdhCD) and isocitrate dehydrogenase (Icd). In contrast, subunits and proteins of the downstream part of the TCA cycle, succinyl-CoA synthetase (SucCD), succinate dehydrogenase (SdhBC), malate dehydrogenase (Mdh), and NADP⁺-dependent malic enzyme (YtsJ) were present in lower amounts, which nicely matched with the flux re-routing from the TCA cycle to proline.

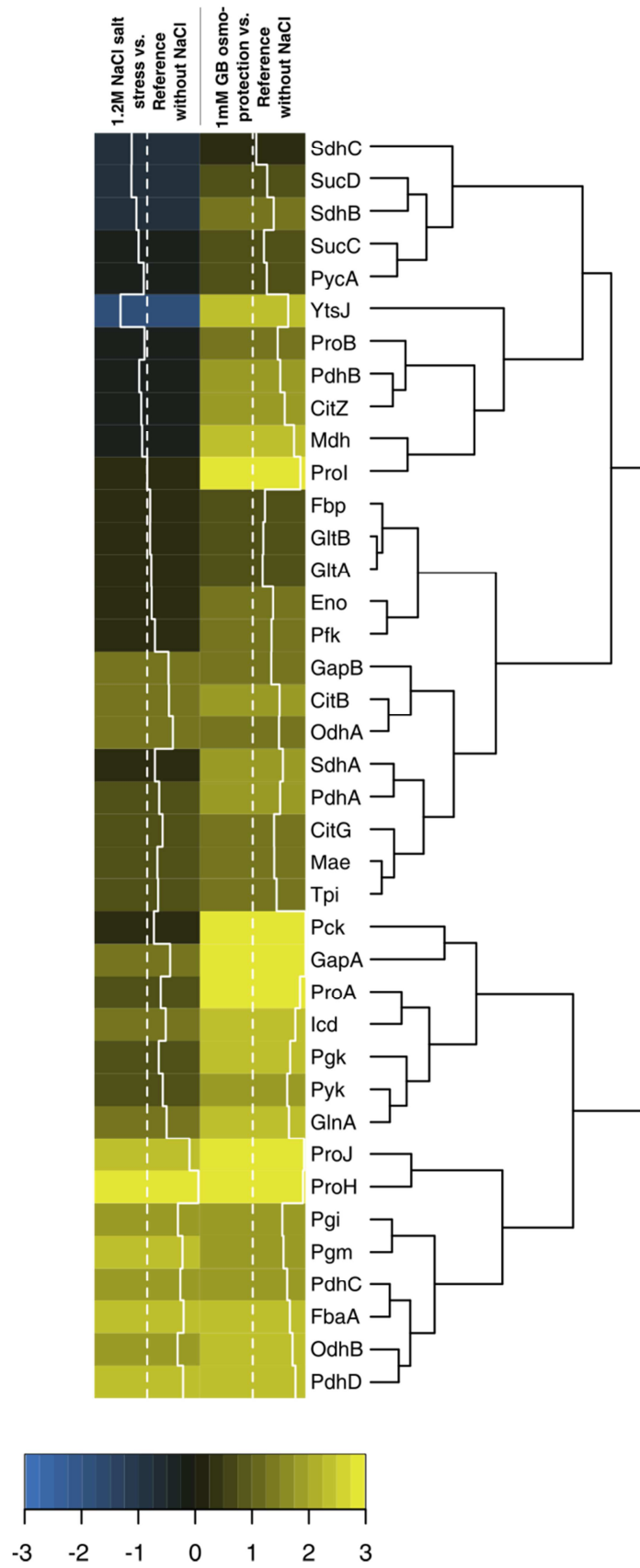


Figure 3.20: Hierarchical cluster analysis of expression of 39 proteins and protein complex subunits of carbon core metabolism and proline metabolism.

The intracellular abundance of about half of all detected proteins was even further increased, when glycine betaine was added to the salt-stressed cells (Figure 3.20). The effect was most pronounced for proteins of the TCA cycle metabolon (CitZ-Icd-Mdh), gluconeogenic enzymes (PckA, YtsJ, GapB) and the anabolic proline synthesis pathway (ProA, ProB, ProI), but impacts also complexes or individual subunits such as SucCD, SdhABC and PdhAB and the glycolytic enzymes. Interestingly, changes in the amount of protein complex subunits were not always stoichiometric. For instance, whereas the quantity of subunit PdhA and PdhB of the pyruvate dehydrogenase complex was not affected by salt stress, the two remaining subunits PdhC and PdhD showed an about four-fold increase, suggesting that the original protein complex stoichiometry under reference conditions is not necessarily maintained. SdhABC was affected in a similar manner. Despite the reduced requirement for proline under osmoprotection, ProJ and ProH were still present in the same quantities as under salt stress without glycine betaine.

Salt-dependent inhibition of enzyme activity is counterbalanced by increase in metabolic protein amounts

On first view, the obviously homeostatic flux state of many of the biochemical conversions in carbon core metabolism (Figure 3.17) seemed to be in contradiction to the strongly increased level of many of the involved high flux proteins (Figure 3.20). However, salt-stressed cells of *B. subtilis* exhibit not only elevated levels of proline, but also increases in their intracellular potassium reaching concentrations up to 600 mM (Whatmore *et al.*, 1990). This obviously results in an altered chemical environment (Wood, 2011). To shed light on the underlying mechanisms, the impact of salt ions on protein activity was investigated for selected proteins by *in vitro* measurements that try to mimic the three different *in vivo* scenarios in the chemostat. Indeed, elevated levels of potassium reduced the catalytic activity of enzymes of all pathways of central carbon metabolism (Table 3.5). Cell extracts were exposed to a K⁺ shift from physiologically normal levels of 300 mM to 600 mM in presence or absence of proline and glycine betaine.

Table 3.5: Specific activity of enzymes from carbon core metabolism of *B. subtilis* grown on M9 medium. The assay mixture was untreated for the reference, and amended with effectors to mimic salt stress (600 mM KCl, 500 mM proline), and osmoprotection (600 mM KCl, 25 mM proline, 650 mM glycine betaine). Effector concentrations were chosen according to (Hoffmann *et al.*, 2013) and (Whatmore *et al.*, 1990). In addition, the effect of potassium ions alone was studied by addition of 300 mM and 600 mM KCl. All experiments are carried out in triplicates (n=3). The enzyme activity is given in $\mu\text{mol min}^{-1} (\text{mg protein})^{-1}$.

Enzyme	Condition			
	Reference	600 mM K ⁺	Salt stress	Osmoprotection
	300 mM KCl, 25 mM proline	600 mM KCl	600 mM KCl, 500 mM proline	600 mM KCl, 25 mM proline, 650 mM glycine betaine
Glucose 6-phosphate isomerase	2.101 ± 0.009	1.387 ± 0.031	1.233 ± 0.017	1.798 ± 0.023
Fructose 1,6-bisphosphate aldolase	0.049 ± 0.003	0.030 ± 0.003	0.030 ± 0.003	0.051 ± 0.006
Pyruvate kinase	0.231 ± 0.014	0.191 ± 0.000	0.191 ± 0.000	0.183 ± 0.014
Glucose 6-phosphate dehydrogenase	0.375 ± 0.003	0.302 ± 0.009	0.301 ± 0.010	0.315 ± 0.009
6-phosphogluconate dehydrogenase	0.205 ± 0.010	0.090 ± 0.005	0.103 ± 0.010	0.151 ± 0.010
Citrate synthase	0.141 ± 0.005	0.089 ± 0.004	0.101 ± 0.014	0.120 ± 0.019
Isocitrate dehydrogenase	1.640 ± 0.031	1.140 ± 0.020	1.199 ± 0.004	1.406 ± 0.039
Malate dehydrogenase	0.561 ± 0.054	0.585 ± 0.028	0.519 ± 0.042	0.670 ± 0.031
Fructose 1,6-bisphosphatase	0.203 ± 0.008	0.116 ± 0.012	0.107 ± 0.002	0.184 ± 0.005
Malic enzyme	0.009 ± 0.003	0.015 ± 0.006	0.018 ± 0.003	0.018 ± 0.003

Obviously, the cell partially compensates for the reduced enzyme activities by producing more of these enzymes (Figure 3.20). The specific activity of malic enzyme and malate dehydrogenase were not affected by elevated potassium concentrations. It is interesting to note that proline itself, added in stress-induced amounts, could not regain the catalytic efficiency of the proteins. However, addition of 650 mM glycine betaine, reflecting the intracellular state at 1.2 M NaCl and 1 mM glycine betaine in the medium, could partially restore the original enzyme activity (Table 3.5). The adaption of the catalytic protein amounts to compensate for lower specific activity at the increased salt concentration seemed a fundamental strategy of *B. subtilis* to cope with the stress conditions. The observed stabilizing and activating effect of glycine betaine on enzyme activity might explain its efficient osmoprotection in *B. subtilis*. Together with previous reports, one can assume that glycine betaine is a better osmoprotectant than proline (Cayley and Record, 2003; Wood, 2011).

The cell recruits functional modules across individual metabolic pathways

The here presented multi-omics approach provides a complex picture of the cellular adjustment of *B. subtilis* to dual stress conditions. The above inspection of the various omics data sets reveals a link between the different cellular components during the stress response (Figure 3.21). However, pairwise comparison of changes in gene expression, protein abundance, metabolite level and flux reveal only poor correlations (Figure 3.21).

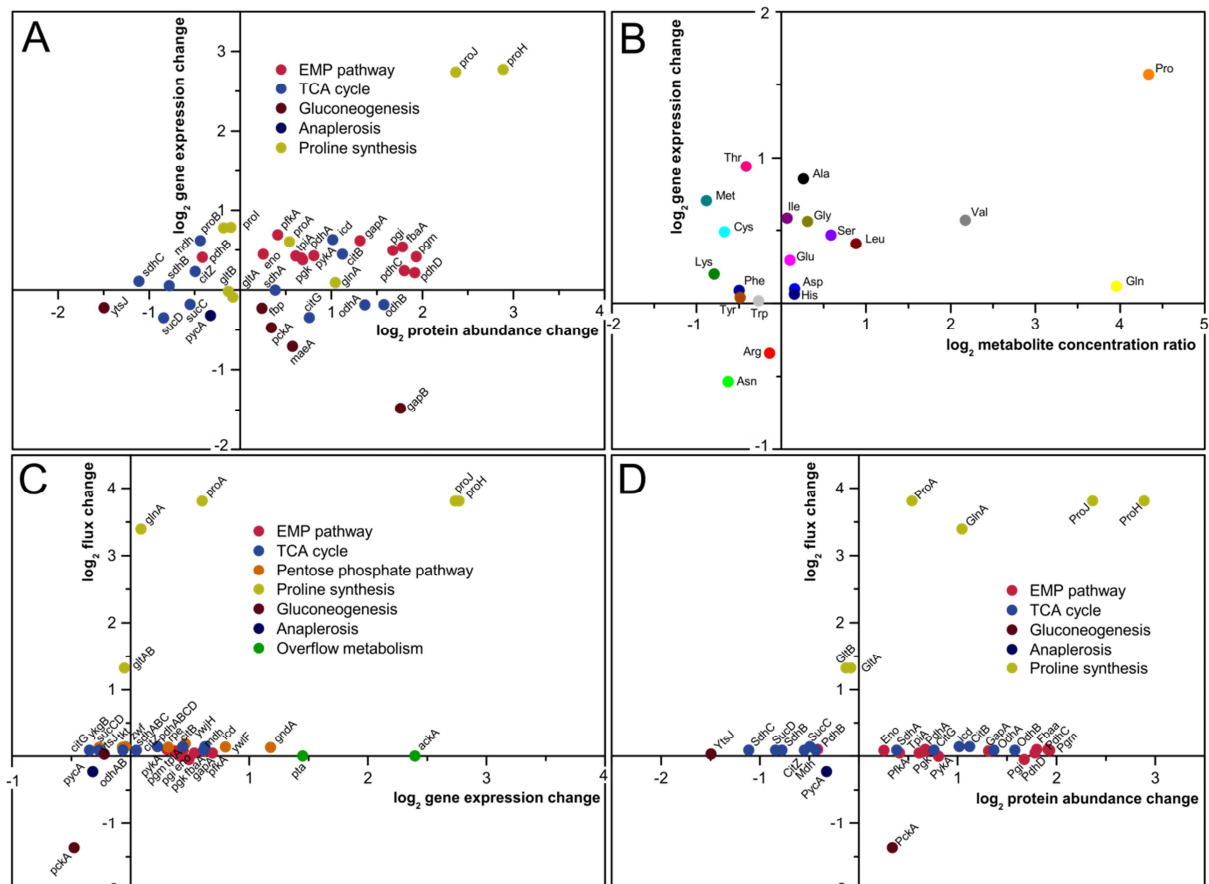


Figure 3.21: Multi-omics correlation plots of gene expression, protein and metabolite level, and metabolic flux in central carbon metabolism of salt-stressed *B. subtilis* compared to non-stressed cells. Pairwise comparison of logarithmic changes in (A) gene expression and protein level, (B) expression of amino acid biosynthesis genes and the corresponding intracellular amino acid concentration (transcription level reflects the average expression of all genes coding for the biosynthesis pathway of the corresponding amino acid), (C) metabolic flux and gene expression, as well as (D) metabolic flux and protein abundance. NADP⁺-dependent enzyme YtsJ was considered as sole active malic enzyme (Lerondel et al., 2006). ProH and ProJ were regarded as the active pathway enzymes under osmotic stress (Brill et al., 2011a). The expression of a protein complex is given as the average expression of its subunits (i. e. PdhABCD, OdhABPdhD, SucCD, SdhABC and GltAB).

Except for genes, proteins and fluxes involved in proline biosynthesis, no linear relationship between gene expression and corresponding metabolic flux can be observed. There are different mechanisms by which the bacterial cell can adjust their metabolism to various environments: i) variations in gene transcription, ii) changes in protein stability, and iii) modulation of the enzyme activity by effectors (Pietack *et al.*, 2010). Under osmotic stress and simultaneous carbon substrate limitation, *B. subtilis* partially compensates for the potassium-related reduction in enzyme activity by producing more of the corresponding protein. Already small changes in gene expression in addition to the stabilizing effect of available osmoprotectants trigger the increased production and/or enzyme stability. The shutdown of protein degradation or other posttranslational protein modifications may also be involved. Nevertheless, the cellular compensation for lower enzyme activities is needed to maintain flux homeostasis (Figure 3.17).

To exploit further correlations, regularized canonical correlation analysis (Lê Cao *et al.*, 2009), enabling the discovery of possible interactions between omics data sets of different nature, was applied. Data from all tested conditions and all analyzed replicates were used as input for this unsupervised statistical approach. Three intuitive clusters of metabolites and transcripts, co-regulated during stress responses under simultaneous constrain in carbon supply and challenges by high salinity (Figure 3.22), were identified. The first group contains proline, glutamine and fumarate in association with genes involved in glutamate synthesis (*glnA*, *gltAB*) and gluconeogenesis (*pckA*, *gapB*), and is thus central to providing precursors for the synthesis of the osmoprotectant proline. In addition, also proline biosynthesis itself is part of a larger, pathway-overspanning cluster. This group contains compounds of lower glycolysis and of the entrance into the TCA cycle (3-phosphoglycerate, phosphoenolpyruvate, pyruvate, and citrate) and it clusters with genes for proline synthesis and degradation (*proA*, *proB*, *proH*, *proJ*, *putB*, *putC*, *putP*). Finally, the third cluster comprises energy metabolites (ATP, GTP) and different intermediates of central carbon metabolic pathways (fructose 1,6-bisphosphate, acetyl-CoA, erythrose 4-phosphate, ribose 5-phosphate, and malate) and transcripts of the anaplerotic pyruvate carboxylase *pycA* and fumarase *citG*. These correlations thus substantiate the main conclusion that the cell recruits metabolic modules across individual pathways in order to achieve both a robust metabolism and appropriate metabolic responses to stress conditions.

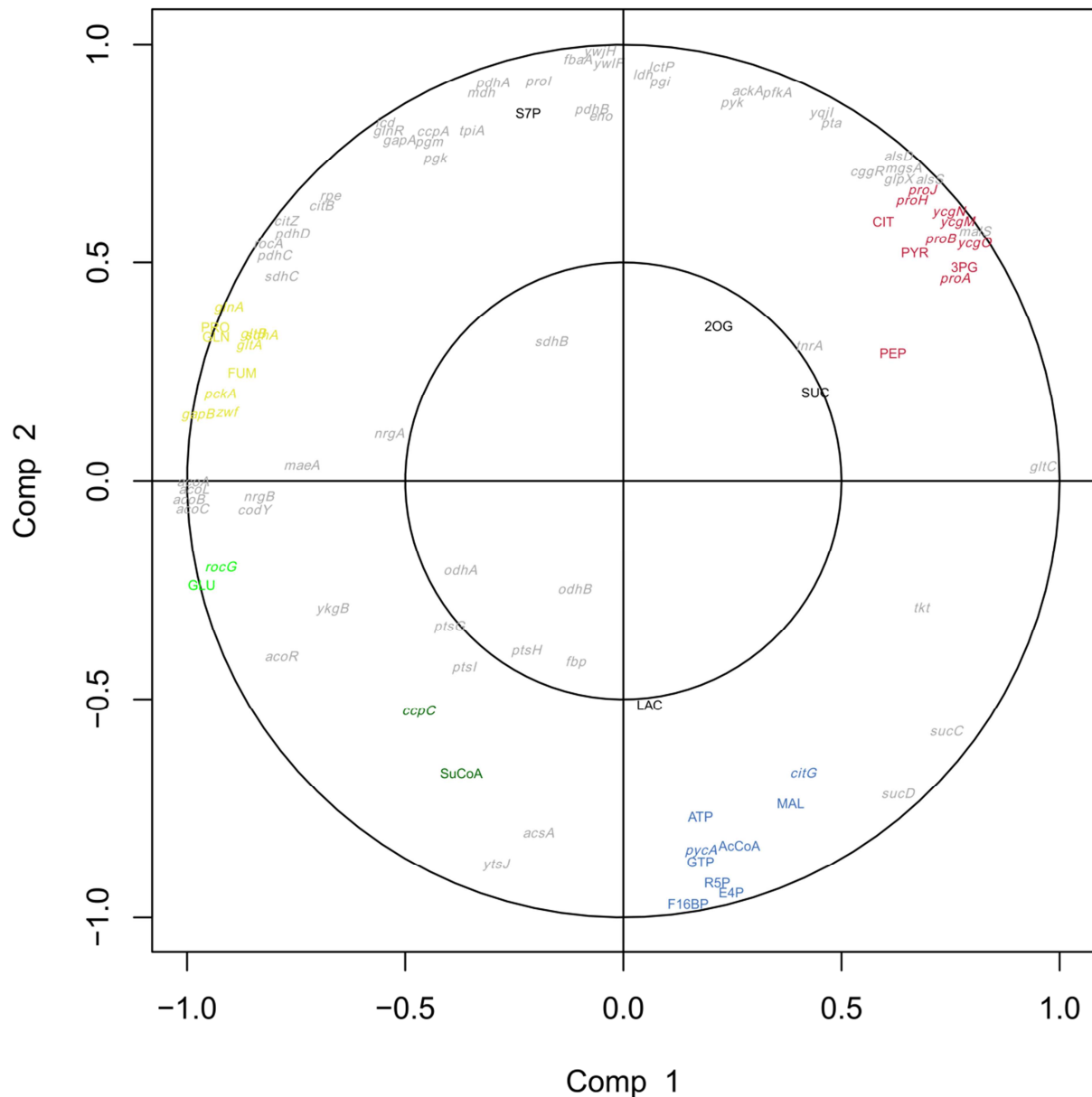


Figure 3.22: Two-dimensional loading plot of regularized canonical correlation analysis reveals regulatory associations between metabolites and transcripts in central metabolism. Three groups of associations can be identified: the first group shown in blue contains cofactors (ATP, GTP) and different intermediates of EMP and PP pathway, and TCA cycle (F1,6BP, AcCoA, E4P, R5P, MAL) clustering with anaplerotic pyruvate carboxylase *pycA* and fumarase *citG*; the second group shown in yellow contains proline, glutamine and fumarate in association with genes involved in ammonium utilization (*glnA*, *gltA*) and gluconeogenesis (*pckA*, *gapB*); the third group shown in red contains compounds of lower glycolysis and of the entrance into TCA cycle (3PG, PEP, PYR, CIT) clustering with genes of proline synthesis and degradation (*proA*, *proB*, *proH*, *proJ*, *putB*, *putC*, *putP*). Components in green are regulatory related and form less pronounced clusters.

3.4 Adaptation of *Bacillus subtilis* carbon core metabolism under nitrogen limitation, ionic and non-ionic osmotic stress

The elevated demand for proline and metabolic enzymes in *B. subtilis* under salt stress makes adequate nitrogen sources a particular prerequisite in such stress situations. In soil, the principal habitate of *B. subtilis*, assimilable nitrogen can be found in the form of ammonium salts, nitrate, urea, amino acids or peptides. Ammonium assimilation is realized by the interplay of glutamine synthetase and glutamate synthase (GS-GOGAT cycle) and is tightly regulated by the global transcription factors TnrA (Gunka and Commichau, 2012).

Next to its scientific relevance, *B. subtilis* is widely used in industrial fermentation processes for a variety of biotechnological products (Harwood, 1992; Schallmeyer *et al.*, 2004; van Dijl and Hecker, 2013). During cultivation, cells are subjected to changing osmotic burdens due to high carbon substrate and salt concentrations or caused by accumulating product titers. To answer the question, how the availability of nitrogen influences osmostress adaptation in *B. subtilis*, cells were investigated by applying the before established systems-level approach to a new set of conditions. The set comprised a nitrogen-limited reference, a salt-stress condition (0.69 M NaCl) and an iso-osmolar high-sugar condition (1.39 M glucose). The growth rate of $D = 0.1 \text{ h}^{-1}$ was kept equal to that of the carbon-limitation study.

Altered cell physiology of nitrogen-limited *B. subtilis*

Residual ammonium concentrations below the detection limit in the three stress conditions and unconsumed glucose levels of 1.75 ± 0.03 and $1.64 \pm 0.04 \text{ g L}^{-1}$ under reference and salt-stress conditions illustrate the successful establishment of nitrogen-limitation in the new set of cultivations. The biomass yield of nitrogen-limited *B. subtilis* was higher, as compared to carbon-limited cells, whereas CO_2 formation and glucose uptake rate were lower. As observed in glucose-limited cultivations, biomass yield was reduced, when cells are osmotically challenged, whereas glucose uptake rate and CO_2 formation increased. By-product formation was rather weak. However, high glucose levels (sugar stress) triggered the production of more overflow metabolites (acetate, acetoin, 2,3-butanediol, lactate) and

pyruvate, whose concentration (about 0.5 mM in the supernatant) exceeded even that of acetate.

Table 3.6: Physiological data and carbon balance for *B. subtilis* BSB1 during carbon-limited and nitrogen-limited chemostat growth on M9 minimal medium without further addition (reference), supplemented with 0.69 M NaCl (salt stress), and supplemented with 1.39 M glucose (sugar stress). The data comprise biomass yield ($Y_{X/S}$), specific rates for glucose uptake (q_s) and extracellular product formation ($n=4$).

	Unit	Reference C-limitation	Reference N-limitation	Salt stress	Sugar stress
$Y_{X/S}$	$g_{DCW} mol^{-1}$	55.6 ± 5.8	63.7 ± 5.6	44.8 ± 1.3	47.8 ± 3.0
q_s	$mmol g_{DCW}^{-1} h^{-1}$	1.8 ± 0.2	1.6 ± 0.1	2.2 ± 0.1	2.1 ± 0.1^b
q_{CO_2}	$mmol g_{DCW}^{-1} h^{-1}$	6.7 ± 0.2	4.5 ± 0.2	5.1 ± 0.3	7.8 ± 0.4
$q_{acetate}$	$\mu mol g_{DCW}^{-1} h^{-1}$	10.9 ± 1.1	3.7 ± 0.2	7.6 ± 0.2	18.4 ± 0.3
$q_{pyruvate}$	$\mu mol g_{DCW}^{-1} h^{-1}$	1.3 ± 0.3	0.7 ± 0.3	14.1 ± 0.3	170.7 ± 0.1
$q_{succinate}$	$\mu mol g_{DCW}^{-1} h^{-1}$	0.6 ± 0.2	0.6 ± 0.1	0.4 ± 0.1	1.0 ± 0.2
$q_{lactate}$	$\mu mol g_{DCW}^{-1} h^{-1}$	6.8 ± 1.4	1.7 ± 0.3	2.6 ± 0.5	11.2 ± 0.2
$q_{oxoglutarate}$	$\mu mol g_{DCW}^{-1} h^{-1}$	< 0.1	1.6 ± 0.7	5.7 ± 0.3	< 0.1
$q_{isobutyrate}$	$\mu mol g_{DCW}^{-1} h^{-1}$	3.0 ± 1.2	9.7 ± 0.4	10.0 ± 0.6	4.9 ± 0.3
$q_{isovalerate}$	$\mu mol g_{DCW}^{-1} h^{-1}$	3.4 ± 1.5	5.5 ± 0.4	1.7 ± 0.5	< 0.1
$q_{acetoin}$	$\mu mol g_{DCW}^{-1} h^{-1}$	< 0.1	3.5 ± 0.3	2.0 ± 0.4	25.1 ± 0.1
$q_{2,3-butanediol}$	$\mu mol g_{DCW}^{-1} h^{-1}$	< 0.1	0.6 ± 0.5	0.4 ± 0.2	3.5 ± 0.2
C recovery^a	%	98.3 ± 6.5	96.8 ± 3.6	100.6 ± 5.9	100.0 ± 2.2

^a Estimation of the carbon recovery considered carbon content of the biomass, which was assumed to be 48.4 % in nitrogen-limited *B. subtilis* (Dauner *et al.*, 2001b). ^b Specific substrate uptake at constantly high glucose concentrations was assumed to range between nitrogen-limited cells and salt-stressed cells as changes in glucose concentration were not detectable with a sufficient resolution.

Although ATP and GTP levels were lower in nitrogen-limited cells, as compared to carbon limitation (Table 3.7), the high energy level, equivalent to an AEC above 0.8, was always maintained. Furthermore, nitrogen-limitation led to a reduction of most intracellular amino acid pools (data not shown), especially glutamate and proline. The level of arginine, however, was increased by a factor of five, thus providing an alternative nitrogen storage compound.

On protein level, the intracellular amount of ammonium-assimilating glutamine synthetase (GlnA, also GS) was drastically increased under nitrogen limitation (data not shown). GS catalyzes the formation of glutamine from ammonium and glutamate. Obviously, the synthesis and activity of GS is tightly regulated in response to the nitrogen availability (Fisher, 1999; Gunka and Commichau, 2012).

Table 3.7: Intracellular levels of nucleotides for non-stressed, salt-stressed and sugar-stressed *B. subtilis* cells, grown in nitrogen-limited chemostat cultures at $D = 0.1 \text{ h}^{-1}$ ($n=3$). The energy level is expressed by the adenylate energy charge (AEC) (Atkinson, 1968).

	Unit	Reference C-limitation	Reference N-limitation	Salt stress	Sugar stress
AMP	$\mu\text{mol g}_{\text{DCW}}^{-1}$	1.9 ± 0.5	0.5 ± 0.3	0.2 ± 0.1	1.1 ± 0.4
ADP	$\mu\text{mol g}_{\text{DCW}}^{-1}$	4.1 ± 0.6	2.0 ± 0.3	2.8 ± 0.3	3.6 ± 0.4
ATP	$\mu\text{mol g}_{\text{DCW}}^{-1}$	19.2 ± 2.3	5.2 ± 0.4	10.9 ± 0.5	10.6 ± 1.8
GTP	$\mu\text{mol g}_{\text{DCW}}^{-1}$	5.2 ± 2.5	1.2 ± 0.1	2.2 ± 0.2	2.7 ± 0.4
AEC		0.84 ± 0.03	0.81 ± 0.05	0.89 ± 0.02	0.81 ± 0.05

Less pronounced, but still significantly increased under nitrogen limitation, were triose phosphate isomerase (Tpi), phosphoglucerate mutase (Pgm) and enolase (Eno) of the CggR-regulon (Ludwig *et al.*, 2001; Meinken *et al.*, 2003) and gluconeogenic fructose 1,6-bisphosphatase (Fbp) (Fujita *et al.*, 1998). Among the less abundant proteins were enzymes of the TCA cycle such as citrate synthase (CitZ), succinate dehydrogenase (SdhABC), fumarase (CitG) and malate dehydrogenase (Mdh). Most TCA cycle enzymes in *B. subtilis* are subject to transcriptional regulation, since carbon catabolite repression controlled by CcpA and CcpC reduces the expression of these enzymes in the presence of glucose (Tobisch *et al.*, 1999; Kim *et al.*, 2003; Sonenshein, 2007). A stronger catabolite repression caused by higher residual glucose levels (compared to carbon-limitation) might be responsible for the lower abundance of these enzymes under nitrogen-limitation. Additionally, malic enzyme (YtsJ), gluconeogenic glyceraldehyde 3-phosphate dehydrogenase (GapB) and glutamate 5-semialdehyde dehydrogenase (ProA) of the proline synthesis pathway were reduced in their intracellular abundance.

Obtained physiological data (Table 3.6) and mass isotopomer distributions (Appendix Table 6.4), as well as an adjusted anabolic precursor demand (Appendix Table 6.2) were again integrated to calculate metabolic fluxes under the given conditions. Nitrogen-limited *B. subtilis* exhibited slightly higher fluxes through EMP pathway down to PEP accompanied by a lower flux into the PP pathway (Figure 3.23 and Figure 3.24A), as compared to carbon-limited cells. The trend is in agreement with previous studies on *B. subtilis* under nitrogen-limitation although to a lesser extent (Dauner *et al.*, 2001b; Fürch *et al.*, 2007). Despite high residual

glucose levels, carbon back flux through the malic enzymes and a minor activity of gluconeogenic PEP carboxykinase were observed, indicating involvement of ATP-futile cycles in energy balancing (Dauner *et al.*, 2001b; Sauer and Eikmanns, 2005). Additionally, less carbon was drained off the TCA cycle via PEP carboxykinase. Apart from these minor adjustments, the central carbon metabolism maintained its homeostatic flux distribution (Figure 3.24A).

Facing the osmotic challenge under nitrogen-limitation

As before, changes in gene expression, protein amounts and metabolite concentrations obtained from the chemostat experiments were integrated and compared in order to get an insight into the long-term osmoadaptation of *B. subtilis* under simultaneous nutrient-limitation (Figure 3.25). When nitrogen-limited cells were challenged by the addition of 0.69 M NaCl, the osmosensitive proline pathway was again activated. To fulfill the demand for the compatible solute proline, precursor synthesis of glutamate and glutamine from 2-oxoglutarate was likewise induced. Despite the nitrogen-limiting conditions, the cell was still able to accumulate about $370 \mu\text{mol g}_{\text{DCW}}^{-1}$ of proline to counteract the high-salinity. Genes for the degradation and recycling of proline were also activated, probably due to the need for nitrogen. Figure 3.25 furthermore shows the induction of osmoprotectant uptake systems (*opuA-E*), the import and release of potassium ions (*ktrAB-CD*), the up-regulation of genes involved in the synthesis of the osmoprotectant glycine betaine from choline (*gbsAB*) and the activation of mechanosensitive channels; well-known adaptation mechanisms when cells have to cope with high osmolyte levels (Figure 3.25) (Kempf and Bremer, 1998; Steil *et al.*, 2003; Holtmann *et al.*, 2003; Nau-Wagner *et al.*, 2012). Most genes belonging to one of the main carbon metabolizing pathways (i.e. EMP pathway, PP pathway and TCA cycle) were unchanged or slightly induced by salt, as for example *pgi* (two-fold), *gndA* (two-fold), *citZ* (two-fold) or *ywjH* (two-fold). Certain key enzymes and protein complexes (e.g. GapA, PdhABCD, CitB and Icd) were again up-regulated as in carbon-limited cells (Figure 3.14). However, in contrast to salt stress under carbon limitation, no transcriptional and proteomic down-regulation of the second part of the TCA cycle downwards from the 2-oxoglutarate node was observed. In fact, the overall increase in protein amounts affected the whole central metabolism.

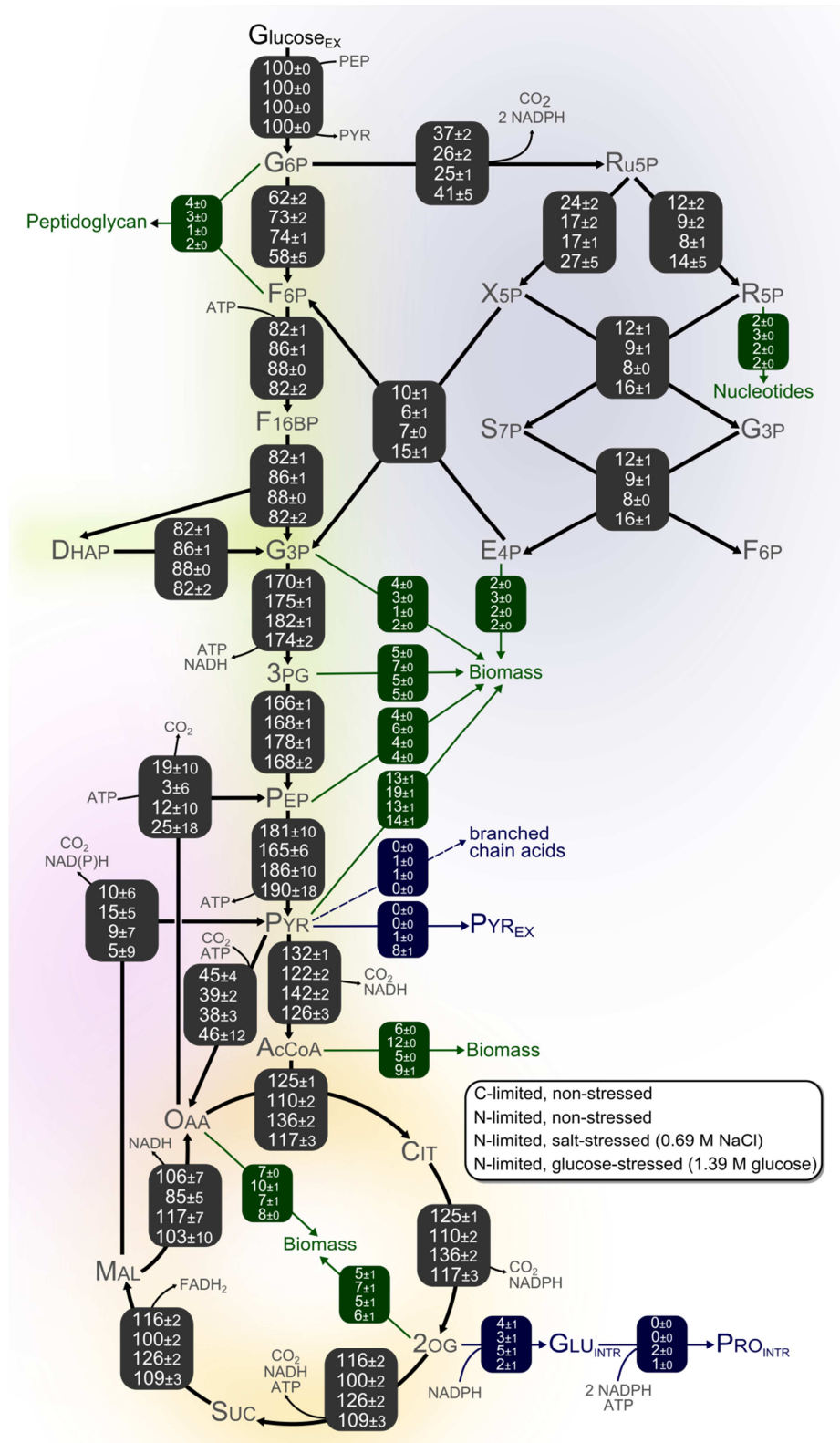


Figure 3.23: Metabolic flux response of chemostat-grown *B. subtilis* BSB1 ($D = 0.1 \text{ h}^{-1}$) to comparable levels of ionic and non-ionic osmotic stress (0.69 M NaCl and 1.39 M glucose, respectively) under simultaneous nitrogen limitation. Upper values represent reference data from glucose-limited grown *B. subtilis*. Values are normalized to the respective specific glucose uptake rate (Table 3.6). Anabolic precursor demand and a comparison between experimental and simulated mass isotopomer distribution are provided in the appendix (Appendix Table 6.2 and Table 6.4).

This included also the interlinking NADP⁺-dependent malic enzyme (YtsJ) and gluconeogenic PEP-carboxykinase (PckA). However, *in vivo* fluxes through the TCA cycle and the PEP-PYR-OAA node were similar to those under carbon-limitation at higher salinity (Figure 3.23 and Figure 3.16).

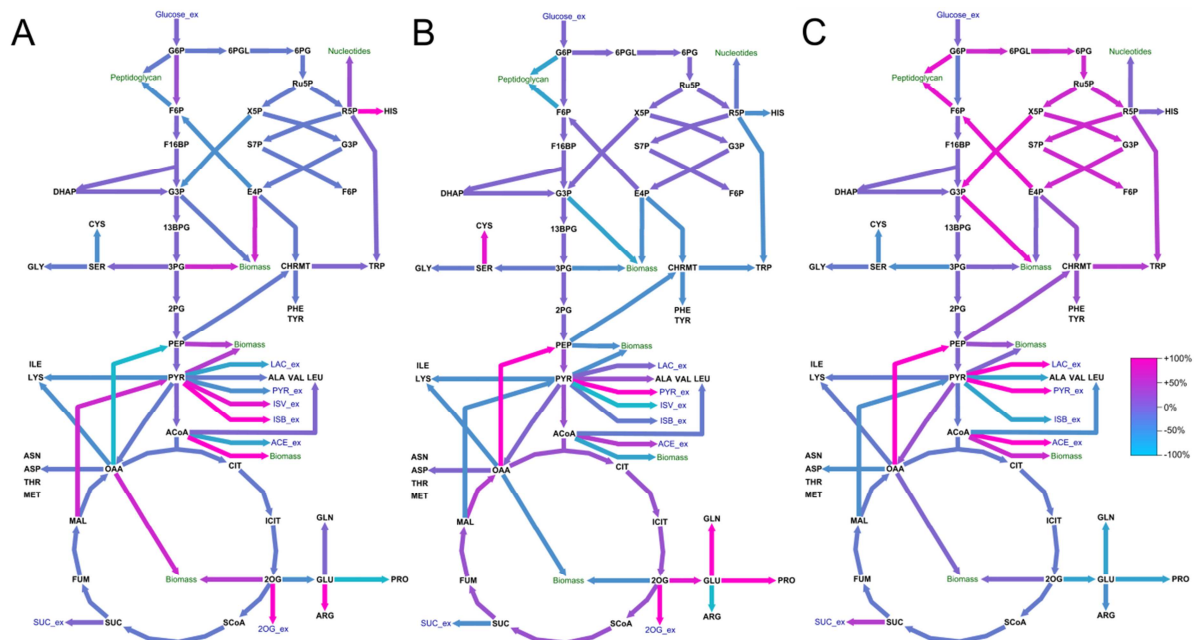


Figure 3.24: Carbon core metabolism largely maintains flux homeostasis under nitrogen limitation and osmotic stress. **(A)** Flux change in percent in nitrogen-limited cells compared to carbon limitation; **(B)** Flux change in salt-stressed cells under nitrogen limitation (0.69 M NaCl) compared to solely nitrogen-limited cells; **(C)** Flux change in percent in cells exposed to high-glucose compared to high-salinity challenged cells (both under simultaneous nitrogen-limitation). Arrow colors indicate positive (fuchsia) and negative (cyan) flux changes. Unchanged fluxes are given as violet arrows. Non-standard abbreviations for metabolites: ACE, acetate; ACoA, acetyl-coenzyme A; CHRMT, chorismate; CIT, citrate; DHAP, dihydroxyacetone phosphate; E4P, erythrose 4-phosphate; F6P, fructose 6-phosphate; F16BP, fructose 1,6-bisphosphate; FUM, fumarate; G6P, glucose 6-phosphate; G3P, glyceraldehyde 3-phosphate; 13BPG, 1,3-bisphosphoglycerate; 2PG, 2-phosphoglycerate; 3PG, 3-phosphoglycerate; ISB, isobutyrate; ICIT, isocitrate; ISV, isovalerate; LAC, lactate; MAL, malate; OAA, oxaloacetate; 2OG, 2-oxoglutarate; 6PG, 6-phosphogluconate; 6PGL, 6-phosphogluconolactone; PEP, phosphoenolpyruvate; PYR, pyruvate; R5P, ribose 5-phosphate; Ru5P, ribulose 5-phosphate; S7P, sedoheptulose 7-phosphate; SUC, succinate; SCoA, succinyl-coenzyme A; X5P, xylulose 5-phosphate Amino acids are abbreviated according to the standard three letter code.

The amino acids glutamate and glutamine are well known signal metabolites for the transcriptional regulation of TCA cycle genes (Commichau *et al.*, 2006; Sonenshein, 2007). The intracellular level of glutamine was six-fold lower in salt-stressed cells under nitrogen-limitation, compared to carbon-limited salt stress. This can be partially explained by the lower osmolarity applied to nitrogen-limited cells (about 1.560 mosm kg⁻¹ compared to 2.560

mosm kg⁻¹ in the carbon-limited high-salinity experiments) and thus the lower demand for proline, but may also be a cause for the still active second part of the TCA cycle. The glycolytic intermediate fructose 1,6-bisphosphate (F1,6BP) is another signal compound involved in carbon catabolite repression (Deutscher *et al.*, 1995; Stülke and Hillen, 2000). When F1,6BP is available in sufficient amounts, expression of genes coding for alternative substrate catabolizing enzymes is repressed. As shown in Figure 3.25, the intracellular level of F1,6BP dropped significantly in the presence of salt, probably leading to a partial relief of catabolite repression, and enables derepression of numerous TCA cycle genes (*citZ-icd-mdh*, *citB*). Previous studies on *Escherichia coli* actually proposed a direct link between osmolarity and carbon catabolite repression by altering the gene transcription of the principal regulatory protein complex CRP-cAMP (Balsalobre *et al.*, 2006).

The apparent consequence of the overall up-regulation of glycolysis, TCA cycle, malic enzyme and PEP-carboxykinase was a drastically increased intracellular pyruvate pool (750 %) (Figure 3.25). This effect was not observed in carbon-limited *B. subtilis* (Figure 3.14). Here, the exact fate of pyruvate is not fully clear as it serves as starting point of multiple pathways (overflow metabolism, anaplerosis, TCA cycle) and it is the precursor of several cellular compounds (amino acids, branched-chain keto acids, acetyl-CoA, fatty acids). Metabolic flux analysis revealed a higher flux through PEP carboxykinase and pyruvate kinase, providing more pyruvate from OAA and PEP (Figure 3.23). Part of the pyruvate was secreted in the culture broth (Figure 3.23, Figure 3.24B and Figure 3.25). The main reason for the elevated pyruvate level might be the supply of sufficient acetyl-CoA to replenish the TCA cycle branch, which provides 2-oxoglutarate for proline biosynthesis. It is also possible, that the catalytic activity of pyruvate dehydrogenase or citrate synthase is limiting, making it necessary to maintain the whole TCA cycle activity, in order to regenerate OAA for a continuous flux. Altogether, the pyruvate and 2-oxoglutarate nodes also constitute main switchpoints in central metabolism, as seen for carbon-limitation.

concentrations (see also Appendix Figure 6.2 for a comparison to non-stressed cells). On the first view, the cellular response differed substantially from salt-stress adaptation. The cell accumulated 3 times less proline and glutamine in response to the high-sugar environment. Expression of genes involved in glucose uptake, glycolysis, pentose phosphate pathway, gluconeogenesis, overflow metabolism and osmosensitive proline synthesis was stronger compared to cells grown in the presence of salt. Consequently, overflow metabolite formation was higher. Most of the corresponding protein concentrations did not change. Genes of the TCA cycle, anaplerotic pyruvate carboxylase, malic enzymes and anabolic synthesis of glutamate, glutamine and proline, however, were widely unchanged in their expression, whereas the amount of the involved enzymes was considerably reduced. The intracellular F1,6BP pool increased to its reference level under nitrogen-limitation, however, not leading to a reduced expression of lower glycolysis genes (*gapA*, *pgk*, *tpi*, *pgm*, *eno*) and pyruvate dehydrogenase (*pdhABCD*) (Doan and Aymerich, 2003; Blencke *et al.*, 2003). Genes of upper glycolysis (*pgi*, *pfkA*, *fbaA*), pyruvate kinase (*pykA*) and PP pathway are constitutively expressed (Tobisch *et al.*, 1999; Ludwig *et al.*, 2001; Blencke *et al.*, 2003). Carbon flux through glycolysis and TCA cycle was comparable to reference conditions. Some additional minor changes were identified: more carbon was channeled into the oxidative PP pathway and drained back into glycolysis by a higher activity of transketolase (Tkt), and an ATP futile cycle via PEP carboxykinase, pyruvate kinase and pyruvate carboxylase was activated, consuming 25 % of the total carbon, and contributed to intracellular ATP balancing.

The comparison of non-ionic and ionic osmotic stress indicated different cellular mechanisms of the bacterial response. The adaptation strongly depends on the nature of the stressor. Both types of stress had a profound impact on a large number of cellular functions, with over 1,200 genes being significantly (two-fold, $p < 0.05$) up- or down-regulated in both stress scenarios (data not shown). Only 43 % of the up-regulated and 83 % of the down-regulated genes under salt stress were similarly expressed in response to high glucose levels, further suggesting a specificity of the osmoadaptation in *B. subtilis*. Common changes included mainly genes involved in sporulation, general stress response, cell motility and chemotaxis, DNA repair, cell wall and lipid metabolism. The remaining expression pattern was stressor-specific. Additionally, sugar-induced gene expression changes taking part for instance in coping with cell envelope stress, genetic competence, trace metal homeostasis, metabolism of signaling nucleotides, protein folding and translation. On the other hand, salt triggered

especially gene transcription involved in iron acquisition and metabolism, protein modification and diverse transport processes.

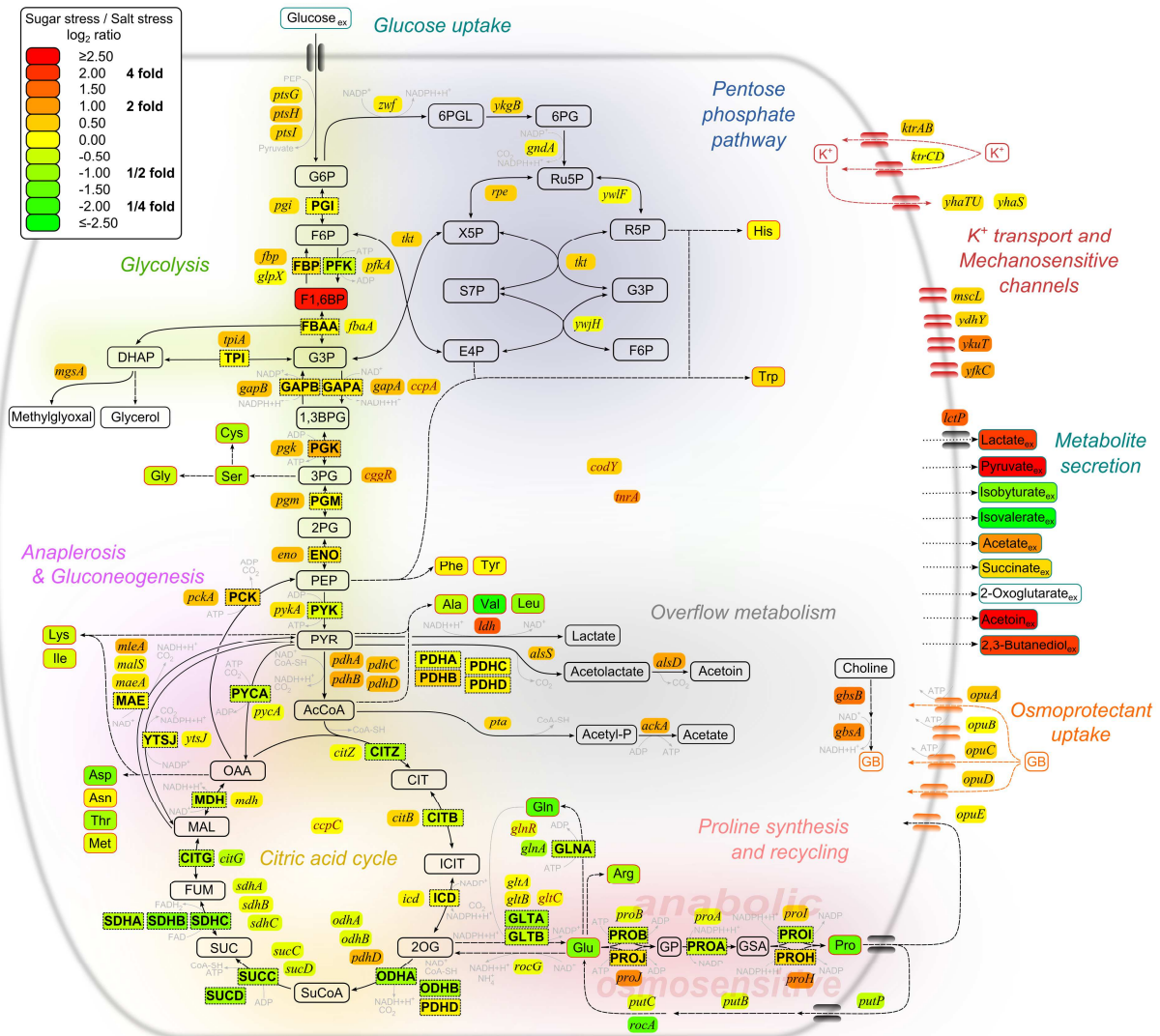


Figure 3.26: Integrated view of relative transcript, protein and metabolite concentrations in *B. subtilis*. Shown are changes in glucose-stressed cells under nitrogen-limitation (in the presence of 1.39 M glucose) compared to salt-stressed cells (0.69 M NaCl). The data format is as follows: gene expression, italics; protein abundances, dashed rectangles; metabolite pools, rounded rectangles. Most intracellular intermediates of glycolysis and TCA cycle were undetectable due to the high glucose background.

Differences in the stress response to ionic and non-ionic inducers have been previously described in *Bacilli* (Vilhelmsson and Miller, 2002; Brill *et al.*, 2011; Hoffmann *et al.*, 2013), *Enterobacteriaceae* (Le Rudulier and Bouillard, 1983; Weber *et al.*, 2006; Balsalobre *et al.*, 2006;

Shabala *et al.*, 2009), *Brevibacterium* (Bernard *et al.*, 1993; Onraedt *et al.*, 2004) and lactic acid bacteria (Glaasker *et al.*, 1998; Le Marrec *et al.*, 2007). Most studies registered a different growth behavior, intracellular solute composition and osmoprotectant uptake in the investigated organisms, comparing growth in the presence of salt and non-electrolytes (Le Rudulier and Bouillard, 1983; Houssin *et al.*, 1991; Glaasker *et al.*, 1998; Onraedt *et al.*, 2004; Le Marrec *et al.*, 2007; Shabala *et al.*, 2009). Glaasker and co-workers observed in *Lactobacillus plantarum* that the imposed high concentrations of sugars (lactose or sucrose) provoke only transient osmotic stress because external and internal sugar levels equilibrate after short time (Glaasker *et al.*, 1998). In *E. coli*, a similar growth restoration upon sugar shock was described (Houssin *et al.* 1991). Furthermore, *E. coli* accumulates a large number of metabolic proteins only in the presence of NaCl, whereas an iso-osmolar concentration of sorbitol resulted in a different proteome pattern (Weber *et al.*, 2006). A comparative microarray analysis in *E. coli* revealed that only 57 % of all up-regulated and 63 % of all down-regulated genes show a similar response to iso-osmolar concentrations of NaCl and sucrose (Shabala *et al.*, 2009) The remaining genes (43 % and 37 %, respectively) were stress-specific. In *B. subtilis* JH642 grown in shake flasks on LB medium, the osmotic induction of *proHJ* (coding for the osmosensitive proline synthesis route) and *opuA* (osmoprotectant uptake) is about three- to four-fold higher, when osmostress is induced by sugars (Brill *et al.*, 2011; Hoffmann *et al.*, 2013). When the compatible solute glycine betaine is additionally supplemented to the medium, intracellular pool sizes vary to the same extent in salt- and sugar-stressed cells, respectively (Hoffmann *et al.*, 2013).

Accordingly, the nature of the applied osmostressor impacts cell growth and central metabolism in many different ways. A prerequisite for the active osmoprotection by solute import or osmoprotectant biosynthesis is an osmotically effective gradient (Hoffmann *et al.*, 2013). Probability is high, that this gradient is much lower in sugar-stressed cells, due to the uptake of sugar close to equilibrium levels (Houssin *et al.*, 1991; Glaasker *et al.*, 1998). Also the impact on transporter capacities and other membrane-linked cellular functions, such as K⁺ in- and efflux and electron transport in cell respiration, differs in cells grown at high-salinity and high sugar levels, respectively (Houssin *et al.*, 1991; Shabala *et al.*, 2009). Further physicochemical and thermodynamical factors like the ionic strength, alterations in membrane potential or permeability, and changes in the internal pH may additionally contribute to observed dissimilarities (Houssin *et al.*, 1991; Shabala *et al.*, 2009). The *in vivo*

enzyme activity strongly depends on the cytosolic environment and the nature of potentially present stressors, as shown in Chapter 3.3 (Table 3.5) and previous studies (Le Marrec *et al.*, 2007; Vilhelmsson and Miller, 2002).

To which extent each of the above mentioned factors influences the different osmoadaptation mechanisms remains open. However, integrated analysis of gene transcription, the active protein inventory, intracellular metabolite levels and carbon fluxes, allowed first insights into cellular adjustments in central metabolism of *B. subtilis* to maintain homeostasis even under severe osmotic stress and nutrient-restricted conditions. The partially drastic changes on the transcriptome and proteome level (Figure 3.25 and Figure 3.26) resulted in a widely rigid carbon flux distribution in glycolysis and the TCA cycle (Figure 3.24) with only minor fine-tuning at selected key metabolite nodes. The availability of signal metabolites, such as F1,6BP, glutamate or glutamine that continuously monitor the cellular energetic state, links the regulation of central carbon and nitrogen metabolism, modulated by global transcriptional regulators, to the appropriate osmostress response. This interplay between metabolism and long-term stress adaptation enables the cell to survive extreme environmental burdens meanwhile staying highly adaptive.

3.5 Biotechnological production of the high-value compatible solute ectoine

The chemical chaperone ectoine

The above chapters provided an excellent insight into stress metabolism under high-salt conditions, using *B. subtilis* as a model. Obviously, bacterial cells activate *de novo* synthesis of compatible solutes to compensate for the imposed stress. In addition to proline, formed by *B. subtilis*, also glycine betaine, ectoine and hydroxyectoine are produced by microorganisms to counteract osmotic imbalances (Kuhlmann and Bremer, 2002; Roberts, 2005). They have substantial commercial value because of their stabilizing and function-preserving effects on biomolecules (i.e. DNA, proteins, membranes) under heat, cold, osmotic and chemical stress (Diamant *et al.*, 2001; Chattopadhyay *et al.*, 2004; Schubert *et al.*, 2007; Hoffmann and Bremer, 2011). Until today, most of the biotechnological production processes are high-salt-induced and thus very demanding in terms of process operation and downstream processing (Sauer and Galinski, 1998). Very recently, superior strains of *Corynebacterium glutamicum* for production of ectoine were developed in this laboratory (Becker *et al.*, 2013). *C. glutamicum* is a well-established cell factory with a long history for production of various bioproducts, such as amino acids, biopolymers or bio-based fuels (Becker and Wittmann, 2012). The new strain *C. glutamicum* ECT-1 constitutively expresses a synthetic ectoine cluster *ectABCD* from *Pseudomonas stutzeri* (Stöveken *et al.*, 2011) together with a feedback resistant aspartokinase (*lysC*) and secretes significant amounts of ectoine (Becker *et al.*, 2013). A further mutant ECT-2 additionally comprises a deletion of the lysine exporter *lysE*, in order to minimize loss of carbon into lysine.

Availability of intracellular amino acids of the aspartate family affects ectoine synthesis

Following strain construction and basic screening of suitable process parameters, as conducted by Becker and co-workers (Becker *et al.*, 2013), this work now aimed at a metabolic characterization of the mutant strains. Particularly, it was relevant to investigate intracellular concentrations of precursor compounds of ectoine to study the impact of the implemented genetic modifications and search for metabolic bottlenecks. Aspartate

semialdehyde (ASA) is an important metabolite and critical branch point with regard to biosynthesis of the aspartate family of amino acids (Lo *et al.*, 2009). Since ectoine biosynthesis is dependent on a sufficient supply of ASA as well (Bestvater *et al.*, 2008; Stöveken *et al.*, 2011), intracellular pools of amino acids belonging to the aspartate family were examined. A cultivation temperature of 35 °C appeared promising for later production. Most desirable, integration of the synthetic ectoine cluster into the dehydrogenase branch of lysine synthesis resulted in a substantial decrease of intracellular lysine as major competitor in the ECT-1 strain (Table 3.8). This was taken as positive indication of a successfully lowered carbon flux towards lysine biosynthesis, thus increasing ASA availability for ectoine. Ectoine indeed accumulated in substantially higher levels in the cytosol than lysine did (Table 3.8). Upon elimination of the lysine exporter, however, the metabolite pattern completely changed. The novel ECT-2 strain accumulated up to 53 $\mu\text{mol g}_{\text{DCW}}^{-1}$ of lysine even exceeding that of the basic lysine producer LYS-1 by more than two fold. Simultaneously, the ectoine level dropped substantially (Table 3.8). Obviously, elimination of lysine secretion did not circumvent high carbon fluxes towards this amino acid but resulted in increased intracellular accumulation. In addition, formation of aspartate and threonine was slightly affected. As compared to the parent lysine producer LYS-1, their cytosolic levels were slightly reduced in the synthetic ectoine producers. The intracellular asparagine level, however, was strongly increased. Whereas only marginal amounts were found in LYS-1, both ECT-1 and ECT-2 exhibited comparably high intracellular asparagine (Okino *et al.*, 2005) levels, also competing with ectoine biosynthesis and secretion. Additional studies at 30 °C (Becker *et al.*, 2013) revealed that the cultivation temperature only had a marginal effect on intracellular amino acid accumulation.

Table 3.8: Concentration of free intracellular amino acids of the aspartate-family and of intracellular ectoine of lysine-producing *C. glutamicum* strains LYS-1 and its ectoine-producing derivatives *C. glutamicum* ECT-1 and *C. glutamicum* ECT-2.

Strain ^a	Aspartate [$\mu\text{mol g}_{\text{DCW}}^{-1}$]	Asparagine [$\mu\text{mol g}_{\text{DCW}}^{-1}$]	Threonine [$\mu\text{mol g}_{\text{DCW}}^{-1}$]	Lysine [$\mu\text{mol g}_{\text{DCW}}^{-1}$]	Ectoine [$\mu\text{mol g}_{\text{DCW}}^{-1}$]
<i>C. glutamicum</i> LYS-1	9.1 ± 0.9	1.4 ± 0.2	6.8 ± 0.5	24.4 ± 6.3	-
<i>C. glutamicum</i> ECT-1	7.6 ± 0.6	28.1 ± 4.0	6.5 ± 0.4	16.3 ± 2.0	158.5 ± 20.7
<i>C. glutamicum</i> ECT-2	7.9 ± 0.6	17.0 ± 2.4	5.2 ± 0.4	52.8 ± 12.6	36.1 ± 7.6

^a Cells were grown at 35 °C in mineral salt medium. The data represent mean values with standard deviations from two biological replicates, each sampled at three different optical densities (OD 2, OD 4 and OD 8).

High-cell density fed-batch fermentation reveals excellent production performance

To take benefit from high cell densities (Okino *et al.*, 2005; Becker *et al.*, 2011) that cannot readily be achieved in shake-flask experiments, the production performance of second generation ectoine producer *C. glutamicum* ECT-2 was benchmarked under carefully controlled fed-batch conditions (Figure 3.27).

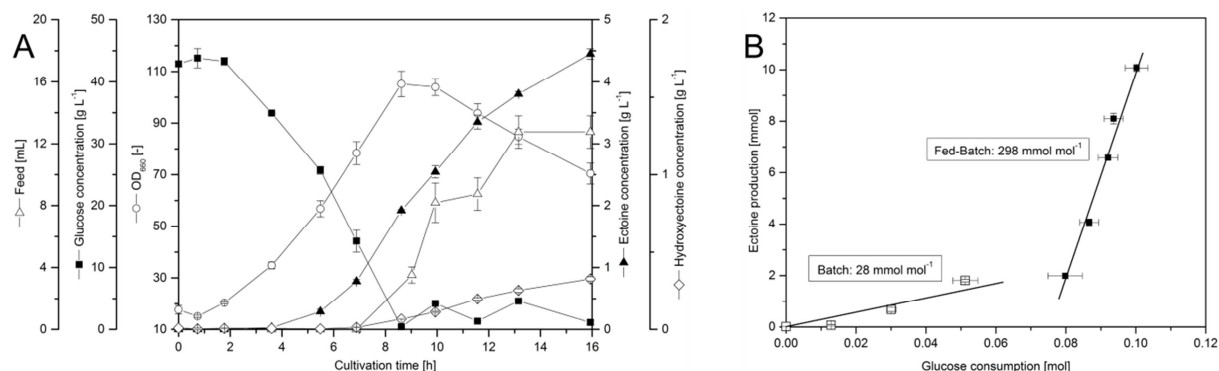


Figure 3.27: Production performance of the advanced ectoine-producer strain *C. glutamicum* ECT-2 during fed-batch fermentation. **(A)** Cultivation profile of strain ECT-2; **(B)** Ectoine yield achieved in the different cultivation phases. The oxygen saturation in the fermenter was kept constant at 30 % by variation of the stirrer velocity and the aeration rate. Automated feeding was initiated by a DO-based signal (Becker *et al.*, 2011). Glucose concentration was thereby kept below 5 g L⁻¹. The data shown represent mean values from two independent fermentation experiments.

Ectoine production efficiency differed significantly during batch and feeding phase of the fermentation process. A ten-fold increase in ectoine yield in the feeding phase of the fermentation was observed (Figure 3.27). Though there was detectable growth-associated ectoine production during the batch phase, the predominant fraction of ectoine (about 80 %) was produced during the feeding phase. The finally achieved titer of 4.5 g L⁻¹ already approached to that of currently described industrial systems (Fallet *et al.*, 2010; Van-Thuoc *et al.*, 2010; Lang *et al.*, 2011). *C. glutamicum* ECT-2, however, takes benefit from fast growth and vitality. This resulted in an overall spacetime yield of 6.7 g L⁻¹ ectoine per day, which is among the highest productivities reported so far (Fallet *et al.*, 2010; Van-Thuoc *et al.*, 2010; Lang *et al.*, 2011). Better performance was only achieved with *Halomonas boliviensis* (Van-Thuoc *et al.*, 2010), and *Chromohalobacter salexigens* (Fallet *et al.*, 2010). These processes do, however, rely on high salinity and involve complex process operation strategies thus driving up production and downstream processing costs.

4 Conclusion and Outlook

The present work describes the establishment and application of an experimental and analytical systems biology approach for the investigation of *Bacillus subtilis* under osmotic stress and simultaneous nutrient-limitation. The applied wet and dry lab procedures yielded high-quality data sets for whole genome expression, absolute concentrations of central metabolic enzymes, extra- and intracellular metabolite levels and *in vivo* fluxes for different environmental stress scenarios. In general, *B. subtilis* is able to maintain cellular integrity and metabolic pathway activity by adjusting its metabolic machinery to the imposed burden. The adaptation comprises the *de novo* synthesis of the compatible solute proline and its precursors, the compensation of reduced enzyme activities by increasing the protein amount, the partial restoration of enzyme operation by the osmoprotectant glycine betaine and the carbon flux-re-routing into the corresponding key pathways at the level of pyruvate and 2-oxoglutarate. Pathway-overspanning associations between metabolites and transcripts reveal the complexity of the regulatory network. Even when nitrogen, a key factor for protein and proline synthesis becomes limiting, cell functioning can be ensured.

B. subtilis is industrially used as cell factory for the biosynthesis of a broad range of bioproducts, such as enzymes, vitamins and antibiotics, constantly facing osmotic challenges caused by high substrate and salt concentrations or accumulating product titers during the fermentation process. Non-ionic osmotic stress caused by high glucose concentrations provokes a rather different metabolic response compared to iso-osmolar salt concentrations, and seems less stressful to the cell. The exact mechanisms leading to the observed differences in salt and sugar-stressed cells remain to be elucidated. In summary, the cell aims for a virtually optimal carbon flux distribution which is widely maintained. Thereby, flux homeostasis relies on widespread adaptations of cellular components. The resulting stress response is not simply the sum of individual changes, but concerted responses to nutritional and environmental challenges obviously require the functional network as a whole.

Bacterial compatible solutes have substantial commercial value because of their stabilizing and function-preserving effects on biomolecules. Using *Corynebacterium glutamicum* as versatile cell factory, a fed-batch process was established that allowed salinity-decoupled production of the chemical chaperone ectoine with an overall productivity of $6.7 \text{ g L}^{-1} \text{ day}^{-1}$ which is among the highest productivities reported so far in the literature.

5 References

- Alice, A.F., and Sanchez-Rivas, C. (1997) DNA supercoiling and osmoresistance in *Bacillus subtilis* 168. *Curr Microbiol* **35**: 309-315.
- Antoniewicz, M.R., Kelleher, J.K., and Stephanopoulos, G. (2007a) Elementary metabolite units (EMU): A novel framework for modeling isotopic distributions. *Metab Eng* **9**: 68-86.
- Antoniewicz, M.R., Kraynie, D.F., Laffend, L.A., González-Lergier, J., Kelleher, J.K., and Stephanopoulos, G. (2007b) Metabolic flux analysis in a nonstationary system: Fed-batch fermentation of a high yielding strain of *E. coli* producing 1,3-propanediol. *Metab Eng* **9**: 277-299.
- Antoniewicz, M.R. (2013) Dynamic metabolic flux analysis – tools for probing transient states of metabolic networks. *Curr Opin Biotech* **24**: 973-978.
- Arakawa, T., and Timasheff, S.N. (1985) The stabilization of proteins by osmolytes. *Biophys J* **47**: 411-414.
- Atkinson, D.E. (1968) Energy charge of the adenylate pool as a regulatory parameter. Interaction with feedback modifiers. *Biochemistry* **7**: 4030-4034.
- Balsalobre, C., Johansson, J., and Uhlin, B.E. (2006) Cyclic AMP-dependent osmoregulation of *crp* gene expression in *Escherichia coli*. *J Bacteriol* **188**: 5935-5944.
- Barbe, V., Cruveiller, S., Kunst, F., Lenoble, P., Meurice, G., Sekowska, A., et al. (2009) From a consortium sequence to a unified sequence: the *Bacillus subtilis* 168 reference genome a decade later. *Microbiology* **155**: 1758-1775.
- Bartholomae, M., Meyer, F.M., Commichau, F.M., Burkovski, A., Hillen, W., and Seidel, G. (2013) Complex formation between malate dehydrogenase and isocitrate dehydrogenase from *Bacillus subtilis* is regulated by TCA cycle metabolites. *FEBS J* **281**: 1132-1143.
- Becker, J., Klopprogge, C., Schröder, H., and Wittmann, C. (2009) Metabolic engineering of the tricarboxylic acid cycle for improved lysine production by *Corynebacterium glutamicum*. *Appl Environ Microb* **75**: 7866-7869.
- Becker, J., Zelder, O., Häfner, S., Schröder, H., and Wittmann, C. (2011) From zero to hero – Design-based systems metabolic engineering of *Corynebacterium glutamicum* for L-lysine production. *Metab Eng* **13**: 159-168.
- Becker, J., and Wittmann, C. (2012) Bio-based production of chemicals, materials and fuels – *Corynebacterium glutamicum* as versatile cell factory. *Curr Opin Biotech* **23**: 631-640.
- Becker, J., Schäfer, R., Kohlstedt, M., Harder, B., Borchert, N., Stöveken, N., Bremer, E., and Wittmann, C. (2013) Systems metabolic engineering of *Corynebacterium glutamicum* for production of the chemical chaperone ectoine. *Microb Cell Fact* **12**: 110.
- Bernard, T., Jebbar, M., Rassouli, Y., Himdi-Kabbab, S., Hamelin, J., and Blanco, C. (1993) Ectoine accumulation and osmotic regulation in *Brevibacterium linens*. *J Gen Microbiol* **139**: 129-136.
- Bestvater, T., Louis, P., and Galinski, E. (2008) Heterologous ectoine production in *Escherichia coli*: By-passing the metabolic bottle-neck. *Saline Syst* **4**: 12.
- Beynon, R.J., Doherty, M.K., Pratt, J.M., and Gaskell, S.J. (2005) Multiplexed absolute quantification in proteomics using artificial QCAT proteins of concatenated signature peptides. *Nat Methods* **2**: 587-589.
- Blencke, H.-M., Homuth, G., Ludwig, H., Mäder, U., Hecker, M., and Stülke, J. (2003) Transcriptional profiling of gene expression in response to glucose in *Bacillus subtilis*: regulation of the central metabolic pathways. *Metab Eng* **5**: 133-149.
- Boch, J., Kempf, B., and Bremer, E. (1994) Osmoregulation in *Bacillus subtilis*: synthesis of the osmoprotectant glycine betaine from exogenously provided choline. *J Bacteriol* **176**: 5364-5371.
- Boer, V.M., Crutchfield, C.A., Bradley, P.H., Botstein, D., and Rabinowitz, J.D. (2010) Growth-limiting intracellular metabolites in yeast growing under diverse nutrient limitations. *Mol Biol Cell* **21**: 198-211.

- Bolten, C.J., Kiefer, P., Letisse, F., Portais, J.-C., and Wittmann, C. (2007) Sampling for metabolome analysis of microorganisms. *Anal Chem* **79**: 3843-3849.
- Bolten, C., and Wittmann, C. (2008) Appropriate sampling for intracellular amino acid analysis in five phylogenetically different yeasts. *Biotechnol Lett* **30**: 1993-2000.
- Borodina, I., Siebring, J., Zhang, J., Smith, C.P., van Keulen, G., Dijkhuizen, L., and Nielsen, J. (2008) Antibiotic overproduction in *Streptomyces coelicolor* A3(2) mediated by phosphofructokinase deletion. *J Biol Chem* **283**: 25186-25199.
- Brill, J., Hoffmann, T., Bleisteiner, M., and Bremer, E. (2011) Osmotically controlled synthesis of the compatible solute proline is critical for cellular defense of *Bacillus subtilis* against high osmolarity. *J Bacteriol* **193**: 5335-5346.
- Čáslavská, J., Kodešová, J., and Horáková, I. (1972) Effect of prolonged cultivation in a chemostat under nitrogen limitation on the morphology and ultrastructure of *Bacillus subtilis*. *Folia Microbiol* **17**: 126-131.
- Cayley, S., and Record, M.T. (2003) Roles of cytoplasmic osmolytes, water, and crowding in the response of *Escherichia coli* to osmotic stress: Biophysical basis of osmoprotection by glycine betaine. *Biochemistry* **42**: 12596-12609.
- Cazorla, F.M., Romero, D., Pérez-García, A., Lugtenberg, B.J.J., de Vicente, A., and Bloemberg, G. (2007) Isolation and characterization of antagonistic *Bacillus subtilis* strains from the avocado rhizoplane displaying biocontrol activity. *J Appl Microbiol* **103**: 1950-1959.
- Charbonnier, Y., Gettler, B., François, P., Bento, M., Renzoni, A., Vaudaux, P., Schlegel, W., and Schrenzel, J. (2005) A generic approach for the design of whole-genome oligoarrays, validated for genotyping, deletion mapping and gene expression analysis on *Staphylococcus aureus*. *BMC Genomics* **6**: 95.
- Chattopadhyay, M.K., Kern, R., Mistou, M.-Y., Dandekar, A.M., Uratsu, S.L., and Richarme, G. (2004) The chemical chaperone proline relieves the thermosensitivity of a *dnaK* deletion mutant at 42°C. *J Bacteriol* **186**: 8149-8152.
- Chien, L.-J., and Lee, C.-K. (2007) Enhanced hyaluronic acid production in *Bacillus subtilis* by coexpressing bacterial hemoglobin. *Biotechnol Progr* **23**: 1017-1022.
- Chong, L., and Ray, L.B. (2002) Whole-istic biology. *Science* **295**: 1661.
- Christensen, B., and Nielsen, J. (1999) Isotopomer analysis using GC-MS. *Metab Eng* **1**: 282-290.
- Christensen, B., and Nielsen, J. (2000) Metabolic network analysis. In *Bioanalysis and Biosensors for Bioprocess Monitoring*. Sonnleitner, B. (ed) Berlin-Heidelberg, Germany: Springer, pp. 209-231.
- Christiansen, T., Christensen, B., and Nielsen, J. (2002) Metabolic network analysis of *Bacillus clausii* on minimal and semirich medium using ¹³C-labeled glucose. *Metab Eng* **4**: 159-169.
- Chubukov, V., Uhr, M., Le Chat, L., Kleijn, R.J., Jules, M., Link, H., et al. (2013) Transcriptional regulation is insufficient to explain substrate-induced flux changes in *Bacillus subtilis*. *Mol Syst Biol* **9**: 709.
- von Wachenfeldt, and Hederstedt, L. (2003) Respiratory cytochromes, other heme proteins, and heme biosynthesis. In *Bacillus subtilis and Its Closest Relatives*. Sonenshein, A.L., Hoch, J.A., and Losick, R. (eds). Washington, DC, USA: ASM Press, pp. 163-179.
- Commichau, F.M., Forchhammer, K., and Stülke, J. (2006) Regulatory links between carbon and nitrogen metabolism. *Curr Opin Microbiol* **9**: 167-172.
- Commichau, F.M., Gunka, K., Landmann, J.J., and Stülke, J. (2008) Glutamate metabolism in *Bacillus subtilis*: Gene expression and enzyme activities evolved to avoid futile cycles and to allow rapid responses to perturbations of the system. *J Bacteriol* **190**: 3557-3564.
- Commichau, F.M., Rothe, F.M., Herzberg, C., Wagner, E., Hellwig, D., Lehnik-Habrink, M., et al. (2009) Novel activities of glycolytic enzymes in *Bacillus subtilis*. *Mol Cell Proteomics* **8**: 1350-1360.
- Cruz Ramos, H., Hoffmann, T., Marino, M., Nedjari, H., Presecan-Siedel, E., Dreesen, O., Glaser, P., and Jahn, D. (2000) Fermentative metabolism of *Bacillus subtilis*: Physiology and regulation of gene Expression. *J Bacteriol* **182**: 3072-3080.

- Dartois, V., Débarbouillé, M., Kunst, F., and Rapoport, G. (1998) Characterization of a novel member of the DegS-DegU regulon affected by salt stress in *Bacillus subtilis*. **180**: 1855-1861.
- Dauner, M., and Sauer, U. (2000) GC-MS analysis of amino acids rapidly provides rich information for isotopomer balancing. *Biotechnol Progr* **16**: 642-649.
- Dauner, M., Bailey, J.E., and Sauer, U. (2001a) Metabolic flux analysis with a comprehensive isotopomer model in *Bacillus subtilis*. *Biotechnol Bioeng* **76**: 144-156.
- Dauner, M., Storni, T., and Sauer, U. (2001b) *Bacillus subtilis* metabolism and energetics in carbon-limited and excess-carbon chemostat culture. *J Bacteriol* **183**: 7308-7317.
- Dauner, M., and Sauer, U. (2001) Stoichiometric growth model for riboflavin-producing *Bacillus subtilis*. *Biotechnol Bioeng*, **76**: 132-143.
- Dauner, M., Sonderegger, M., Hochuli, M., Szyperski, T., Wüthrich, K., Hohmann, H.-P., Sauer, U., and Bailey, J.E. (2002) Intracellular carbon fluxes in riboflavin-producing *Bacillus subtilis* during growth on two-carbon substrate mixtures. *Appl Environ Microb* **68**: 1760-1771.
- Des Rosiers, C., Lloyd, S., Comte, B., and Chatham, J.C. (2004) A critical perspective of the use of ¹³C-isotopomer analysis by GCMS and NMR as applied to cardiac metabolism. *Metab Eng* **6**: 44-58.
- Des Rosiers, C., and Chatham, J.C. (2005) Myocardial phenotyping using isotopomer analysis of metabolic fluxes. *Biochem Soc T* **33**: 1413-1417.
- Deutscher, J., Küster, E., Bergstedt, U., Charrier, V., and Hillen, W. (1995) Protein kinase-dependent HPr/CcpA interaction links glycolytic activity to carbon catabolite repression in gram-positive bacteria. *Mol Microbiol* **15**: 1049-1053.
- Deutscher, J., Galinier, A., and Martin-Verstraete, I. (2003) Carbohydrate uptake and metabolism. In *Bacillus subtilis and Its Closest Relatives*. Sonenshein, A.L., Hoch, J.A., and Losick, R. (eds). Washington, DC, USA: ASM Press, pp. 129-150.
- Diamant, S., Eliahu, N., Rosenthal, D., and Goloubinoff, P. (2001) Chemical chaperones regulate molecular chaperones *in vitro* and in cells under combined salt and heat stresses. *J Biol Chem* **276**: 39586-39591.
- Diesterhaft, M.D., and Freese, E. (1973) Role of pyruvate carboxylase, phosphoenolpyruvate carboxykinase, and malic enzyme during growth and sporulation of *Bacillus subtilis*. *J Biol Chem* **248**: 6062-6070.
- van Dijk, J.M., and Hecker, M. (2013) *Bacillus subtilis*: From soil bacterium to super-secreting cell factory. *Microb Cell Fact* **12**: 3.
- Doan, T., and Aymerich, S. (2003) Regulation of the central glycolytic genes in *Bacillus subtilis*: binding of the repressor CggR to its single DNA target sequence is modulated by fructose 1,6-bisphosphate. *Mol Microbiol* **47**: 1709-1721.
- Dominguez, H., Rollin, C., Guyonvarch, A., Guerquin-Kern, J.-L., Coccagn-Bousquet, M., and Lindley, N.D. (1998) Carbon-flux distribution in the central metabolic pathways of *Corynebacterium glutamicum* during growth on fructose. *Eur J Biochem* **254**: 96-102.
- Earl, A.M., Losick, R., and Kolter, R. (2008) Ecology and genomics of *Bacillus subtilis*. *Trends Microbiol* **16**: 269-275.
- Engels, V., Lindner, S.N., and Wendisch, V.F. (2008) The global repressor SugR controls expression of genes of glycolysis and of the L-lactate dehydrogenase LdhA in *Corynebacterium glutamicum*. *J Bacteriol* **190**: 8033-8044.
- Eymann, C., Homuth, G., Scharf, C., and Hecker, M. (2002) *Bacillus subtilis* functional genomics: Global characterization of the stringent response by proteome and transcriptome analysis. *J Bacteriol* **184**: 2500-2520.
- Fallet, C., Rohe, P., and Franco-Lara, E. (2010) Process optimization of the integrated synthesis and secretion of ectoine and hydroxyectoine under hyper/hypo-osmotic stress. *Biotechnol Bioeng* **107**: 124-133.
- Fischer, E., Zamboni, N., and Sauer, U. (2004) High-throughput metabolic flux analysis based on gas chromatography-mass spectrometry derived ¹³C constraints. *Anal Biochem* **325**: 308-316.
- Fischer, E., and Sauer, U. (2005) Large-scale *in vivo* flux analysis shows rigidity and suboptimal performance of *Bacillus subtilis* metabolism. *Nat Genet* **37**: 636-640.

- Fischer, K.E., and Bremer, E. (2012) Activity of the osmotically regulated *yqiHIK* promoter from *Bacillus subtilis* is controlled at a distance. *J Bacteriol* **194**: 5197-5208.
- Fisher, S.H. (1999) Regulation of nitrogen metabolism in *Bacillus subtilis*: Vive la difference! *Mol Microbiol* **32**: 223-232.
- Fong, S.S., Nanchen, A., Palsson, B.Ø., and Sauer, U. (2006) Latent pathway activation and increased pathway capacity enable *Escherichia coli* adaptation to loss of key metabolic enzymes. *J Biol Chem* **281**: 8024-8033.
- Fuhrer, T., and Sauer, U. (2009) Different biochemical mechanisms ensure network-wide balancing of reducing equivalents in microbial metabolism. *J Bacteriol* **191**: 2112-2121.
- Fujisawa, M., Ito, M., and Krulwich, T.A. (2007) Three two-component transporters with channel-like properties have monovalent cation/proton antiport activity. *P Natl Acad Sci USA* **104**: 13289-13294.
- Fujita, Y., Yoshida, K.-I., Miwa, Y., Yanai, N., Nagakawa, E., and Kasahara, Y. (1998) Identification and expression of the *Bacillus subtilis* fructose 1,6-bisphosphatase gene (*fbp*). *J Bacteriol* **180**: 4309-4313.
- Fürch, T., Wittmann, C., Wang, W., Franco-Lara, E., Jahn, D., and Deckwer, W.-D. (2007) Effect of different carbon sources on central metabolic fluxes and the recombinant production of a hydrolase from *Thermobifida fusca* in *Bacillus megaterium*. *J Biotechnol* **132**: 385-394.
- Fürch, T., Hollmann, R., Wittmann, C., Wang, W., and Deckwer, W.-D. (2007) Comparative study on central metabolic fluxes of *Bacillus megaterium* strains in continuous culture using ¹³C labelled substrates. *Bioproc Biosyst Eng* **30**: 47-59.
- Galindo, E., Serrano-Carreón, L., Gutiérrez, C.R., Allende, R., Balderas, K., Patiño, M., et al. (2013) The challenges of introducing a new biofungicide to the market: A case study. *Electron J Biotechnol* **16**: 3.
- Glaasker, E., Tjan, F.S.B., ter Steeg, P.F., Konings, W.N., and Poolman, B. (1998) Physiological response of *Lactobacillus plantarum* to salt and nonelectrolyte stress. *J Bacteriol* **180**: 4718-4723.
- Goel, A., Ferrance, J., Jeong, J., and Atai, M.M. (1993) Analysis of metabolic fluxes in batch and continuous cultures of *Bacillus subtilis*. *Biotechnol Bioeng* **42**: 686-696.
- Goelzer, A., and Fromion, V. (2011) Bacterial growth rate reflects a bottleneck in resource allocation. *Biochim Biophys Acta* **1810**: 978-988.
- Güell, M., van Noort, V., Yus, E., Chen, W.-H., Leigh-Bell, J., Michalodimitrakis, K., et al. (2009) Transcriptome complexity in a genome-reduced bacterium. *Science* **326**: 1268-1271.
- Gunka, K., and Commichau, F.M. (2012) Control of glutamate homeostasis in *Bacillus subtilis*: a complex interplay between ammonium assimilation, glutamate biosynthesis and degradation. *Mol Microbiol* **85**: 213-224.
- Hahne, H., Mäder, U., Otto, A., Bonn, F., Steil, L., Bremer, E., Hecker, M., and Becher, D. (2010) A comprehensive proteomics and transcriptomics analysis of *Bacillus subtilis* salt stress adaptation. *J Bacteriol* **192**: 870-882.
- Harwood, C.R. (1992) *Bacillus subtilis* and its relatives: Molecular biological and industrial workhorses. *Trends Biotechnol* **10**: 247-256.
- Hecker, M., and Völker, U. (2001) General stress response of *Bacillus subtilis* and other bacteria. *Adv Microb Physiol* **44**: 35-91.
- Hoffmann, T., Schütz, A., Brosius, M., Völker, A., Völker, U., and Bremer, E. (2002) High-salinity-induced iron limitation in *Bacillus subtilis*. *J Bacteriol* **184**: 718-727.
- Hoffmann, T., Boiangiu, C., Moses, S., and Bremer, E. (2008) Responses of *Bacillus subtilis* to hypotonic challenges: Physiological contributions of mechanosensitive channels to cellular survival. *Appl Environ Microbiol* **74**: 2454-2460.
- Hoffmann, T., and Bremer, E. (2011) Protection of *Bacillus subtilis* against cold stress via compatible-solute acquisition. *J Bacteriol* **193**: 1552-1562.
- Hoffmann, T., Blohn, C., Stanek, A., Moses, S., Barzantny, H., and Bremer, E. (2012) Synthesis, release, and recapture of compatible solute proline by osmotically stressed *Bacillus subtilis* cells. *Appl Environ Microbiol* **78**: 5753-5762.

- Hoffmann, T., Wensing, A., Brosius, M., Steil, L., Völker, U., and Bremer, E. (2013) Osmotic control of *opuA* expression in *Bacillus subtilis* and its modulation in response to intracellular glycine betaine and proline pools. *J Bacteriol* **195**: 510-522.
- Holtmann, G., Bakker, E.P., Uozumi, N., and Bremer, E. (2003) KtrAB and KtrCD: Two K⁺ uptake systems in *Bacillus subtilis* and their role in adaptation to hypertonicity. *J Bacteriol* **185**: 1289-1298.
- Höper, D., Bernhardt, J., and Hecker, M. (2006) Salt stress adaptation of *Bacillus subtilis*: A physiological proteomics approach. *Proteomics* **6**: 1550-1562.
- Hoskisson, P.A. (2005) Continuous culture – making a comeback? *Microbiology* **151**: 3153-3159.
- Houssin, C., Eynard, N., Shechter, E., and Ghazi, A. (1991) Effect of osmotic pressure on membrane energy-linked functions in *Escherichia coli*. *Biochim Biophys Acta* **1056**: 76-84.
- Hua, Q., Joyce, A.R., Palsson, B.Ø., and Fong, S.S. (2007) Metabolic characterization of *Escherichia coli* strains adapted to growth on lactate. *Appl Environ Microbiol* **73**: 4639-4647.
- Ishii, N., Nakahigashi, K., Baba, T., Robert, M., Soga, T., Kanai, A., et al. (2007) Multiple high-throughput analyses monitor the response of *E. coli* to perturbations. *Science* **316**: 593-597.
- Junker, B., Klukas, C., and Schreiber, F. (2006) VANTED: A system for advanced data analysis and visualization in the context of biological networks. *BMC Bioinformatics* **7**: 109.
- Kajiyama, Y., Otagiri, M., Sekiguchi, J., Kosono, S., and Kudo, T. (2007) Complex formation by the *mrpABCDEFG* gene products, which constitute a principal Na⁺/H⁺ antiporter in *Bacillus subtilis*. *J Bacteriol* **189**: 7511-7514.
- Katz, J., and Rognstad, R. (1978) Futile cycling in glucose metabolism. *Trends Biochem Sci* **3**: 171-174.
- Kayser, A., Weber, J., Hecht, V., and Rinas, U. (2005) Metabolic flux analysis of *Escherichia coli* in glucose-limited continuous culture. I. Growth-rate-dependent metabolic efficiency at steady state. *Microbiology*, **151**: 693-706.
- Kelleher, J.K. (2001) Flux estimation using isotopic tracers: Common ground for metabolic physiology and metabolic engineering. *Metab Eng* **3**: 100-110.
- Kempf, B., and Bremer, E. (1998) Uptake and synthesis of compatible solutes as microbial stress responses to high-osmolality environments. *Arch Microbiol* **170**: 319-330.
- Kim, S.-I., Jourlin-Castelli, C., Wellington, S.R., and Sonenshein, A.L. (2003) Mechanism of repression by *Bacillus subtilis* CcpC, a LysR family regulator. *J Mol Biol* **334**: 609-624.
- Kleijn, R.J., Buescher, J.M., Le Chat, L., Jules, M., Aymerich, S., and Sauer, U. (2010) Metabolic fluxes during strong carbon catabolite repression by malate in *Bacillus subtilis*. *J Biol Chem* **285**: 1587-1596.
- Klein, T., Heinzle, E., and Schneider, K. (2013) Metabolic fluxes in *Schizosaccharomyces pombe* grown on glucose and mixtures of glycerol and acetate. *Appl Microbiol Biotechnol* **97**: 5013-5026.
- Kolkman, A., Olsthoorn, M.M.A., Heeremans, C.E.M., Heck, A.J.R., and Slijper, M. (2005) Comparative proteome analysis of *Saccharomyces cerevisiae* grown in chemostat cultures limited for glucose or ethanol. *Mol Cell Proteomics* **4**: 1-11.
- Krispin, O., and Allmansberger, R. (1995) Changes in DNA supertwist as a response of *Bacillus subtilis* towards different kinds of stress. *FEMS Microbiology Lett* **134**: 129-135.
- Krömer, J.O., Sorgenfrei, O., Klopprogge, K., Heinzle, E., and Wittmann, C. (2004) In-depth profiling of lysine-producing *Corynebacterium glutamicum* by combined analysis of the transcriptome, metabolome, and fluxome. *J Bacteriol* **186**: 1769-1784.
- Krömer, J.O., Fritz, M., Heinzle, E., and Wittmann, C. (2005) *In vivo* quantification of intracellular amino acids and intermediates of the methionine pathway in *Corynebacterium glutamicum*. *Anal Biochem* **340**: 171-173.
- Kuhlmann, A.U., and Bremer, E. (2002) Osmotically regulated synthesis of the compatible solute ectoine in *Bacillus pasteurii* and related *Bacillus* spp. *Appl Environ Microbiol* **68**: 772-783.
- Kuhn, D., Blank, L.M., Schmid, A., and Bühler, B. (2010) Systems biotechnology – Rational whole-cell biocatalyst and bioprocess design. *Eng Life Sci* **10**: 384-397.

- Kühner, S., van Noort, V., Betts, M.J., Leo-Macias, A., Batisse, C., Rode, M., *et al.* (2009) Proteome organization in a genome-reduced bacterium. *Science* **326**: 1235-1240.
- Kunst, F., Ogasawara, N., Moszer, I., Albertini, A.M., Alloni, G., Azevedo, V., *et al.* (1997) The complete genome sequence of the gram-positive bacterium *Bacillus subtilis*. *Nature* **390**: 249-256.
- Kunst, F., and Rapoport, G. (1995) Salt stress is an environmental signal affecting degradative enzyme synthesis in *Bacillus subtilis*. *J Bacteriol* **177**: 2403-2407.
- Lang, Y.-j., Bai, L., Ren, Y.-n., Zhang, L.-h., and Nagata, S. (2011) Production of ectoine through a combined process that uses both growing and resting cells of *Halomonas salina* DSM 5928T. *Extremophiles* **15**: 303-310.
- Lapidot, A., and Nissim, I. (1980) Regulation of pool sizes and turnover rates of amino acids in humans: ¹⁵N-glycine and ¹⁵N-alanine single-dose experiments using gas chromatography mass spectrometry analysis. *Metabolism* **29**: 230-239.
- Lê, S., Josse, J., and Husson, F. (2008) FactoMineR: an R package for multivariate analysis. *J Stat Softw* **25**: 1.
- Lê Cao, K.-A., González, I., and Déjean, S. (2009) integrOmics: an R package to unravel relationships between two omics datasets. *Bioinformatics* **21**: 2855-2856.
- Le Marrec, C., Bon, E., and Lonvaud-Funel, A. (2007) Tolerance to high osmolality of the lactic acid bacterium *Oenococcus oeni* and identification of potential osmoprotectants. *Int J Food Microbiol* **115**: 335-342.
- Le Rudulier, D., and Bouillard, L. (1983) Glycine betaine, an osmotic effector in *Klebsiella pneumoniae* and other members of the *Enterobacteriaceae*. *Appl Environ Microbiol* **46**: 152-159.
- Lee, S.Y., Lee, D.-Y., and Kim, T.Y. (2005) Systems biotechnology for strain improvement. *Trends Biotechnol* **23**: 349-358.
- Lentzen, G., and Schwarz, T. (2006) Extremolytes: natural compounds from extremophiles for versatile applications. *Appl Microbiol Biotechnol* **72**: 623-634.
- Lerondel, G., Doan, T., Zamboni, N., Sauer, U., and Aymerich, S. (2006) YtsJ has the major physiological role of the four paralogous malic enzyme isoforms in *Bacillus subtilis*. *J Bacteriol* **188**: 4727-4736.
- Liebeke, M., Pöther, D.-C., van Duy, N., Albrecht, D., Becher, D., Hochgräfe, F., *et al.* (2008) Depletion of thiol-containing proteins in response to quinones in *Bacillus subtilis*. *Mol Microbiol* **69**: 1513-1529.
- Liebeke, M., Meyer, H., Donat, S., Ohlsen, K., and Lalk, M. (2010) A metabolomic view of *Staphylococcus aureus* and its Ser/Thr kinase and phosphatase deletion mutants: Involvement in cell wall biosynthesis. *Chem Biol* **17**: 820-830.
- Liebeke, M., Dörries, K., Zühlke, D., Bernhardt, J., Fuchs, S., Pané-Farré, J., *et al.* (2011) A metabolomics and proteomics study of the adaptation of *Staphylococcus aureus* to glucose starvation. *Mol Biosyst* **7**: 1241-1253.
- ter Linde, J. J. M., Liang, H., Davis, R.W., Steensma, H.Y., van Dijken, J. P., and Pronk, J.T. (1999) Genome-wide transcriptional analysis of aerobic and anaerobic chemostat cultures of *Saccharomyces cerevisiae*. *J Bacteriol* **181**: 7409-7413.
- Lo, C.-C., Bonner, C.A., Xie, G., D'Souza, M., and Jensen, R.A. (2009) Cohesion group approach for evolutionary analysis of aspartokinase, an enzyme that feeds a branched network of many biochemical pathways. *Microbiol Mol Biol R* **73**: 594-651.
- López, C.S., Heras, H., Ruzal, S.M., Sánchez-Rivas, C., and Rivas, E.A. (1998) Variations of the envelope composition of *Bacillus subtilis* during growth in hyperosmotic medium. *Curr Microbiol* **36**: 55-61.
- López, C.S., Garda, H.A., and Rivas, E.A. (2002) The effect of osmotic stress on the biophysical behavior of the *Bacillus subtilis* membrane studied by dynamic and steady-state fluorescence anisotropy. *Arch Biochem Biophys* **408**: 220-228.
- López, C.S., Alice, A.F., Heras, H., Rivas, E.A., and Sánchez-Rivas, C. (2006) Role of anionic phospholipids in the adaptation of *Bacillus subtilis* to high salinity. *Microbiology* **152**: 605-616.
- Ludwig, H., Homuth, G., Schmalisch, M., Dyka, F.M., Hecker, M., and Stülke, J. (2001) Transcription of glycolytic genes and operons in *Bacillus subtilis*: evidence for the presence of multiple levels of control of the *gapA* operon. *Mol Microbiol* **41**: 409-422.

- Maaß, S., Sievers, S., Zühlke, D., Kuzinski, J., Sappa, P.K., Muntel, J., *et al.* (2011) Efficient, global-scale quantification of absolute protein amounts by integration of targeted mass spectrometry and two-dimensional gel-based proteomics. *Anal Chem* **83**: 2677-2684.
- MacLean, B., Tomazela, D.M., Abbatiello, S.E., Zhang, S., Whiteaker, J.R., Paulovich, A.G., Carr, S.A., and MacCoss, M.J. (2010a) Effect of collision energy optimization on the measurement of peptides by selected reaction monitoring (SRM) mass spectrometry. *Anal Chem* **82**: 10116-10124.
- MacLean, B., Tomazela, D.M., Shulman, N., Chambers, M., Finney, G.L., Frewen, B., *et al.* (2010b) Skyline: an open source document editor for creating and analyzing targeted proteomics experiments. *Bioinformatics* **26**: 966-968.
- Mäder, U., Schmeisky, A.G., Flórez, L.A., and Stülke, J. (2012) SubtiWiki – a comprehensive community resource for the model organism *Bacillus subtilis*. *Nucleic Acids Res* **40**: D1278-D1287.
- Mandal, M., Boese, B., Barrick, J.E., Winkler, W.C., and Breaker, R.R. (2003) Riboswitches control fundamental biochemical pathways in *Bacillus subtilis* and other bacteria. *Cell* **113**: 577-586.
- Matsumoto, K., Okada, M., Horikoshi, Y., Matsuzaki, H., Kishi, T., Itaya, M., and Shibuya, I. (1998) Cloning, sequencing, and disruption of the *Bacillus subtilis psd* gene coding for phosphatidylserine decarboxylase. *J Bacteriol* **180**: 100-106.
- Meinken, C., Blencke, H.-M., Ludwig, H., and Stülke, J. (2003) Expression of the glycolytic *gapA* operon in *Bacillus subtilis*: Differential syntheses of proteins encoded by the operon. *Microbiology* **149**: 751-761.
- de Mendoza, D., Schujman, G.E., and Aguilar, P.S. (2003) Biosynthesis and function of membrane lipids. In *Bacillus subtilis and Its Closest Relatives*. Sonenshein, A.L., Hoch, J.A., and Losick, R. (eds). Washington, DC, USA: ASM Press, pp. 43-55.
- Metallo, C.M., Walther, J.L., and Stephanopoulos, G. (2009) Evaluation of ¹³C isotopic tracers for metabolic flux analysis in mammalian cells. *J Biotechnol* **144**: 167-174.
- Meyer, F.M., Gerwig, J., Hammer, E., Herzberg, C., Commichau, F.M., Völker, U., and Stülke, J. (2011) Physical interactions between tricarboxylic acid cycle enzymes in *Bacillus subtilis*: evidence for a metabolon. *Metab Eng* **13**: 18-27.
- Meyer, H., Liebeke, M., and Lalk, M. (2010) A protocol for the investigation of the intracellular *Staphylococcus aureus* metabolome. *Anal Biochem* **401**: 250-259.
- Meyer, H., Weidmann, H., and Lalk, M. (2013) Methodological approaches to help unravel the intracellular metabolome of *Bacillus subtilis*. *Microb Cell Fact* **12**: 69.
- Michna, R.H., Commichau, F.M., Tödter, D., Zschiedrich, C.P., and Stülke, J. (2014) SubtiWiki – a database for the model organism *Bacillus subtilis* that links pathway, interaction and expression information. *Nucleic Acids Res* **42**: D692-D698.
- Moritz, B., Striegel, K., Graaf, A.A. de, and Sahm, H. (2000) Kinetic properties of the glucose 6-phosphate and 6-phosphogluconate dehydrogenases from *Corynebacterium glutamicum* and their application for predicting pentose phosphate pathway flux *in vivo*. *Eur J Biochem* **267**: 3442-3452.
- Moses, S., Sinner, T., Zapras, A., Stöveken, N., Hoffmann, T., Belitsky, B.R., Sonenshein, A.L., and Bremer, E. (2012) Proline utilization by *Bacillus subtilis*: Uptake and catabolism. *J Bacteriol* **194**: 745-758.
- Moxley, J.F., Jewett, M.C., Antoniewicz, M.R., Villas-Boas, S.G., Alper, H., Wheeler, R.T., *et al.* (2009) Linking high-resolution metabolic flux phenotypes and transcriptional regulation in yeast modulated by the global regulator Gcn4p. *P Natl Acad Sci USA* **16**: 6477-6482.
- Mukhopadhyay, A., Redding, A.M., Rutherford, B.J., and Keasling, J.D. (2008) Importance of systems biology in engineering microbes for biofuel production. *Curr Opin Biotechnol* **19**: 228-234.
- Nakahigashi, K., Toya, Y., Ishii, N., Soga, T., Hasegawa, M., Watanabe, H., *et al.* (2009) Systematic phenome analysis of *Escherichia coli* multiple-knockout mutants reveals hidden reactions in central carbon metabolism. *Mol Syst Biol* **5**: 306.

- Nakano, M.M., Dailly, Y.P., Zuber, P., and Clark, D.P. (1997) Characterization of anaerobic fermentative growth of *Bacillus subtilis*: Identification of fermentation end products and genes required for growth. *J Bacteriol* **179**: 6749-6755.
- Nau-Wagner, G., Opper, D., Rolbetzki, A., Boch, J., Kempf, B., Hoffmann, T., and Bremer, E. (2012) Genetic control of osmoadaptive glycine betaine synthesis in *Bacillus subtilis* through the choline-sensing and glycine betaine-responsive GbsR repressor. *J Bacteriol* **194**: 2703-2714.
- Netzer, R., Krause, M., Rittmann, D., Peters-Wendisch, P., Eggeling, L., Wendisch, V., and Sahm, H. (2004) Roles of pyruvate kinase and malic enzyme in *Corynebacterium glutamicum* for growth on carbon sources requiring gluconeogenesis. *Arch Microbiol* **182**: 354-363.
- Neuweger, H., Persicke, M., Albaum, S., Bekel, T., Dondrup, M., Huser, A., et al. (2009) Visualizing post genomics data-sets on customized pathway maps by ProMeTra – aeration-dependent gene expression and metabolism of *Corynebacterium glutamicum* as an example. *BMC Syst Biol* **3**: 82.
- Nicolas, P., Mäder, U., Dervyn, E., Rochat, T., Leduc, A., Pigeonneau, N., et al. (2012) Condition-dependent transcriptome reveals high-level regulatory architecture in *Bacillus subtilis*. *Science* **335**: 1103-1106.
- Nissim, I., Yudkoff, M., Yang, W., Terwilliger, T., and Segal, S. (1981) Rapid gas chromatographic-mass spectrometric analysis of [¹⁵N] urea: Application to human metabolic studies. *Clin Chim Acta* **109**: 295-304.
- Nissim, I., and Lapidot, A. (1986) Dynamic aspects of amino acid metabolism in alloxan-induced diabetes and insulin-treated rabbits: *In vivo* studies with ¹⁵N and gas chromatography-mass spectrometry. *Biochem Med Metab Bio* **35**: 88-100.
- Nöh, K., Grönke, K., Luo, B., Takors, R., Oldiges, M., and Wiechert, W. (2007) Metabolic flux analysis at ultra short time scale: Isotopically non-stationary ¹³C labeling experiments. *J Biotechnol* **129**: 249-267.
- Oh, Y.-K., Palsson, B.Ø., Park, S.M., Schilling, C.H., and Mahadevan, R. (2007) Genome-scale reconstruction of metabolic network in *Bacillus subtilis* based on high-throughput phenotyping and gene essentiality data. *J Biol Chem* **282**: 28791-28799.
- Okino, S., Inui, M., and Yukawa, H. (2005) Production of organic acids by *Corynebacterium glutamicum* under oxygen deprivation. *Appl Microbiol Biotechnol* **68**: 475-480.
- Onraedt, A., Muynck, C. de, Walcarius, B., Soetaert, W., and Vandamme, E. (2004) Ectoine accumulation in *Brevibacterium epidermis*. *Biotechnol Lett* **26**: 1481-1485.
- Papagianni, M. (2012) Recent advances in engineering the central carbon metabolism of industrially important bacteria. *Microb Cell Fact* **11**: 50.
- Pastor, J.M., Salvador, M., Argandoña, M., Bernal, V., Reina-Bueno, M., Csonka, L.N., et al. (2010) Ectoines in cell stress protection: Uses and biotechnological production. *Biotechnol Adv* **28**: 782-801.
- Pazlarova, J. (2010) Chemostat-induced uneven division of *Bacillus subtilis*. *J Ind Microbiol Biot* **37**: 1257-1261.
- Perkins, J. B., Pero, J. G. (1993) Biosynthesis of riboflavin, biotin, folic acid, and cobalamin. In *Bacillus subtilis and Its Closest Relatives*. Sonenshein, A.L., Hoch, J.A., and Losick, R. (eds). Washington, DC, USA: ASM Press, pp. 319-334.
- Pietack, N., Becher, D., Schmidl, S.R., Saier, M.H., Hecker, M., Commichau, F.M., and Stülke, J. (2010) *In vitro* phosphorylation of key metabolic enzymes from *Bacillus subtilis*: PrkC phosphorylates enzymes from different branches of basic metabolism. *J Mol Microbiol Biotechnol* **18**: 129-140.
- Piggot, P.J., and Hilbert, D.W. (2004) Sporulation of *Bacillus subtilis*. *Curr Opin Microbiol* **7**: 579-586.
- Piper, M.D.W., Daran-Lapujade, P., Bro, C., Regenber, B., Knudsen, S., Nielsen, J., and Pronk, J.T. (2002) Reproducibility of oligonucleotide microarray transcriptome analyses: An interlaboratory comparison using chemostat cultures of *Saccharomyces cerevisiae*. *J Biol Chem* **277**: 37001-37008.
- Pirt, S.J. (1965) The maintenance energy of bacteria in growing cultures. *P Roy Soc Lond B Bio* **163**: 224-231.
- Pratt, J.M., Simpson, D.M., Doherty, M.K., Rivers, J., Gaskell, S.J., and Beynon, R.J. (2006) Multiplexed absolute quantification for proteomics using concatenated signature peptides encoded by QconCAT genes. *Nat Protoc* **1**: 1029-1043.

- Quek, L.-E., Wittmann, C., Nielsen, L.K., and Krömer, J.O. (2009) OpenFLUX: efficient modelling software for ^{13}C -based metabolic flux analysis. *Microb Cell Fact* **8**: 25.
- R Core Team (2013) R: A language and environment for statistical computing. URL: <http://www.r-project.org>.
- Radmacher, E., and Eggeling, L. (2007) The three tricarboxylate synthase activities of *Corynebacterium glutamicum* and increase of L-lysine synthesis. *Appl Microbiol Biotechnol* **76**: 587-595.
- Roberts, M. (2005) Organic compatible solutes of halotolerant and halophilic microorganisms. *Saline Syst* **1**: 5.
- Rohn, H., Hartmann, A., Junker, A., Junker, B.H., and Schreiber, F. (2012) FluxMap: A VANTED add-on for the visual exploration of flux distributions in biological networks. *BMC Syst Biol* **6**: 33.
- Romero, S., Merino, E., Bolívar, F., Gosset, G., and Martinez, A. (2007) Metabolic engineering of *Bacillus subtilis* for ethanol production: Lactate dehydrogenase plays a key role in fermentative metabolism. *Appl Environ Microbiol* **73**: 5190-5198.
- Romero-Garcia, S., Hernandez-Bustos, C., Merino, E., Gosset, G., and Martinez, A. (2009) Homolactic fermentation from glucose and cellobiose using *Bacillus subtilis*. *Microb Cell Fact* **8**: 23.
- Rühl, M., Zamboni, N., and Sauer, U. (2010) Dynamic flux responses in riboflavin overproducing *Bacillus subtilis* to increasing glucose limitation in fed-batch culture. *Biotechnol Bioeng* **105**: 795-804.
- Rühl, M., Le Coq, D., Aymerich, S., and Sauer, U. (2012) ^{13}C -flux analysis reveals NADPH-balancing transhydrogenation cycles in stationary phase of nitrogen-starving *Bacillus subtilis*. *J Biol Chem* **287**: 27959-27970.
- Ruzal, S.M., López, C., Rivas, E., and Sánchez-Rivas, C. (1998) Osmotic strength blocks sporulation at stage II by impeding activation of early sigma factors in *Bacillus subtilis*. *Curr Microbiol* **36**: 75-79.
- Ruzal, S.M., and Sanchez-Rivas, C. (1998) In *Bacillus subtilis* DegU-P is a positive regulator of the osmotic response. *Curr Microbiol* **37**: 368-372.
- Saito, H., Shibata, T., and Ando, T. (1979) Mapping of genes determining nonpermissiveness and host-specific restriction to bacteriophages in *Bacillus subtilis* Marburg. *Mol Gen Genet* **170**: 117-122.
- Sauer, T., and Galinski, E.A. (1998) Bacterial milking: A novel bioprocess for production of compatible solutes. *Biotechnol Bioeng* **57**: 306-313.
- Sauer, U., Hatzimanikatis, V., Hohmann, H.P., Manneberg, M., van Loon, A.P., and Bailey, J.E. (1996) Physiology and metabolic fluxes of wild-type and riboflavin-producing *Bacillus subtilis*. *Appl Environ Microbiol* **62**: 3687-3696.
- Sauer, U., Hatzimanikatis, V., Bailey, J.E., Hochuli, M., Szyperski, T., and Wüthrich, K. (1997) Metabolic fluxes in riboflavin-producing *Bacillus subtilis*. *Nat Biotechnol* **15**: 448-452.
- Sauer, U., and Bailey, J.E. (1999) Estimation of P-to-O ratio in *Bacillus subtilis* and its influence on maximum riboflavin yield. *Biotechnol Bioeng* **64**: 750-754.
- Sauer, U., and Eikmanns, B.J. (2005) The PEP-pyruvate-oxaloacetate node as the switch point for carbon flux distribution in bacteria. *FEMS Microbiol Rev* **29**: 765-794.
- Sauer, U. (2006) Metabolic networks in motion: ^{13}C -based flux analysis. *Mol Syst Biol* **2**: 1.
- Sauer, U., Heinemann, M., and Zamboni, N. (2007) Getting closer to the whole picture. *Science* **316**: 550-551.
- Schallmeyer, M., Singh, A., and Ward O.P. (2004) Developments in the use of *Bacillus* species for industrial production. *Can J Microbiol* **50**: 1-17.
- Schilling, O., Frick, O., Herzberg, C., Ehrenreich, A., Heinzle, E., Wittmann, C., and Stülke, J. (2007) Transcriptional and metabolic responses of *Bacillus subtilis* to the availability of organic acids: Transcription regulation is important but not sufficient to account for metabolic adaptation. *Appl Environ Microbiol* **73**: 499-507.
- Schubert, T., Maskow, T., Benndorf, D., Harms, H., and Breuer, U. (2007) Continuous synthesis and excretion of the compatible solute ectoine by a transgenic, nonhalophilic bacterium. *Appl Environ Microbiol* **73**: 3343-3347.
- Servant, P., Le Coq, D., and Aymerich, S. (2005) CcpN (YqzB), a novel regulator for CcpA-independent catabolite repression of *Bacillus subtilis* gluconeogenic genes. *Mol Microbiol* **55**: 1435-1451.

- Shabala, L., Bowman, J., Brown, J., Ross, T., McMeekin, T., and Shabala, S. (2009) Ion transport and osmotic adjustment in *Escherichia coli* in response to ionic and non-ionic osmotic stress. *Environ Microbiol* **11**: 137-148.
- Shimizu, K. (2004) Metabolic flux analysis based on ^{13}C -labeling experiments and integration of the information with gene and protein expression patterns. In *Recent Progress of Biochemical and Biomedical Engineering in Japan II*. Kobayashi, T. (ed) Berlin-Heidelberg, Germany: Springer, pp. 1-49.
- Singh, K.D., Schmalisch, M.H., Stülke, J., and Görke, B. (2008) Carbon catabolite repression in *Bacillus subtilis*: Quantitative analysis of repression exerted by different carbon sources. *J Bacteriol* **190**: 7275-7284.
- Sonenshein, A.L. (2003) The Krebs citric acid cycle. In *Bacillus subtilis and Its Closest Relatives*. Sonenshein, A.L., Hoch, J.A., and Losick, R. (eds). Washington, DC, USA: ASM Press, pp. 151-162.
- Sonenshein, A.L. (2007) Control of key metabolic intersections in *Bacillus subtilis*. *Nat Rev Microbiol* **5**: 917-927.
- Starcher, B. (2001) A ninhydrin-based assay to quantitate the total protein content of tissue samples. *Anal Biochem* **292**: 125-129.
- Steil, L., Hoffmann, T., Budde, I., Völker, U., and Bremer, E. (2003) Genome-wide transcriptional profiling analysis of adaptation of *Bacillus subtilis* to high salinity. *J Bacteriol* **185**: 6358-6370.
- Stöveken, N., Pittelkow, M., Sinner, T., Jensen, R.A., Heider, J., and Bremer, E. (2011) A specialized aspartokinase enhances the biosynthesis of the osmoprotectants ectoine and hydroxyectoine in *Pseudomonas stutzeri* A1501. *J Bacteriol* **193**: 4456-4468.
- Stülke, J., and Hillen, W. (2000) Regulation of carbon catabolism in *Bacillus* species. *Annu Rev Microbiol* **54**: 849-80.
- Szyperski, T. (1995) Biosynthetically directed fractional ^{13}C -labeling of proteinogenic amino acids. *Eur J Biochem* **232**: 433-448.
- Tännler, S., Decasper, S., and Sauer, U. (2008) Maintenance metabolism and carbon fluxes in *Bacillus* species. *Microb Cell Fact* **7**: 19.
- Thomas, K.C., and Dawson, P.S.S. (1977) Variations in the adenylate energy charge during phased growth (cell cycle) of *Candida utilis* under energy excess and energy-limiting growth conditions. *J Bacteriol* **132**: 36-43.
- Tobisch, S., Zühlke, D., Bernhardt, J., Stülke, J., and Hecker, M. (1999) Role of CcpA in regulation of the central pathways of carbon catabolism in *Bacillus subtilis*. *J Bacteriol* **181**: 6996-7004.
- Tsalikian, E., Howard, C., Gerich, J.E., and Haymond, M.W. (1984) Increased leucine flux in short-term fasted human subjects: Evidence for increased proteolysis. *Am J Physiol-Endoc M* **247**: E323-E327.
- Van-Thuoc, D., Guzmán, H., Quillaguamán, J., and Hatti-Kaul, R. (2010) High productivity of ectoines by *Halomonas boliviensis* using a combined two-step fed-batch culture and milking process. *J Biotechnol* **147**: 46-51.
- Varela, C., Agosin, E., Baez, M., Klapa, M., and Stephanopoulos, G. (2003) Metabolic flux redistribution in *Corynebacterium glutamicum* in response to osmotic stress. *Appl Microbiol Biotechnol* **60**: 547-555.
- Varela, C.A., Baez, M.E., and Agosin, E. (2004) Osmotic stress response: Quantification of cell maintenance and metabolic fluxes in a lysine-overproducing strain of *Corynebacterium glutamicum*. *Appl Environ Microbiol* **70**: 4222-4229.
- Vilhelmsson, O., and Miller, K.J. (2002) Synthesis of pyruvate dehydrogenase in *Staphylococcus aureus* is stimulated by osmotic stress. *Appl Environ Microbiol* **68**: 2353-2358.
- Weber, A., Kögl, S.A., and Jung, K. (2006) Time-dependent proteome alterations under osmotic stress during aerobic and anaerobic growth in *Escherichia coli*. *J Bacteriol* **188**: 7165-7175.
- Weng, M., Nagy, P.L., and Zalkin, H. (1995) Identification of the *Bacillus subtilis pur* operon repressor. *P Natl Acad Sci USA* **92**: 7455-7459.
- Whatmore, A.M., Chudek, J.A., and Reed, R.H. (1990) The effects of osmotic upshock on the intracellular solute pools of *Bacillus subtilis*. *J Gen Microbiol* **136**: 2527-2535.
- Widner, B., Behr, R., Dollen, S. von, Tang, M., Heu, T., Sloma, A., et al. (2005) Hyaluronic acid production in *Bacillus subtilis*. *Appl Environ Microbiol* **71**: 3747-3752.
- Wiechert, W. (2001) ^{13}C metabolic flux analysis. *Metab Eng* **3**: 195-206.

- Wilkinson, L. (2011) Venn and Euler diagrams. URL: <http://www.rforge.net/venneuler/>
- van Winden, W.A., Wittmann, C., Heinzle, E., and Heijnen, J.J. (2002) Correcting mass isotopomer distributions for naturally occurring isotopes. *Biotechnol Bioeng* **80**: 478-479.
- Wittmann, C., and Heinzle, E. (1999) Mass spectrometry for metabolic flux analysis. *Biotechnol Bioeng* **62**: 739-750.
- Wittmann, C. (2002) Metabolic flux analysis using mass spectrometry. In *Tools and Applications of Biochemical Engineering Science*. Schügerl, K., Zeng, A.-P., Aunins, J., Bader, A., Bell, W., and Biebl, H. et al. (eds) Berlin-Heidelberg, Germany: Springer, pp. 39-64.
- Wittmann, C., and Heinzle, E. (2002) Genealogy profiling through strain improvement by using metabolic network analysis: Metabolic flux genealogy of several generations of lysine-producing *Corynebacteria*. *Appl Environ Microbiol* **68**: 5843-5859.
- Wittmann, C., and Heinzle, E. (2005) Metabolic activity profiling by ¹³C tracer experiments and mass spectrometry in *Corynebacterium glutamicum*. In *Methods in Biotechnology, Vol. 18: Microbial Processes and Products*. Barredo, J.L. (ed) Totowa, NJ, USA: Humana Press, pp. 191-203.
- Wittmann, C. (2007) Fluxome analysis using GC-MS. *Microb Cell Fact* **6**: 6.
- Wittmann, C., Weber, J., Betiku, E., Krömer, J., Böhm, D., and Rinas, U. (2007) Response of fluxome and metabolome to temperature-induced recombinant protein synthesis in *Escherichia coli*. *J Biotechnol* **132**: 375-384.
- Wood, J.M. (2011) Bacterial osmoregulation: A paradigm for the study of cellular homeostasis. *Annu Rev Microbiol* **65**: 215-238.
- Wu, S.-C., Yeung, J.C., Duan, Y., Ye, R., Szarka, S.J., Habibi, H.R., and Wong, S.-L. (2002) Functional production and characterization of a fibrin-specific single-chain antibody fragment from *Bacillus subtilis*: Effects of molecular chaperones and a wall-bound protease on antibody fragment production. *Appl Environ Microbiol* **68**: 3261-3269.
- Wu, X.-C., Ng, S.-C., Near, R.I., and Wong, S.-L. (1993) Efficient production of a functional single-chain antidigoxin antibody via an engineered *Bacillus subtilis* expression-secretion system. *Nat Biotech* **11**: 71-76.
- Wulf, P.D. (1998) Presence of the ribulose monophosphate pathway in *Bacillus subtilis*. *Microbiology* **144**: 596-597.
- Yang, T.H., Heinzle, E., and Wittmann, C. (2005) Theoretical aspects of ¹³C metabolic flux analysis with sole quantification of carbon dioxide labeling. *Comput Biol Chem* **29**: 121-133.
- Yang, T.H., Wittmann, C., and Heinzle, E. (2006) Respirometric ¹³C flux analysis, part I: Design, construction and validation of a novel multiple reactor system using on-line membrane inlet mass spectrometry. *Metab Eng* **8**: 417-431.
- Yoshida, A. (1965) Enzymic properties of malate dehydrogenase of *Bacillus subtilis*. *J Biol Chem* **240**: 1118-1124.
- Yuan, Y., Yang, T.H., and Heinzle, E. (2010) ¹³C metabolic flux analysis for larger scale cultivation using gas chromatography-combustion-isotope ratio mass spectrometry. *Metab Eng* **12**: 392-400.
- Yus, E., Maier, T., Michalodimitrakis, K., van Noort, V., Yamada, T., Chen, W.-H., et al. (2009) Impact of genome reduction on bacterial metabolism and its regulation. *Science* **326**: 1263-1268.
- Zamboni, N., Mouncey, N., Hohmann, H.-P., and Sauer, U. (2003) Reducing maintenance metabolism by metabolic engineering of respiration improves riboflavin production by *Bacillus subtilis*. *Metab Eng* **5**: 49-55.
- Zamboni, N., and Sauer, U. (2003) Knockout of the high-coupling cytochrome aa3 oxidase reduces TCA cycle fluxes in *Bacillus subtilis*. *FEMS Microbiol Lett* **226**: 121-126.
- Zamboni, N., Fischer, E., Laudert, D., Aymerich, S., Hohmann, H.-P., and Sauer, U. (2004) The *Bacillus subtilis* *yqjI* gene encodes the NADP⁺-dependent 6-P-gluconate dehydrogenase in the pentose phosphate pathway. *J Bacteriol* **186**: 4528-4534.
- Zamboni, N., Fischer, E., Muffler, A., Wyss, M., Hohmann, H.-P., and Sauer, U. (2005) Transient expression and flux changes during a shift from high to low riboflavin production in continuous cultures of *Bacillus subtilis*. *Biotechnol Bioeng* **89**: 219-232.

- Zaprasis, A., Brill, J., Thüring, M., Wünsche, G., Heun, M., Barzantny, H., Hoffmann, T., and Bremer, E. (2013) Osmoprotection of *Bacillus subtilis* through import and proteolysis of proline-containing peptides. *Appl Environ Microbiol* **79**: 576-587.
- Zhang, W., Li, F., and Nie, L. (2010) Integrating multiple 'omics' analysis for microbial biology: Application and methodologies. *Microbiology* **156**: 287-301.
- Zhang, X.-Z., Sathitsuksanoh, N., Zhu, Z., and Zhang, Y.-H.P. (2011) One-step production of lactate from cellulose as the sole carbon source without any other organic nutrient by recombinant cellulolytic *Bacillus subtilis*. *Metab Eng* **13**: 364-372.
- Zhang, X.-Z., and Zhang, Y.-H.P. (2011) Simple, fast and high-efficiency transformation system for directed evolution of cellulase in *Bacillus subtilis*. *Microb Biotechnol* **4**: 98-105.

6 Appendix

6.1 Abbreviations and Symbols

Abbreviations

<i>1,3BPG, 13BPG</i>	1,3-bisphosphoglycerate	<i>FAD, FADH₂</i>	Flavin adenine dinucleotide
<i>2OG</i>	2-oxoglutarate	<i>FDR</i>	False discovery rate
<i>2PG</i>	2-phosphoglycerate	<i>FID</i>	Free induction decay
<i>3PG</i>	3-phosphoglycerate	<i>FMOC</i>	9-fluorenylmethylchloroformate
<i>6PG</i>	6-phosphogluconate	<i>FUM</i>	Fumarate
<i>6PGL</i>	6-phosphogluconolactone	<i>FWHM</i>	Full width at half maximum
<i>ABC</i>	ATP-binding cassette	<i>G6P</i>	Glucose 6-phosphate
<i>ABU</i>	α-aminobutyric acid	<i>GAP</i>	Glyceraldehyde 3-phosphate
<i>AcCoA, ACoA</i>	Acetyl-CoA	<i>GB</i>	Glycine betaine
<i>ACE</i>	Acetate	<i>GC</i>	Gas chromatography
<i>ACN</i>	Acetonitrile	<i>GC-IR-MS</i>	Gas chromatography isotope ratio mass spectrometry
<i>ACTN</i>	Acetoin	<i>GEO</i>	Gene Expression Omnibus
<i>ADP</i>	Adenosine diphosphate	<i>GOGAT</i>	Glutamate synthase
<i>AEC</i>	Adenylate energy charge	<i>GP</i>	Glutamate 5-phosphate
<i>AMP</i>	Adenosine monophosphate	<i>GRAS</i>	Generally regarded as safe
<i>ASA</i>	Aspartate semialdehyde	<i>GS</i>	Glutamine synthetase
<i>ATP</i>	Adenosine triphosphate	<i>GSA</i>	Glutamate 5-semialdehyde
<i>BCA</i>	Biological control agent	<i>GTP</i>	Guanosine triphosphate
<i>BSA</i>	Bovine serum albumine	<i>HPr</i>	Histidine protein
<i>cAMP</i>	Cyclic adenosine monophosphate	<i>ICIT</i>	Isocitrate
<i>CcpA</i>	Carbon catabolite control protein A	<i>IP-LC-MS</i>	Ion pairing liquid chromatography mass spectrometry
<i>CcpC</i>	Carbon catabolite control protein C	<i>ISB</i>	Isobutyrate
<i>CcpN</i>	Carbon catabolite control protein N	<i>ISV</i>	Isovalerate
<i>cDNA</i>	Complementary deoxyribonucleic acid	<i>Ktr</i>	Potassium transport
<i>CHRM1</i>	Chorismate	<i>LAC</i>	Lactate
<i>CIT</i>	Citrate	<i>LB</i>	Lysogeny broth
<i>CoA</i>	Coenzyme A	<i>LC-MS/MS</i>	Liquid chromatography tandem-mass spectrometry
<i>CSA</i>	Camphorsulfonic acid	<i>MAL</i>	Malate
<i>CRP</i>	cAMP receptor protein	<i>MBDSFTA</i>	<i>N</i> -methyl- <i>N</i> - <i>tert</i> -butyldimethylsilyl-trifluoroacetamide
<i>dATP</i>	Deoxyadenosine triphosphate	<i>MeOX</i>	<i>O</i> -methoxylamine
<i>dCTP</i>	Deoxycytidine triphosphate	<i>MID</i>	Mass isotopomer distribution
<i>DCW</i>	Dry cell weight	<i>miRNA</i>	Micro-ribonucleic acid
<i>dGTP</i>	Deoxyguanosine triphosphate	<i>mRNA</i>	Messenger ribonucleic acid
<i>DHAP</i>	Dihydroxyacetone phosphate	<i>MS</i>	Mass spectrometry
<i>diff</i>	Difference	<i>Msc</i>	Mechanosensitive channel
<i>Dim</i>	Dimension	<i>MSTFA</i>	<i>N</i> -methyl- <i>N</i> -trimethylsilyl-trifluoroacetamide
<i>DNA</i>	Deoxyribonucleic acid	<i>NAD⁺, NADH</i>	Nicotinamide adenine dinucleotide
<i>dNTP</i>	Deoxyribonucleotide	<i>NADP⁺, NADPH</i>	Nicotinamide adenine dinucleotide phosphate
<i>DTNB</i>	5,5'-dithiobis-(2-nitrobenzoic acid)	<i>NCBI</i>	National Center for Biotechnology Information
<i>DTT</i>	Dithiothreitol	<i>NMR</i>	Nuclear magnetic resonance
<i>dTTP</i>	Deoxythymidine triphosphate	<i>OAA</i>	Oxaloacetate
<i>E4P</i>	Erythrose 4-phosphate	<i>OD</i>	Optical density
<i>EDTA</i>	Ethylenediaminetetraacetic acid	<i>OPA</i>	<i>O</i> -phthaldialdehyde
<i>EI</i>	Enzyme I	<i>Opu</i>	Osmoprotectant uptake
<i>EII</i>	Enzyme II	<i>PCA</i>	Principal component analysis
<i>EMP</i>	Embden-Meyerhof-Parnas	<i>PEP</i>	Phosphoenolpyruvate
<i>EMU</i>	Elementary metabolite unit	<i>PP</i>	Pentose phosphate
<i>ESI</i>	Electrospray ionization	<i>PRO</i>	Proline
<i>F1,6BP, F16BP</i>	Fructose 1,6-bisphosphate	<i>PTS</i>	Phosphotransferase system
<i>F6P</i>	Fructose 6-phosphate	<i>Put</i>	Proline uptake

<i>PYR</i>	Pyruvate	<i>SUC</i>	Succinate
<i>QconCAT</i>	Quantification concatamer	<i>SuCoA, SCoA</i>	Succinyl-CoA
<i>R5P</i>	Ribose 5-phosphate	<i>TBDMS</i>	<i>tert</i> -butyldemthylsilyl
<i>rCCA</i>	Regularized canonical correlation analysis	<i>TCA</i>	Tricarboxylic acid
<i>RI</i>	Refractive index	<i>TE</i>	Tris / ethylenediaminetetraacetic acid
<i>RNA</i>	Ribonucleic acid	<i>TNB</i>	5-thio-2-nitrobenzoic acid
<i>Ru5P</i>	Ribulose 5-phosphate	<i>Trp⁺</i>	Tryptophan-prototroph
<i>S7P</i>	Sedoheptulose 7-phosphate	<i>TSP</i>	Trimethylsilyl propanoic acid
<i>SIM</i>	Selective ion monitoring	<i>UDP</i>	Uridine diphosphate
<i>siRNA</i>	Small interfering ribonucleic acid	<i>UV</i>	Ultraviolet
<i>spec.Act.</i>	Specific enzyme activity	<i>XSP</i>	Xylulose 5-phosphate
<i>SRM</i>	Single reaction monitoring		

Sysmbols

C_{rec}	Carbon recovery	q_s	Glucose uptake rate
D	Dilution rate	S	Substrate concentration
d	Path length	V	Volume
d_f	Film thickness	V_m	Molar volume
F	Flow rate	X	Biomass concentration
id	Inner diameter	x	Relative mass fraction
l	Column length	x_c	Relative carbon fraction
M	Molar mass	Y	Yield
M_0	Monoisotopic mass of the molecule ion	Z	Charge
m_{glc}	Maintenance coefficient	δ	Deviation between measured and simulated labeling data
m	Mass	ϵ	Extinction coefficient
P	Product concentration	μ	Specific growth rate
q_p	Product formation rate		

6.2 Supplementary information

Table 6.1: Biochemical network and reaction stoichiometry for metabolic flux analysis.

rxnID	rxnEQ	cTrans	type	
R01	GLC_EX = G6P	abcdef = abcdef	F	Glucose uptake
R02	G6P = F6P	abcdef = abcdef	FR	EMP
R03	F6P = G6P	abcdef = abcdef	R	
R04	F6P + ATP = F16BP	abcdef + X = abcdef	F	
R05	F16BP = DHAP + G3P	abcdef = abc + def	F	
R06	DHAP = G3P	abc = cba	F	
R07	G3P = 3PG + NADH + ATP	abc = abc + X + X	FR	
R08	3PG + NADH + ATP = G3P	abc + X + X = abc	R	
R09	3PG = PEP	abc = abc	FR	
R10	PEP = 3PG	abc = abc	R	
R11	PEP = PYR	abc = abc	F	
R12	G6P = P5P + CO ₂ + NADPH + NADPH	abcdef = bcdef + a + X + X	F	PPP
R13	P5P + P5P = S7P + G3P	abcde + fghij = fgabcde + hij	FR	
R14	S7P + G3P = P5P + P5P	fgabcde + hij = abcde + fghij	R	
R15	S7P + G3P = E4P + F6P	abcdefg + hij = defg + abchij	FR	
R16	E4P + F6P = S7P + G3P	defg + abchij = abcdefg + hij	R	
R17	E4P + P5P = F6P + G3P	abcd + efghi = efabcd + ghi	FR	
R18	F6P + G3P = E4P + P5P	efabcd + ghi = abcd + efghi	R	
R19	PYR = ACCOA + CO ₂ + NADH	abc = bc + a + X	F	TCA
R20	ACCOA + OAA = CIT	ab + cdef = fedbac	F	
R21	CIT = 2OG + CO ₂ + NADPH	abcdef = abcde + f + X	F	
R22	2OG = 0.5 SUC + 0.5 SUC + CO ₂ + NADH + ATP	abcde = 0.5 edcb + 0.5 bcde + a + X + X	F	
R23	SUC = MAL + NADH	abcd = abcd + X	F	
R24	MAL = OAA + NADH	abcd = abcd + X	F	
R25	MAL = PYR + CO ₂ + NADPH	abcd = abc + d + X	F	Malic enzyme
R26	PYR + CO ₂ + ATP = OAA	abc + d + X = abcd	F	Anaplerosis
R27	OAA + ATP = PEP + CO ₂	abcd + X = abc + d	F	Gluconeogenesis
R28	ACCOA = ACE + ATP	ab = ab + X	F	Metabolites
R29	ACE = ACE_EX		B	
R30	PYR = PYR_EX		B	
R31	PYR + NADPH = LAC	abc + X = abc	F	
R32	LAC = LAC_EX		B	
R33	SUC = SUC_EX		B	
R34	2OG = 2OG_EX		B	
R35	VAL = VAL_EX		B	
R36	ISV = ISV_EX		B	
R37	LEU = LEU_EX		B	
R38	ISB = ISB_EX		B	
R39	CO ₂ = CO ₂ _EX	a = a	FR	
R40	CO ₂ _EX = CO ₂	a = a	R	
R41	G6P = G6P_B		B	Biomass
R42	F6P = F6P_B		B	
R43	P5P = P5P_B		B	
R44	E4P = E4P_B		B	
R45	G3P = G3P_B		B	
R46	3PG = 3PG_B		B	
R47	PEP = PEP_B		B	
R48	PYR = PYR_B		B	
R49	ACCOA = ACCOA_B		B	
R50	2OG = 2OG_B		B	
R51	OAA = OAA_B		B	

R52	SER + CYS + GLY = SERCYSGLY_B		B
R53	CYS = CYS_B		B
R54	GLY = GLY_B		B
R55	HIS = HIS_B		B
R56	GLU + GLN + ARG + PRO = GLUGLNARGPRO_B		B
R57	GLN = GLN_B		B
R58	ARG = ARG_B		B
R59	PRO = PRO_B		B
R60	ALA + VAL + LEU = ALAVALLEU_B		B
R61	LEU = LEU_B		B
R62	PHE + TYR + TRP = PHETYRTRP_B		B
R63	TRP = TRP_B		B
R64	HIS + TRP = HISTRP_B		B
R65	TYR + PHE = TYRPHE_B		B
R66	ASP + ASN + THR + MET + LYS + ILE = ASPASNTHRMETLYSILE_B		B
R67	LYS + ILE = LYSILE_B		B
R68	ASP + ASN + THR + MET = ASPASNTHRMET_B		B
	0.4083 GLY + 0.2669 ALA + 0.3067 VAL + 0.3464 LEU + 0.2699 ILE + 0.2162 SER + 0.1863 THR + 0.1759 PHE + 0.1108 TYR + 0.0543		
R69	TRP + 0.0567 CYS + 0.1133 MET + 0.3231 LYS + 0.193 ARG + 0.0817 HIS + 0.148 ASP + 0.2604 GLU + 0.148 ASN + 0.2603 GLN + 0.1606 PRO = BIOMASS		B
R70	NADPH = NADPH_B		B
R71	3PG = GLY + MTHF	$abc = ab + c$	S
R72	PYR + PYR = VAL + CO2	$abc + def = abefc + d$	S
R73	E4P + PEP = SHKM	$abcd + efg = efgabcd$	S
R74	SHKM + PEP = CHRM	$abcdefg + hij = abcdefghij$	S
R75	CHRM = PHE + CO2	$abcdefghij = hijbcdefg + a$	S
R76	CHRM = TYR + CO2	$abcdefghij = hijbcdefg + a$	S
R77	CHRM = ANTHR + PYR	$abcdefghij = abcdefg + hij$	S
R78	ANTHR + P5P = CPADR5P	$abcdefg + hijkl = abcdefghijkl$	S
R79	CPADR5P = INDG + CO2	$abcdefghijkl = abcdefghijkl + e$	S
R80	INDG = IND + G3P	$abcdefghijk = abcdefgh + ijk$	S
R81	IND + SER = TRP	$abcdefgh + ijk = abcdefghkji$	S
R82	PYR + PYR = ISV + CO2	$abc + def = abefc + d$	S
R83	ISV + ACCOA = LEU + CO2	$abcde + fg = fgbcde + a$	S
R84	2OG + CO2 = ARG	$abcde + f = abcdef$	S
R85	OAA + PYR = 0.5 LYS + 0.5 LYS + 0.5 CO2 + 0.5 CO2	$abcd + efg = 0.5 abcdgf + 0.5 efgdcb + 0.5 e + 0.5 a$	S
R86	OAA + MTHF = MET	$abcd + e = abcde$	S
R87	P5P + MTHF = HIS	$abcde + f = edcbaf$	S
R88	3PG = CYS	$abc = abc$	S
R89	3PG = SER	$abc = abc$	S
R90	PYR = ALA	$abc = abc$	S
R91	OAA = ASP	$abcd = abcd$	S
R92	OAA = ASN	$abcd = abcd$	S
R93	OAA = THR	$abcd = abcd$	S
R94	PYR + OAA = ILE + CO2	$abc + defg = debfgc + a$	S
R95	2OG = GLU	$abcde = abcde$	S
R96	2OG = GLN	$abcde = abcde$	S
R97	2OG = PRO	$abcde = abcde$	S

Amino acids

Table 6.2: Theoretical precursor demand [$\text{mmol g}_{\text{DCW}}^{-1}$] of wild-type *B. subtilis* under different growth conditions.

Precursor	Exponential	Carbon-limited				Nitrogen-limited		
		0.4 h ⁻¹	Reference 0.1 h ⁻¹	Salt stress	Osmo protection	Reference 0.1 h ⁻¹	Salt stress	Sugar stress
Glucose 6-phosphate	0.046	0.144	0.302	0.085	0.260	0.203	0.130	0.228
Fructose 6-phosphate	0.061	0.183	0.392	0.107	0.328	0.216	0.124	0.218
Ribose 5-phosphate	0.748	0.551	0.428	0.418	0.441	0.435	0.442	0.448
Erythrose 4-phosphate	0.406	0.350	0.284	0.313	0.374	0.403	0.402	0.403
Glyeraldehyde 3-phosphate	0.119	0.356	0.651	0.179	0.540	0.491	0.278	0.485
3-phosphoglycerate	1.159	0.948	0.821	0.885	1.015	1.081	1.086	1.083
Phosphoenolpyruvate	0.830	0.759	0.685	0.660	0.848	0.870	0.842	0.870
Pyruvate	2.718	2.619	2.395	2.362	2.929	2.997	2.927	2.975
Acetyl-CoA	0.767	1.476	1.114	0.557	1.075	1.848	1.240	1.845
2-oxoglutarate	1.654	1.643	1.635	3.339	1.443	1.568	2.265	1.551
Oxaloacetate	1.704	1.480	1.281	1.298	1.602	1.646	1.625	1.637

Table 6.3: Comparison between measured and simulated mass isotopomer distribution in proteinogenic amino acids of carbon-limited *B. subtilis*.

Fragment		C-limitation (Reference)		C-limitation & salt stress		C-limitation & osmoprotection	
		simulated	experimental	simulated	experimental	simulated	experimental
Ala 260	m+0	0.486	0.478	0.489	0.487	0.437	0.432
	m+1	0.368	0.379	0.368	0.374	0.399	0.405
	m+2	0.113	0.110	0.110	0.107	0.126	0.124
	m+3	0.033	0.034	0.033	0.033	0.039	0.039
Val 288	m+0	0.317	0.305	0.320	0.310	0.260	0.251
	m+1	0.401	0.408	0.403	0.407	0.405	0.407
	m+2	0.201	0.206	0.198	0.203	0.234	0.239
	m+3	0.063	0.062	0.061	0.061	0.077	0.077
Thr 404	m+0	0.288	0.287	0.277	0.277	0.236	0.236
	m+1	0.374	0.376	0.374	0.376	0.372	0.372
	m+2	0.221	0.220	0.227	0.226	0.249	0.249
	m+3	0.089	0.089	0.093	0.092	0.107	0.107
Asp 418	m+0	0.287	0.287	0.277	0.278	0.235	0.237
	m+1	0.373	0.375	0.373	0.375	0.372	0.372
	m+2	0.221	0.220	0.227	0.225	0.249	0.248
	m+3	0.090	0.089	0.093	0.092	0.108	0.108
Glu 432	m+0	0.216	0.213	0.210	0.203	0.168	0.161
	m+1	0.354	0.354	0.352	0.353	0.336	0.334
	m+2	0.257	0.260	0.260	0.264	0.283	0.288
	m+3	0.119	0.119	0.122	0.123	0.143	0.146
Ser 390	m+0	0.431	0.424	0.435	0.438	0.387	0.389
	m+1	0.368	0.375	0.368	0.367	0.392	0.393
	m+2	0.148	0.147	0.145	0.144	0.162	0.159
	m+3	0.052	0.053	0.051	0.051	0.060	0.059
Phe 336	m+0	0.236	0.235	0.249	0.247	0.184	0.181
	m+1	0.377	0.375	0.383	0.381	0.359	0.356
	m+2	0.251	0.249	0.243	0.242	0.282	0.281
	m+3	0.099	0.098	0.092	0.092	0.125	0.124
Tyr 466	m+0	0.203	0.202	0.214	0.213	0.158	0.158
	m+1	0.349	0.345	0.355	0.352	0.328	0.325
	m+2	0.262	0.261	0.257	0.255	0.286	0.282
	m+3	0.125	0.124	0.118	0.117	0.149	0.147
Gly 246	m+0	0.739	0.741	0.751	0.750	0.721	0.719
	m+1	0.187	0.185	0.177	0.178	0.202	0.202
	m+2	0.074	0.074	0.072	0.072	0.077	0.079
Lys 431	m+0	0.196	0.198	0.191	0.192	0.148	0.152
	m+1	0.344	0.342	0.342	0.340	0.319	0.316
	m+2	0.266	0.266	0.269	0.269	0.290	0.288
	m+3	0.130	0.129	0.133	0.132	0.158	0.157
Leu 302	m+0	0.218	0.229	0.220	0.227	0.166	0.175
	m+1	0.375	0.368	0.377	0.374	0.354	0.350
	m+2	0.263	0.261	0.263	0.259	0.297	0.291
	m+3	0.105	0.105	0.104	0.103	0.132	0.133
Arg 442	m+0	0.184	0.184	0.174	0.172	0.141	0.141
	m+1	0.334	0.329	0.328	0.326	0.310	0.306
	m+2	0.271	0.270	0.276	0.275	0.291	0.288
	m+3	0.139	0.139	0.145	0.143	0.164	0.162

Table 6.4: Comparison between measured and simulated mass isotopomer distribution in proteinogenic amino acids in nitrogen-limited *B. subtilis*.

Fragment		N-limitation		N-limitation & high-salt		N-limitation & high-glucose	
		simulated	experimental	simulated	experimental	simulated	experimental
Ala 260	m+0	0.451	0.450	0.450	0.446	0.719	0.724
	m+1	0.394	0.396	0.393	0.399	0.194	0.191
	m+2	0.119	0.117	0.120	0.118	0.074	0.072
	m+3	0.036	0.037	0.037	0.037	0.013	0.013
Val 288	m+0	0.274	0.266	0.273	0.264	0.676	0.676
	m+1	0.408	0.409	0.408	0.409	0.223	0.224
	m+2	0.225	0.230	0.225	0.231	0.081	0.080
	m+3	0.071	0.072	0.072	0.073	0.017	0.017
Thr 404	m+0	0.254	0.255	0.241	0.242	0.589	0.591
	m+1	0.377	0.377	0.373	0.373	0.257	0.257
	m+2	0.238	0.237	0.246	0.246	0.115	0.114
Asp 418	m+0	0.099	0.099	0.105	0.105	0.031	0.031
	m+1	0.253	0.255	0.241	0.243	0.588	0.593
	m+2	0.376	0.376	0.372	0.373	0.257	0.255
	m+3	0.238	0.237	0.246	0.245	0.116	0.114
Glu 432	m+0	0.100	0.100	0.106	0.105	0.031	0.031
	m+0	0.181	0.176	0.174	0.168	0.567	0.563
	m+1	0.345	0.344	0.339	0.337	0.268	0.272
	m+2	0.276	0.279	0.280	0.283	0.121	0.120
Ser 390	m+3	0.135	0.136	0.140	0.142	0.034	0.034
	m+0	0.404	0.404	0.403	0.403	0.626	0.629
	m+1	0.389	0.390	0.388	0.390	0.239	0.238
	m+2	0.152	0.151	0.153	0.152	0.109	0.106
Phe 336	m+3	0.055	0.055	0.056	0.056	0.027	0.027
	m+0	0.218	0.217	0.210	0.210	0.636	0.634
	m+1	0.381	0.380	0.374	0.373	0.249	0.249
	m+2	0.263	0.261	0.266	0.266	0.090	0.090
Tyr 466	m+3	0.102	0.101	0.108	0.108	0.021	0.021
	m+0	0.187	0.185	0.181	0.180	0.547	0.548
	m+1	0.350	0.348	0.344	0.340	0.279	0.278
	m+2	0.272	0.271	0.275	0.273	0.125	0.123
Gly 246	m+3	0.128	0.128	0.134	0.134	0.037	0.037
	m+0	0.747	0.748	0.745	0.746	0.764	0.768
	m+1	0.181	0.178	0.183	0.181	0.166	0.163
	m+2	0.072	0.073	0.072	0.073	0.070	0.069
Lys 431	m+0	0.162	0.164	0.155	0.158	0.556	0.552
	m+1	0.330	0.327	0.323	0.320	0.276	0.277
	m+2	0.284	0.284	0.287	0.286	0.122	0.123
	m+3	0.147	0.148	0.153	0.153	0.035	0.036
Leu 302	m+0	0.176	0.186	0.177	0.187	0.645	0.646
	m+1	0.361	0.357	0.361	0.357	0.244	0.244
	m+2	0.291	0.285	0.290	0.285	0.088	0.086
	m+3	0.125	0.125	0.125	0.125	0.019	0.020
Arg 442	m+0	0.150	0.148	0.146	0.144	0.550	0.525
	m+1	0.317	0.308	0.312	0.301	0.279	0.270
	m+2	0.288	0.279	0.289	0.280	0.124	0.120
	m+3	0.158	0.153	0.162	0.157	0.036	0.037

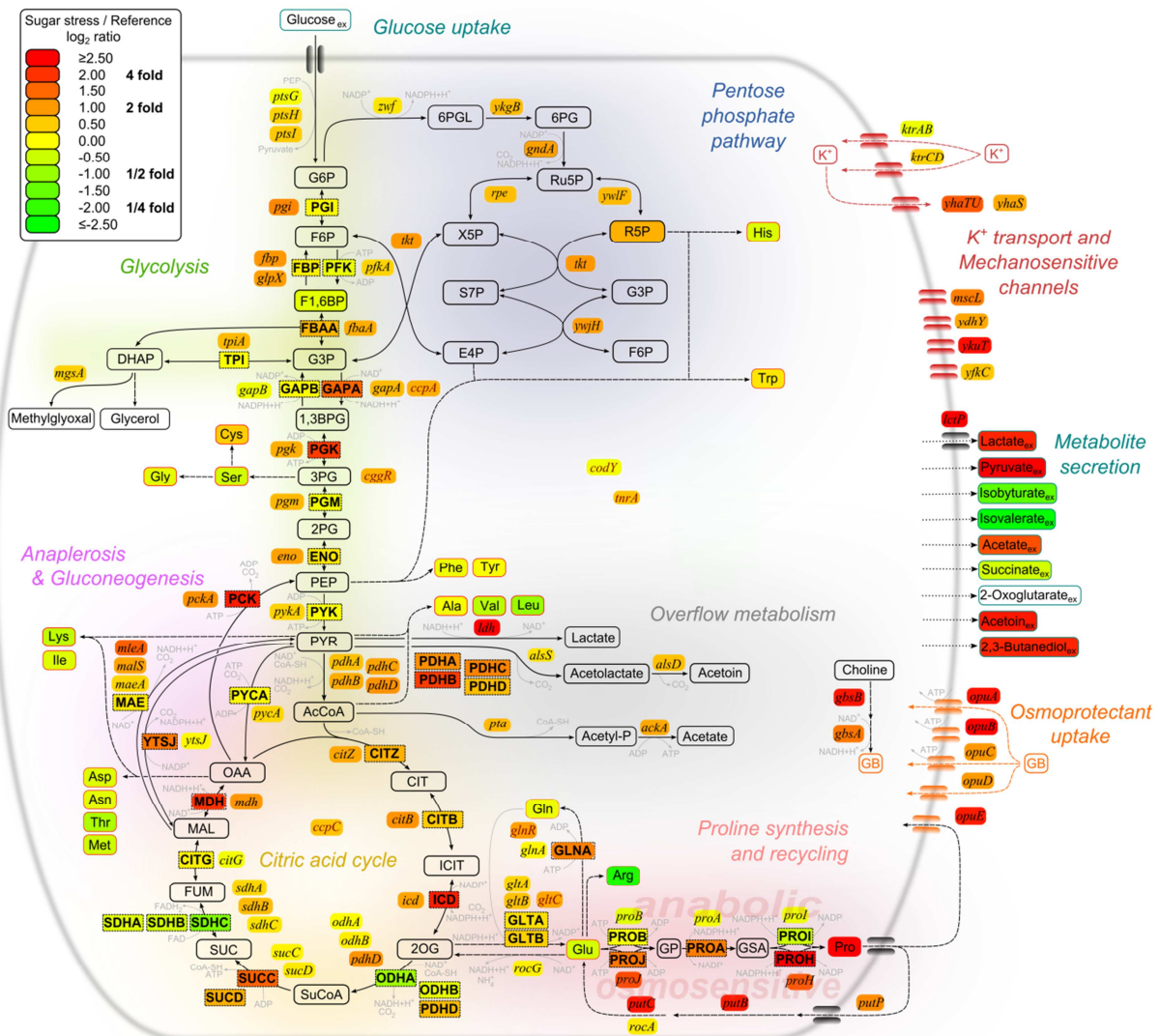


Figure 6.2: Integrated view of relative transcript, protein and metabolite concentrations in *B. subtilis*. Shown are changes in glucose-stressed cells under nitrogen-limitation (in the presence of 1.39 M glucose) compared to unstressed cells. The data format is as follows: gene expression, italics; protein abundances, dashed rectangles; metabolite pools, rounded rectangles.